

Electromagnetic Environment Associated with Lightning Strikes to Tall Strike Objects

THÈSE N° 4903 (2011)

PRÉSENTÉE LE 11 MARS 2011

À LA FACULTÉ SCIENCES ET TECHNIQUES DE L'INGÉNIEUR
GROUPE SCI STI FR (LABORATOIRE DE COMPATIBILITE ELECTROMAGNETIQUE)
PROGRAMME DOCTORAL EN ENERGIE

ÉCOLE POLYTECHNIQUE FÉDÉRALE DE LAUSANNE

POUR L'OBTENTION DU GRADE DE DOCTEUR ÈS SCIENCES

PAR

Seyed Abbas MOSADDEGHI

acceptée sur proposition du jury:

Dr S.-R. Cherkaoui, président du jury
Prof. F. Rachidi-Haeri, directeur de thèse
Prof. M. Rubinstein, rapporteur
Prof. A. Skrivervik Favre, rapporteur
Prof. R. Thottappillil, rapporteur



ÉCOLE POLYTECHNIQUE
FÉDÉRALE DE LAUSANNE

Suisse
2011

Résumé

Depuis peu, les chercheurs spécialisés du domaine de la foudre s'intéressent de près à son interaction avec les objets foudroyés. Plusieurs campagnes de mesures, comprenant des enregistrements du courant et des champs électromagnétiques associés, ont été menées dans le monde, principalement en Russie, en Afrique du Sud, en Allemagne, au Japon et en Autriche. Ce sujet est relativement nouveau, et la résolution des problèmes qui s'y rapportent aura un impact important dans diverses applications fondées sur les mêmes théories, telle la protection contre la foudre ou la détermination des caractéristiques de la foudre à partir des champs mesurés à distance. Le principal objectif de cette thèse de doctorat consiste en développements théoriques et en mesures expérimentales, en vue de comprendre et de résoudre des problèmes récemment apparus à propos des caractéristiques des arcs en retour de la foudre sur les structures élevées, ainsi que des rayonnements électromagnétiques qui leur sont associés

Le Chapitre 2 passe en revue les récents progrès de la modélisation du foudroiement des tours élevées et les données expérimentales obtenues durant les deux dernières décennies. Deux types de modèles d'arc en retour sont discutés : les modèles d'Ingénieurs et les modèles de la Théorie d'Antenne (TA) ou Electromagnétique. Ces modèles ont été généralisés pour prendre en compte les structures foudroyées élevées.

Ce chapitre comprend également une description de la méthode de calcul utilisée pour l'évaluation des champs électromagnétiques générés par une décharge de foudre sur une structure élevée, ainsi qu'une vue d'ensemble des données disponibles sur le courant de foudre et sur le champ électromagnétique associé.

Ce chapitre souligne enfin quelques questions importantes soulevées, ces dernières années, par différents groupes de recherche, et qui donnent lieu à de nouvelles investigations. Ces questions sont les suivantes :

(1) On ne dispose ni d'une analyse théorique systématique, ni de données expérimentales pour les champs électromagnétiques au voisinage d'une structure frappée par la foudre. Or la caractérisation des champs électromagnétiques proches est particulièrement importante dans l'analyse de leur interaction avec des équipements électriques et électroniques situés à proximité.

(2) Aucun modèle d'arc en retour n'est capable de reproduire le passage à zéro des champs lointains pour les coups de foudre sur des structures élevées. De quelle manière ces modèles peuvent-ils être révisés pour rendre compte de cet effet?

(3) Comment les modèles d'ingénieurs peuvent-ils être révisés pour supprimer la discontinuité du courant au niveau du front d'onde de l'arc de retour?

(4) On sait que les mesures de champs électromagnétiques rayonnés par la foudre sont affectées par la présence de bâtiments situés à proximité ou de structures métalliques. Mais actuellement, aucune analyse systématique et quantitative d'un tel effet n'est disponible dans la littérature.

Le travail présenté dans cette thèse aborde toutes les questions mentionnées ci-dessus. Les principales contributions originales de cette thèse, tant théoriques qu'expérimentales, sont présentées dans les chapitres 3 à 6.

Le Chapitre 3 est consacré à une description théorique de la signature des champs électriques et magnétiques à très courte distance, en relation avec le foudroisement d'une tour. Il y est montré que le champ électrique généré par un arc en retour de foudre sur une structure élevée peut changer de polarité à une distance très proche. Ce changement de polarité semble être une signature spécifique du champ électrique vertical très proche. Une équation simple a été développée afin d'obtenir une estimation de la distance critique en deçà de laquelle une telle inversion de polarité peut se produire. Il apparaît également que l'inversion de polarité dépend du coefficient de réflexion à la base de la tour, et disparaît lorsque ce coefficient est proche de 1. En revanche, d'autres paramètres tels que la vitesse de l'arc en retour, le coefficient de réflexion au sommet de l'objet foudroyé et le modèle d'arc en retour adopté ne semblent pas avoir un impact significatif sur l'inversion de polarité. Les résultats de

simulation ont aussi montré que la crête du champ électrique, à des distances supérieures à la hauteur de la tour, témoigne d'une décroissance usuelle en $1/r$. Cependant, à des distances plus rapprochées, la crête du champ électrique se sature à cause de l'effet d'ombrage (*shadowing effect*) de la tour. Cet effet se traduit par une diminution substantielle du champ électrique proche. En outre, la crête du champ magnétique varie inversement proportionnellement à la distance horizontale et ne dépend pas de manière significative de la présence d'un objet élevé foudroyé.

Le Chapitre 4 présente une version améliorée des modèles d'ingénieur pour l'arc en retour d'une décharge sur une structure de grande taille, prenant en compte (1) la présence de réflexions possibles au front d'onde de l'arc en retour, et (2) la présence d'un traceur ascendant de connexion. Nous proposons également une solution itérative élégante qui peut être facilement mise en œuvre dans les programmes de simulation par ordinateur pour prendre en compte de manière simple les réflexions multiples qui se produisent au niveau des discontinuités, aux deux extrémités de la tour ainsi qu'au front d'onde de l'arc en retour.

Les résultats de simulation pour les champs magnétiques sont comparés aux mesures associées aux décharges de la Tour CN (553 m) à Toronto. Il en ressort que la prise en compte de la réflexion au front d'onde de l'arc en retour permet de mieux reproduire la structure fine de l'onde du champ magnétique.

Le Chapitre 5 présente et discute les mesures obtenues en 2007 et 2008 de champs électriques (composantes verticale et radiale) et magnétiques des traceurs et des arcs en retour associés au foudroiement de la tour de Gaisberg en Autriche. Les données comprennent également les enregistrements simultanés des champs électriques verticaux et radiaux, qui ont été obtenus pour la première fois à des distances aussi proches.

Il apparaît que les courbes du champ électrique radial et du champ électrique vertical ont une forme proche de celle d'une impulsion en V asymétrique. Le champ électrique vertical est caractérisé par une variation initiale négative, relativement lente, due au traceur descendant, suivie par une montée rapide due à la phase de l'arc en retour. Pour les champs électriques horizontaux cependant, le fond de l'impulsion en V n'est pas associé à la transition du traceur vers l'arc en retour. Le champ horizontal dû à l'arc en retour est caractérisé par une courte impulsion négative, d'une durée d'environ une microseconde.

En outre, nous avons développé une expression analytique du champ électrique radial en supposant une distribution de charge uniforme le long du traceur et une vitesse de propagation constante.

Il est également montré que le champ électrique vertical de l'arc en retour est beaucoup plus faible que celui qui a été mesuré lors d'expériences de déclenchement artificiel de la foudre. Ce résultat confirme l'effet d'ombrage de la tour prédit, par l'analyse théorique du Chapitre 3, qui se traduit par une diminution significative du champ électrique à des distances inférieures à la hauteur de la tour.

Enfin, l'aptitude des deux modèles d'arc en retour à reproduire les champs électriques vertical et horizontal a été testée sur les mesures obtenues. Les modèles considérés sont (1) le modèle MTLE (Modified Transmission Line with Exponential Decay), et (2) le modèle électromagnétique, mis en œuvre à l'aide du logiciel Numerical Electromagnetics Code NEC-4. Il apparaît que les formes d'onde du champ électrique prédites par les deux modèles concordent avec les formes d'onde mesurées. En général, les champs obtenus par le modèle électromagnétique semblent être en meilleur accord avec les données mesurées, en raison de l'utilisation directe de l'onde de courant mesurée comme données d'entrée et de la représentation plus fine de la tour foudroyée.

Le Chapitre 6 discute de l'effet des bâtiments et des structures métalliques sur les mesures du champ électromagnétique généré par la foudre. En effet, les capteurs utilisés pour la mesure des champs électriques et magnétiques de l'éclair sont souvent placés à proximité ou sur le toit des bâtiments ou d'autres structures. Les parties métalliques, ainsi que d'autres pièces conductrices de ces structures, peuvent affecter les champs mesurés. Afin d'évaluer l'effet de ces structures, des champs électriques et magnétiques ont été mesurés simultanément sur le toit d'un bâtiment et sur le sol aux alentours de ce bâtiment. Les résultats obtenus suggèrent que le champ électrique mesuré sur le toit de l'immeuble pourrait être amplifié par un facteur compris entre 1.7 et 1.9, tandis que les champs électriques mesurés sur le sol peuvent être atténués d'un facteur allant de 5 à 20. En outre, il est démontré que pour un capteur placé sur le sol à proximité d'un bâtiment, la composante du champ magnétique perpendiculaire au bâtiment peut être significativement atténuée, probablement en raison de l'effet des courants induits dans le bâtiment. Le champ magnétique sur le toit de l'immeuble ne semble pas être notablement affecté par le bâtiment.

Dans certaines simulations numériques utilisant le Numerical Electromagnetics Code (NEC-4), le bâtiment a été représenté par un grillage métallique (*wire-grid*). Les résultats de ces simulations confirment les conclusions de l'analyse expérimentale, en dépit de différences quantitatives qui sont attribuées, du moins en partie, au modèle simplifié de l'immeuble.

Liste des mots-clés:

Foudre, Champ électromagnétique, Arc en retour, Modèles d'Ingénieur, Modèles électromagnétiques, Traceur descendant, Structures élevées, Effet d'ombrage, Traceur ascendant de connexion, Bâtiment à proximité.

Abstract

The study of the lightning interaction with tall strike objects has attracted considerable attention of lightning researchers lately. Many lightning measurements including current and associated electromagnetic fields were recently made all over the globe namely in Russia, South Africa, Germany, Brazil, Japan, and Austria. It is a novel area of studies, and the resolution of associated questions will have an impact upon many lightning-related applications such as lightning protection and the determination of lightning parameters from remote field measurements. The main objective of the thesis is to carry out further theoretical investigations and experimental measurements to understand and elucidate recently raised questions on the characteristics of lightning return-strokes to tall structures and their associated electromagnetic radiation.

Chapter 2 presents a review on recent progress in the modeling of lightning strikes to tall towers and associated experimental data obtained during the last decade or so. Two types of return stroke models namely the Engineering Models, and the Electromagnetic or Antenna-Theory (AT) models, extended to take into account the presence of a tall strike object are discussed.

The Chapter contains also a description of the computational methods for the evaluation of electromagnetic fields generated by a lightning strike to a tall structure, as well as an overview of available data on lightning current and associated electromagnetic fields.

The chapter finally highlights some important questions raised by different research groups in the past few years which call for further investigations. These questions are as follows:

(1) No systematic theoretical analysis nor experimental data are available for electromagnetic fields in the immediate vicinity of a tall structure struck by lightning. The characterization of nearby electromagnetic fields is particularly important in the analysis of the interaction to nearby electrical and electronics systems.

(2) Why do lightning return stroke models not reproduce the far-field zero crossing associated with lightning to tall structures? How should these models be revised to be able to reproduce such an effect?

(3) How should the engineering models be revised in order to remove the associated current discontinuity at the return stroke wavefront?

(4) It is well-known that the measurements of electromagnetic fields from lightning are affected by the presence of nearby buildings and metallic structures. However, no systematic and quantitative analysis of such an effect is presently available in the literature.

The work presented in this thesis addresses all of the above questions. The main original contributions of this thesis, consisting of both theoretical and experimental work, are presented in Chapters 3 through 6.

Chapter 3 is devoted to a theoretical description of the signature of electric and magnetic fields at very close distance associated with lightning strikes to a tower. It is shown that the electric field generated by a lightning return stroke to a tall structure can change polarity at very close distance range. This change in the polarity seems to be a specific signature of the very close vertical electric field. A simple equation is derived which provides an estimate of the critical distance below which such an inversion of polarity might occur. It is also shown that the inversion of polarity depends on the value of the reflection coefficient at the base of the tower and disappears for reflection coefficients close to 1. On the other hand, other parameters such as the return stroke speed, the reflection coefficient at the top of the strike object, and the adopted return stroke model seem not to have an impact on the inversion of polarity. Simulation results also showed that the electric field peak at distances beyond the height of the tower or so exhibits the typical $1/r$ dependence. At closer distances, however, the E-field peak features a saturation, due to the so-called tower shadowing effect. This shadowing effect results in a substantial decrease of the nearby electric field. On the other hand, the magnetic field peak varies inversely proportional to the horizontal distance and does not depend significantly on the presence of an elevated strike object.

Chapter 4 introduces an improved version of the engineering models for return-strokes to tall structures which accounts for (1) the presence of possible reflections at the return stroke wavefront, and, (2) a return stroke initiation above the structure due to an upward connecting leader. We also propose an elegant iterative solution that can be easily implemented into computer simulation programs to take into account in a straightforward way multiple reflections occurring at the discontinuities at the tower ends and at the return stroke wavefront.

Simulation results for the magnetic fields are compared with experimental waveforms associated with lightning strikes to the CN Tower (553 m). It is shown that taking into account the reflections at the return-stroke wavefront results in better reproducing the fine structure of the magnetic field waveforms.

Chapter 5 presents and discusses obtained measurements of electric (vertical and radial) and magnetic fields from leaders and return strokes associated with lightning strikes to the Gaisberg tower in Austria obtained in 2007 and 2008. The data include simultaneous records of vertical and radial electric fields, which were obtained for the first time at such close distances.

It is found that the vertical and radial electric field waveforms appear as asymmetrical V-shaped pulses. For the vertical electric field, the initial, relatively slow, negative electric field change is due to the downward leader and the following fast positive field change is due to the upward return stroke phase of the lightning discharge. For the horizontal electric fields, however, the bottom of the V is not associated with the transition from the leader to the return stroke. The horizontal field change due to the return stroke is characterized by a short negative pulse of the order of one microsecond or so, starting with a fast negative excursion followed by a positive one.

In addition, an analytical expression for the radial electric field, assuming a uniform charge distribution along the leader with constant speed is derived.

It is also shown that the return-stroke vertical electric field changes appear to be significantly smaller than similar measurements obtained using triggered lightning. This finding confirms the shadowing effect of the tower predicted by the theoretical analysis of Chapter 3, which results in a significant decrease of the electric field at distances of about the height of the tower or less.

Finally, the ability of two different models for the return stroke in reproducing measured vertical and horizontal electric fields is tested using the obtained measured data. The considered models are (1) the engineering MTLE (Modified Transmission Line with Exponential Decay) model, and (2) the electromagnetic model implemented using the Numerical Electromagnetics Code NEC-4. It is shown that both models predict electric field waveforms which are in reasonable agreement with measured waveforms. In general, the predicted fields by the electromagnetic model appear to be in better agreement with measured data, because of the direct use of the measured current waveform as an input and the more accurate representation of the tower.

Chapter 6 reports on the effect of nearby buildings on electromagnetic fields from lightning. Indeed, sensors used for the measurement of lightning electric and magnetic fields are often placed close to or on top of buildings or other structures. Metallic beams and other conducting parts in those structures may cause enhancement or attenuation effects on the measured fields. Experimental waveforms radiated from distant natural lightning recorded during the summers of 2006 and 2007 are presented. Electric and magnetic field waveforms were measured simultaneously on the roof of a building and on the ground at different distances away from it. The results suggest that the measured electric field on the roof of the building could be enhanced by a factor of 1.7 to 1.9, whereas the electric fields on the ground experienced a significant reduction by a factor ranging from 5 to 20. Also, it is shown that for a sensor located on the ground close to a building, the magnetic field component perpendicular to the building can experience significant attenuation, presumably due to the effect of the induced currents in the building. The magnetic field on the roof of the building seems not to be significantly affected by the building.

Simulations using the Numerical Electromagnetic Code (NEC-4) were also carried out in which the building was represented using a simple wire-grid model. The simulation results support in essence the findings of the experimental analysis, despite quantitative differences which are ascribed, at least in part, to the oversimplified model of the building.

List of keywords:

Lightning, Electromagnetic field, Return Stroke, Engineering Models, Electromagnetic models, Downward leader, Tall structures, Shadowing effect, Upward connecting leader, Nearby building.

Acknowledgements

I am heartily thankful to my supervisor, Prof. Farhad Rachidi, whose continuous guidance and support made it possible for me to finalize this dissertation. Farhad is not only described by his deep knowledge and outstanding scientific achievements in the Lightning research but also his extraordinary personal characteristics made him one of the unique supervisors one can ever had. I am truly fascinated by the kindness, humbleness and friendliness he has shown throughout these years. Thanks Farhad!

I would like also express my profound respect and sincere gratitude to Prof. Alain Germond, may he rest in peace, who accepted me among the staff of the LRE¹ (Power Systems Laboratory) of the EPFL.

Special thanks are addressed to my dear colleague Dr. Davide Pavanello for all the help and support that he gave me. It was a great pleasure to work with Davide whose experience in lightning measuring in Toronto had a considerable contribution to what I have reached in this thesis. Grazie Davide!

I am sincerely grateful to my dear friend and outstanding scientist, Prof. Marcos Rubinstein, for all interesting discussions we have had and his valuable contributions and suggestions to my work. I would like also to thank Marcos for having accepted to be among the experts of the jury for the final examination of my thesis.

¹ The Electromagnetic Compatibility (EMC) group was part of the Power Systems laboratory (LRE) until 2009. It became a separate entity (EMC Laboratory) in 2010.

My sincere gratitude goes equally to my Austrian colleagues in Austrian Lightning Detection and Information System (ALDIS-OVE), Dr. Gerhard Diendorfer, Hannes Pichler, and Dr. Wolfgang Schulz for their continues support, valuable collaboration and interesting discussions during and after the measurement campaign in Salzburg, Austria. I am also thankful to Mrs. Petra Pohl-Fakler, secretary of ALDIS, for her kind hospitality during my short visit in ALDIS in March 2009.

Special thanks are addressed to my colleague and dear friend, Dr. Abdolhamid Shoory, for all the interest he expressed and his valuable support and pertinent advises throughout my work. Thanks Hamid!

I would like to express my sincere thanks to Prof. Rajeev Tottappillil of the Royal Institute of Technology (KTH), Sweden, Prof. Anja Skrivervik Favre of the Laboratory of Electromagnetics and Acoustic (LEMA) of the EPFL, and Dr. Rachid Cherkaoui, for having accepted to be part of the jury for the final examination of my thesis, and for the interest they showed in my work through their interesting questions and suggestions. I am in particular grateful to Rajeev for all the opportunities offered to me by the European COST Action P18 (The Physics of Lightning Flash and Its Effects), chaired by him.

I am especially thankful to Dr. Pierre Zweiacker for sharing his valuable laboratorial experience and contribution to lightning measurement campaigns as well as his kind assistance in revising the French abstract of the thesis.

I would like to address my sincere thanks to Profs. Rouzbeh Moini and Hesamedin Sadeghi my supervisors during my Master's project at AUT for their constant help, support and encouragement, in particular when I was offered the opportunity to continue my studies in Switzerland.

Throughout my professional career I had the opportunity to discuss with numerous members of lightning research community. I am in particular thankful to Prof. Vladimir Rakov (University of Florida, US), Prof. Carlo Alberto Nucci (University of Bologna, Italy), Prof. Mario Paolone (University of Bologna, Italy), Prof. Volodymyr Shostak (Kyiv Polytechnic Institute), Prof. Yoshihio Baba (Doshisha University, Japan), Prof. Akihiro Ametani

(Doshisha University, Japan), Dr. Nelson Theethayi (Bombardier Transportation, Sweden AB), Prof. Alexandre Piantini (University of São Paulo, Brazil), Eric Montandon (EMC Consulting, Worb, Switzerland), and Dr. Célio Barbosa (Centro de Pesquisa e Desenvolvimento em Telecomunicações, Brazil).

This study has been carried out within the framework of the European COST Action P18. Financial support from the Swiss Office for Education and Research SER (grant C05.0149), the Swiss National Science Foundation (project 200021-122457), and Armasuisse Research and Technology is acknowledged. I am sincerely and profoundly grateful to these institutions for the provided support. Thanks are also due to Markus Nyffeler for his interest and support.

I am deeply grateful to Mrs. Andrée Moinat, secretary of the Laboratory, for all her sympathy, support and interesting linguistic discussions. Merci Andrée!

My sincere gratitude equally goes to all of my colleagues not mentioned above, Prof. Michel Ianoz, Simon Cottier, Dr. Abdenabi Mimouni, Dr. Keyhan Sheshyekani, Dr. Abraham Rubinstein, Carlos Romero, Nicolas Mora, Felix Vega, Birgit Meyer, Roxanne Wuilloud, Dr. Ana Vukicevic, Pooyan Manoochehrnia, Isabel Nzazi, Dr. Elena Vdovina-Beck, Dr. Elvira Kaegi, Sylvian Wenger, Ali Ahmadi Khatir, Omid Alizadeh Mousavi, Vivien Etard, Alexander Smorgonskiy, Jean-Michel Buemi, Lazar Bizumic, Anna Arestova, Mathilde Brocard, as well as the former colleagues I had the privilege to meet: Dr. José-Luis Bermudez and Dr. Emmanuel Petrache. Thanks for all interesting discussions, and fantastic memories we shared together.

I shall be forever grateful to my parents for the education I received and my family for all their support and encouragement.

Contents

Résumé:	i
Abstract:	vii
Acknowledgements:	xi
Chapter 1: Introduction	1
1.1 Organization of thesis	2
Chapter 2: Lightning to Tall Structures: State of the Art	5
2.1 Introduction	5
2.2 Modeling Lightning Strikes to Tall Structures	6
2.2.1 Engineering Models	6
2.2.2 Electromagnetic Models	13
2.2.3 Hybrid Electromagnetic Circuit Model (HECM)	17
2.3 Electromagnetic field computation	17
2.3.1 Electromagnetic field expressions for a perfectly conducting ground	18
2.3.2 Electromagnetic field computation for a finitely conducting ground	24
2.4 Experiments	28
2.4.1 Measurements of lightning current	28
2.4.2 Measurements of lightning electromagnetic fields from tall towers	30
2.5 Conclusions	33
Chapter 3: Characteristics of Very Close Electromagnetic Fields in the Vicinity of a Tall Struck Object	35
3.1 Introduction	35
3.2 Theory and adopted model	36
3.3 Considered configurations, channel-base current and return-stroke model	37
3.4 Simulation results and discussion	38
3.4.1 168-m tall tower	38
3.4.2 553-m tall tower	39
3.5 Theoretical explanation for the inversion of polarity	40
3.5.1 Explanation using general field equations	40
3.5.2 Explanation using the formula derived by Baba and Rakov [35]	43
3.6 Sensitivity of the polarity inversion to different parameters	44
3.6.1 Return-stroke speed	44

3.6.2 Reflection coefficients.....	45
3.6.3 Shadowing effect of the tower	46
3.6.4 Return-stroke models	47
3.7 Summary and conclusions.....	48
Chapter 4: Radiated Fields from Lightning Strikes to Tall Structures: Effect of Upward Connecting Leader and Reflections at the Return Stroke Wavefront	51
4.1 Introduction	51
4.2 Proposed Model.....	53
4.3 Simulation and comparison with experimental data of Pavanello et al. [110].....	56
4.3.1 Current.....	57
4.3.2 Magnetic Field.....	60
4.4 Conclusions	64
Chapter 5: Lightning Electromagnetic Fields at Very Close Distances Associated with Lightning Strikes to the Gaisberg Tower in Austria	67
5.1 Introduction	67
5.2 Experimental setup.....	69
5.2.1 Gaisberg Tower	69
5.2.2 Current Measurement System	69
5.3 Presentation of experimental data	70
5.4 Data analysis	71
5.4.1 Magnetic fields.....	74
5.4.2 Vertical Electric fields.....	77
5.4.3 Radial Electric Fields	85
5.5 Test of Electromagnetic and Engineering Models for the Return Stroke	89
5.5.1 Channel-Base Current	89
5.5.2 Antenna Theory Model (AT)	90
5.5.3 Engineering Models	92
5.5.4 Simulation Results and Comparison with Experimental Data	92
5.6 Summary and Conclusions.....	96
5.7 Appendix	98
Chapter 6: Effect of Nearby Buildings on Electromagnetic Fields from Lightning	101
6.1 Introduction	101
6.2 Considered configurations and simulation parameters	102
6.3 Experimental results.....	105

6.3.1 Setup One	105
6.3.2 Setup Two	108
6.3.3 Setup Three	110
6.4 Simulations.....	112
6.5 Conclusions	114
Chapter 7: Conclusions, Summaries and Perspective	115
7.1 Summary and conclusions.....	115
7.2 Perspectives	120
References	121

Chapter 1

Introduction

The lightning discharge is the first cause of weather-related casualties after flash floods, well above tornadoes and hurricanes (Chapter 19 of [1]). It is also well known as a natural source of electromagnetic disturbances. The generated electromagnetic field could cause very costly damages in nearby telecommunication systems and equipment. Thirty to sixty percent of all power outages annually are lightning-related [2]. The evaluation of lightning electromagnetic effects and the design of an efficient protection system require a good knowledge of the phenomenon and an accurate estimation of the radiated electromagnetic fields. However, lightning occurrence is nearly unpredictable and its experimental characterization is quite a challenging task.

The lightning current is certainly one of the most significant parameters to be determined for all the studies on the electromagnetic effects of lightning. It is worth noting that this current can only be measured at the base of the channel and the use of models is needed to predict the current spatial-temporal distribution along the channel. Tall structures or elevated objects located in urban areas or in countryside -particularly on mountain tops- are interesting means to measure lightning currents because they are often struck by lightning. Indeed, most of the available data on lightning currents are obtained using instrumented towers.

Lightning initiated by tall strike-objects has attracted considerable attention of lightning researchers lately (e.g. [3-5]). Many lightning measurements including current and associated electromagnetic fields have been made all over the globe namely in Russia [4], South Africa

[6-7], Germany [8], Brazil [9], Japan [10], and Austria [11]. It is a novel area of studies, and the resolution of associated questions will have an impact upon many lightning-related applications such as lightning protection and the determination of lightning parameters from remote field measurements.

The main objective of the thesis is to carry out further theoretical investigations and experimental measurements to understand and elucidate recently raised questions [5] on the characteristics of lightning return-strokes to tall structures and their associated electromagnetic radiation.

1.1 Organization of thesis

Chapter 2 presents a review on recent progress in the modeling of lightning strikes to tall towers and associated experimental data obtained during the last decade or so. Two types of return stroke models namely the Engineering Models, and the Electromagnetic or Antenna-Theory (AT) models, extended to take into account the presence of a tall strike object are discussed. The Chapter contains also a description of the computational methods for the evaluation of electromagnetic fields generated by a lightning strike to a tall structure, as well as an overview of available data on lightning current and associated electromagnetic fields.

Chapter 3 presents a theoretical description of the signature of electric and magnetic fields at very close distance associated with lightning strikes to a tower. It is shown that the electric field generated by a lightning return stroke to a tall structure can change polarity at very close distance range. This change in the polarity seems to be a specific signature of the very close vertical electric field. Two different theoretical explanations of such an inversion of polarity are given. In addition, a simple equation is derived which provides an estimate of the critical distance below which such an inversion of polarity might occur. The dependence of such an inversion of polarity on the value of the reflection coefficients at the base and top of the tower as well as other parameters such as the return stroke speed, and the adopted return stroke model are analyzed and discussed.

Chapter 4 introduces an improved model for a lightning return stroke to tall structures that takes into account the presence of possible reflections at the return stroke wavefront and the presence of an upward connecting leader. Closed-form, iterative solutions for the current

distribution along the channel and the strike object are derived. Simulation results for the magnetic fields are compared with experimental waveforms associated with lightning strikes to the CN Tower (553 m tall).

Chapter 5 presents and discusses measurements of electric (vertical and radial) and magnetic fields from leaders and return strokes associated with lightning strikes to the 100 m tall Gaisberg tower in Austria obtained in 2007 and 2008. The fields were measured at a distance of about 20 m from the tower. Simultaneously, return stroke currents were also measured at the top of the tower. The data include, for the first time at such close distances, simultaneous records of vertical and horizontal electric fields.

The statistical parameters of the vertical and radial (horizontal) electric field changes due to the downward leader and the return stroke are presented and discussed. The obtained data are compared with available measurements obtained using triggered lightning and possible effects of the tower on the electromagnetic field signature are discussed. Finally, the ability of different lightning return stroke models in reproducing measured vertical and horizontal electric fields are tested using the obtained measured data.

Chapter 6 presents an analysis of the effect of nearby buildings on the electric and magnetic fields radiated by lightning. Indeed, sensors used for the measurement of lightning electric and magnetic fields are often placed on top of buildings. Metallic beams and other conducting parts in those structures may cause enhancement or attenuation effects on the measured fields. The chapter describes an experimental campaign during which electric and magnetic fields radiated from distant natural lightning were measured simultaneously on the roof of a building (the Power Systems Laboratory of the Swiss Federal Institute of Technology, Lausanne, Switzerland) and on the ground at different distances away from it. The possible enhancement or reduction in the electromagnetic fields due the presence of such a building are investigated and discussed. Simulations using the Numerical Electromagnetics Code (NEC-4) in which the building was represented using a simple wire-grid model are also presented and compared with the experimental data.

Finally, the conclusions of this study as well as proposed future work are presented in **Chapter 7**.

Chapter 2

Lightning to Tall Structures: State of the Art

2.1 Introduction

The lightning discharge is an unpredictable electromagnetic source and therefore its experimental characterization is quite a complex task. The lightning current is certainly one of the most significant parameters to be determined for all the studies on the electromagnetic effects of lightning. It is worth noting that this current can only be measured at the base of the channel and the use of return-stroke models is needed to predict the current spatial-temporal distribution along the channel. Tall structures or elevated objects located in urban areas or in the countryside -particularly on the mountain's top- are interesting means to measure lightning currents because they are often struck by lightning. Indeed, most of the available data on lightning currents are obtained using instrumented towers. Another technique with which data on lightning current can be obtained is the artificial initiation of lightning using small rockets (Chapter 7 of [1]). However, in this thesis, we will essentially focus on lightning to tall structures and we will not cover data from rocket-triggered lightning.

In this Chapter, we will present a review of recent progress in the analysis of lightning strikes to tall structures. The Chapter is organized as follows. In Section 2.2, we consider the modeling aspect of the problem and we present a review of the extension of lightning return stroke models to include the presence of an elevated strike object. Section 2.3 deals with the computation of electromagnetic fields generated by a lightning strike to a tall structure. A

review of available data on lightning current and associated electromagnetic fields is presented in Section 2.4. Finally, summary and conclusions are given in Section 2.5.

2.2 Modeling Lightning Strikes to Tall Structures²

Some of the return-stroke models, initially developed for the case of return-strokes initiated at ground, were generalized to take into account the presence of a vertically-extended strike object. The presence of an elevated strike object has been included in two classes of return-stroke models, namely the engineering models and the electromagnetic or Antenna-Theory (AT) models, as defined by Rakov and Uman [12]. In the engineering return-stroke models, the spatial and temporal distribution of the channel current is specified based on observed characteristics such as the channel-base current, return-stroke speed and remote electromagnetic fields. The presence of an elevated strike object in such models has been considered by assuming the object as a uniform, lossless transmission line (e.g. [13]). In Antenna-Theory-type models (e.g. [14-17]) known as AT models, the strike object and the lightning channel are represented using thin wires. Maxwell's equations are numerically solved using the Method of Moments (MoM) [18] to find the current distribution along the lightning channel, from which the radiated electromagnetic fields can be computed. Spatial and temporal current data out of electromagnetic and engineering models can be further used for computing electromagnetic fields. Beside electromagnetic and engineering models, the so-called Hybrid Electromagnetic Circuit Model (HECM) could be considered as a third class of models based on electromagnetic and circuit theory (e.g. [19-20]).

2.2.1 Engineering Models

To analyze the interaction of lightning with tall strike objects, some of the engineering return-stroke models, initially developed for the case of return-strokes initiated at ground, were extended to take into account the presence of a vertically-extended strike object e.g., [3, 22-35]. In some of these models, it is assumed that a current pulse $i_o(t)$ associated with the return-stroke process is injected at the lightning attachment point both into the strike object and into the lightning channel, e.g., [3, 23, 26-32, 36]. The upward-moving wave propagates along the channel at the return-stroke speed v as specified by the return-stroke model. The downward-

² This Section is heavily drawn from [5].

moving wave propagates at the speed of light along the strike object, assumed to be a lossless uniform transmission line characterized by constant non-zero reflection coefficients at its top and its bottom. As noted in [24], the assumption of two identical current waves injected into the lightning channel and into the strike object implies that their characteristic impedances are equal to each other. This assumption makes the models not self-consistent in that there is no impedance discontinuity at the tower top at the time of the lightning attachment to the tower, but there is one when the reflections from ground arrive at the tower top.

2.2.1.1 Extension of engineering models based on a distributed source representation

Rachidi et al. [13] presented an extension of the so-called engineering return-stroke models, taking into account the presence of a vertically-extended strike object, which does not employ the assumption that identical current pulses are launched both upward and downward from the object top. The extension is based on a distributed-source representation of the return-stroke channel [37-38], which allows more general and straightforward formulations of these models than the traditional representations implying a lumped current source at the bottom of the channel.

The general equations for the spatial-temporal distribution of the current along the lightning channel and along the strike object have been derived in [13]:

$$i(z', t) = \left[P(z' - h) i_o \left(h, t - \frac{z' - h}{v^*} \right) - \rho_t i_o \left(h, t - \frac{z' - h}{c} \right) \right. \\ \left. + (1 - \rho_t)(1 + \rho_t) \sum_{n=0}^{\infty} \rho_g^{n+1} \rho_t^n i_o \left(h, t - \frac{h + z'}{c} - \frac{2nh}{c} \right) \right] u \left(t - \frac{z' - h}{v} \right) \quad (2.1)$$

for $h < z' < H_0$

$$i(z', t) = (1 - \rho_t) \sum_{n=0}^{\infty} \left[\rho_t^n \rho_g^n i_o \left(h, t - \frac{h - z'}{c} - \frac{2nh}{c} \right) + \rho_t^n \rho_g^{n+1} i_o \left(h, t - \frac{h + z'}{c} - \frac{2nh}{c} \right) \right] \quad (2.2)$$

for $0 \leq z' \leq h$

where h is the height of the tower, ρ_t and ρ_g are the top and bottom current reflection coefficients for upward and downward propagating waves, respectively, given by

$$\rho_t = \frac{Z_t - Z_{ch}}{Z_t + Z_{ch}} \quad (2.3)$$

$$\rho_g = \frac{Z_t - Z_g}{Z_t + Z_g} \quad (2.4)$$

H_0 is the height of the extending return-stroke channel, c is the speed of light, $P(z')$ is a model-dependent attenuation function, $u(t)$ the Heaviside unit-step function, v is the return-stroke front speed, and v^* is the current-wave speed. Expressions for $P(z')$ and v^* for some of the most commonly used return-stroke models are summarized in Table 2.1, in which λ is the attenuation height for the MTLE model and H_{tot} is the total height of the lightning channel.

Table 2.1 $P(z')$ and v^* for different return-stroke models (Adapted from [12]).

Model	$P(z')$	v^*
BG	1	∞
TCS	1	$-c$
TL	1	v
MTLL	$1-z'/H_{tot}$	v
MTLE	$\exp(-z'/\lambda)$	v

Equations (2.1) and (2.2) are based on the concept of ‘undisturbed current’ $i_o(t)$, which represents the ‘ideal’ current that would be measured at the tower top if the current reflection coefficients at its both extremities were equal to zero.

It is assumed that the current reflection coefficients ρ_t and ρ_g are constant. In addition, any upward connecting leader and any reflections at the return-stroke wavefront [30] are disregarded.

2.2.1.2 Extension of engineering models based on a lumped series voltage source

Baba and Rakov [35, 39] proposed an alternative approach to Rachidi et al.’s distributed source representation [13], using a lumped series voltage source at the junction point between the channel and the strike object. They showed that such a representation ensures appropriate boundary conditions at the attachment point and is equivalent to the distributed source representation [39]. In their representation, Baba and Rakov expressed the spatial-temporal distribution of the current along the strike object and along the channel in terms of the short-circuit current $i_{sc}(t)$, which is related to the undisturbed current through

$$i_{sc}(t) = 2i_o(t) \quad (2.5)$$

Furthermore, in [39], Baba and Rakov considered in their expressions a different speed v_{ref} for the upward propagating current waves reflected from the ground and then transmitted into the lightning channel.

Note that an equivalent representation in terms of the so-called reference current – the current that would flow through the return-stroke channel in the absence of the elevated struck object – has also been proposed by Shigihara and Piantini ([40]).

2.2.1.3 On the representation of the elevated strike object

In all engineering models, the elevated strike object is modeled as an ideal transmission line. To include the structural nonuniformities of the elevated strike object, several transmission line sections in cascade have also been considered (e.g. [25, 41]). The transmission line representation of the elevated strike object has been shown to yield reasonable results in comparison with experimental data. However, one should bear in mind that experimental data associated with lightning to tall structures are ‘affected’ by other, less-easily controlled factors such as the variability of lightning channel impedance and possible reflections at the return-stroke wavefront [42]. In [43], Bermudez et al. presented an experimental validation of the transmission line representation of an elevated object struck by lightning. The experimental results were obtained using a reduced-scale model and injected signals with narrow pulse widths (down to 500 ps). The validation is performed using a reduced scale structure representing the Toronto CN Tower in Canada. Two models consisting, respectively, of 1-section and 3-section uniform transmission lines were considered for the comparison. It was shown that the 3-section model is able to accurately reproduce the obtained experimental data. The overall agreement between the 1-section model and the experimental results was also satisfactory, at least for the early-time response.

More recently, FDTD simulations performed by Baba and Rakov [44] and confirmed by Shoory et al. [45] suggest that the waveguide properties of a conical tower above ground depend on the direction of propagation. Precisely, while the current pulses suffer no attenuation while traveling from the tower apex to its base, the attenuation is significant when pulses propagate from the base to the apex [44]. This finding might render questionable the validity of reflection coefficients at ground level inferred from the measurements of the current at the top of the tower.

2.2.1.4 Current distribution along the channel as predicted by engineering models

Pavanello et al. [46] compared the spatial-temporal distribution of the current predicted by engineering models, employing an undisturbed current $i_o(t)$, given by

$$i_o(h,t) = \frac{I_{o1}}{\eta} \frac{(t/\tau_1)^2}{1+(t/\tau_1)^2} e^{(-t/\tau_2)} + I_{o2} (e^{-t/\tau_3} - e^{-t/\tau_4}) \quad (2.6)$$

This undisturbed current is shown in Fig. 2.1, where the values of the parameters chosen are: $I_{o1} = 9.9$ kA, $\eta = 0.845$, $\tau_1 = 0.072$ μ s, $\tau_2 = 5.0$ μ s, $I_{o2} = 7.5$ kA, $\tau_3 = 100.0$ μ s, $\tau_4 = 6.0$ μ s. These values correspond to the channel-base current adopted in [47] to compare ground-initiated lightning return-stroke models. Starting from the same undisturbed current, the spatial-temporal distribution of the current along the channel and along the strike object were calculated for each model.

In the calculation, the elevated strike object was assumed to have a height $h = 168$ m, corresponding to the Peissenberg tower in Germany, and reflection coefficients were set respectively to $\rho_t = -0.53$ and $\rho_g = 0.7$ [8].

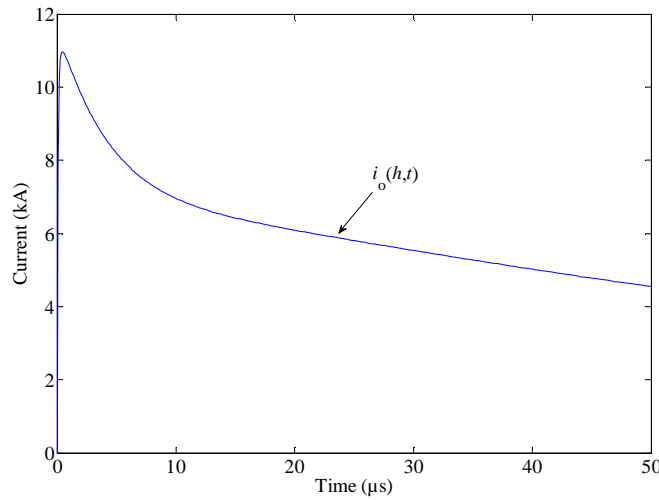


Fig. 2.1 Undisturbed current (Adapted from[46])

Fig 2.2 shows the current distribution along the tower and along the channel, at different time instants ($t = 1, 2, \dots, 10$ μ s), predicted by each model. It can be seen that [46]

- In accordance with (2.2), the current distribution along the tower is independent of the model;
- The BG and TCS models exhibit a strong discontinuity at the return-stroke wavefront, inherent in these models [12]
- Although the vertical scale of Fig. 2.2 does not allow resolution of current variation at the return-stroke wavefront for TL, MTLL and MTLE models, these models have also a

discontinuity at the front. This discontinuity arises from the fact that the current injected into the tower at its top is reflected back and forth at its top and bottom ends, and portions of this current are transmitted into the channel; these transmitted pulses, which are assumed to travel at the speed of light, catch up with the return-stroke wavefront travelling at a lower speed, but not allowed to propagate in the leader channel above the return-stroke front [48].

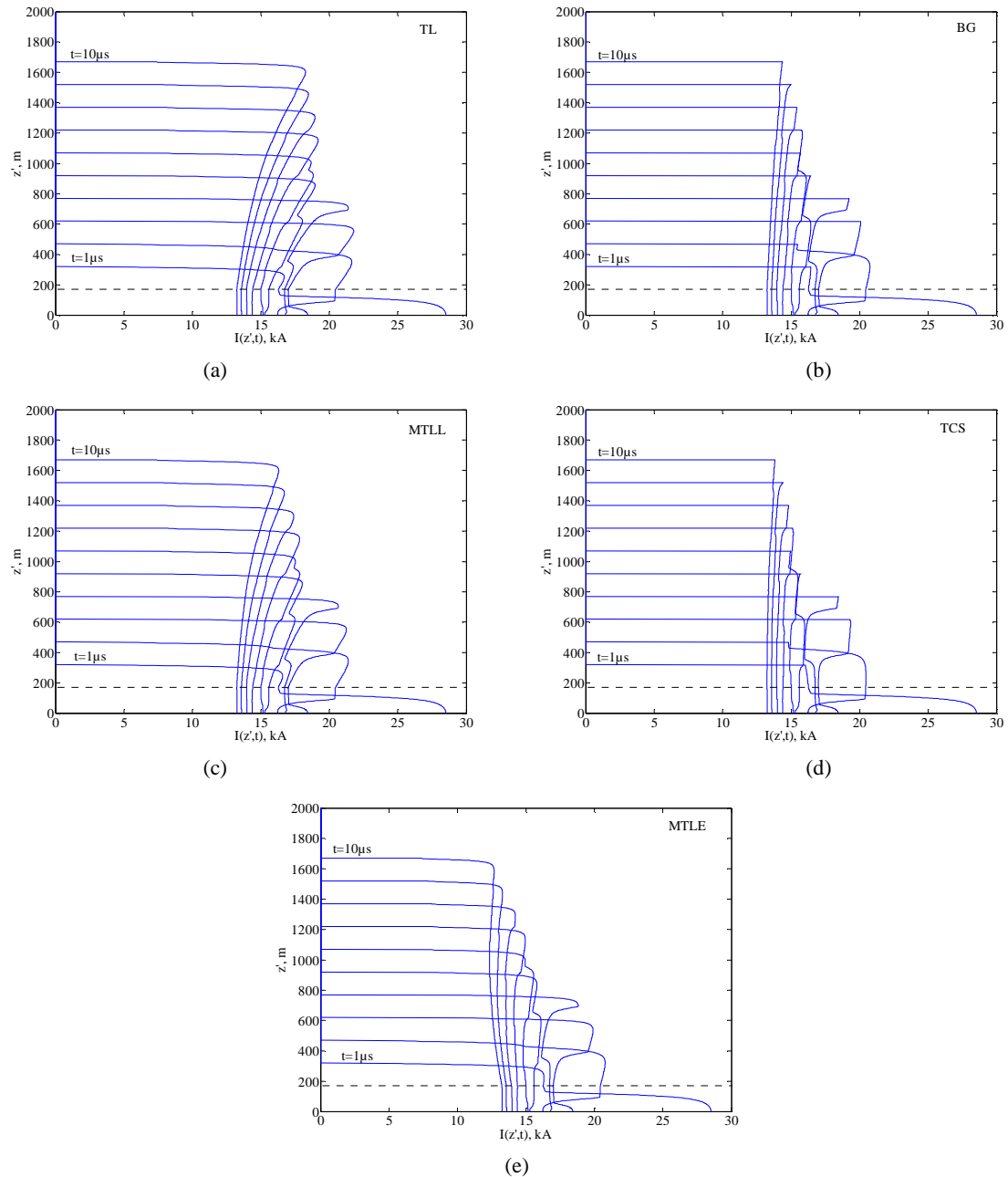


Fig. 2.2 Current (horizontal axis) as a function of height z' (vertical axis) at ten instants of time, $t = 1, 2, \dots, 10 \mu\text{s}$, for five models starting from the same undisturbed current (shown in Fig. 2.1). (a) TL model, (b) BG model, (c) MTL model, (d) TCS model, (e) MTLE model. The horizontal dashed line indicates the height of the tower (168 m). (Adapted from [46])

Fig. 2.3 shows the waveforms of current evaluated at the top (168 m) and the base of the tower (0 m). The effects of the multiple reflections at the tower extremities are clearly visible in the waveforms. It can also be seen that the current at the tower base has a higher peak value due to the contribution from the reflected wave at ground level [46].

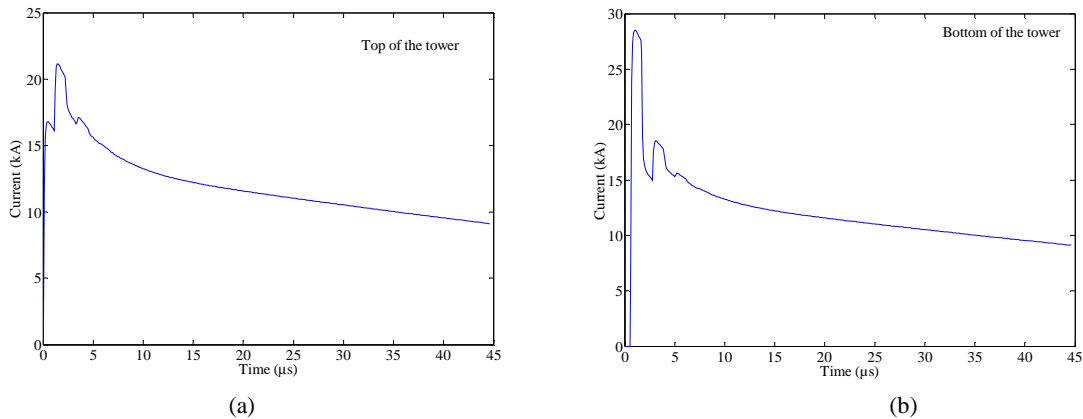


Fig. 2.3 Current at the top (a) and at the bottom (b) of a 168-m tower. (Adapted from [46])

2.2.1.5 Determination of reflection coefficients at the top and the bottom of the strike object

Engineering models require that the reflection coefficients at the top and bottom of the strike object be known. In most of the studies, those coefficients are assumed to be constant and frequency-independent. The values of the reflection coefficients have been inferred by several authors from a limited experimental set of current waveforms found in the literature [49-51]. The knowledge of reflection coefficients is also required to extract the ‘primary’ (or undisturbed) current exempt from the disturbances introduced by the transient processes along the tower. Guerrieri et al. [3] proposed a formula, corrected by Rachidi et al. [13], to extract the undisturbed current. The formula involves an infinite summation in the time domain, assuming that the reflection coefficients are constant and known. Gavric [52] proposed an iterative method based on the Electromagnetic Transient Program (EMTP) to remove superimposed reflections caused by a strike tower from digitally recorded lightning flash currents. Janischewskyj et al. [53] derived reflection coefficients at the CN Tower in Toronto and stated that the values depend on the initial rise time of the measured current, although the limited number of points in their plots render the drawing of conclusions difficult. A dependence on the risetime would suggest that at least one of the reflection coefficients is a function of the frequency. They also proposed a method to extract the reflection coefficients

from the measured current waveform. However, their method is applicable only assuming a simplified current waveform (double ramp) and neglecting any frequency dependence for the reflection coefficients. The last consideration was relaxed in a first approximation by Bermudez et al. [33]. They derive a frequency-domain counterpart of expressions (2.1) and (2.2) which include the frequency-dependence of reflection coefficients. They also derived an expression to calculate the reflection coefficient as a function of the frequency at the bottom of the lightning strike object from two currents measured at different heights along the strike object.

They showed that [33], if the current and its time derivative overlap with reflections at the top or bottom of the strike object, it is impossible to derive the reflection coefficient at the top of the strike object exactly from any number of simultaneous current measurements. They proposed an extrapolation method to estimate this reflection coefficient. The proposed methodology was applied to experimental data obtained on the Peissenberg Tower (Germany) consisting of lightning currents measured at two heights. The obtained results suggest that the reflection coefficient at ground level can be considered as practically constant in the frequency range 100 kHz to 800 kHz [33].

2.2.2 Electromagnetic Models

Electromagnetic models have been widely employed by lightning researchers for investigating lightning strikes to tall structures. An Antenna-Theory-type model was first proposed by Podgorski and Landt in 1985 [14, 54] and it was applied to analyze lightning strikes to the CN Tower. In AT-type models (e.g. [15-17, 55]), the elevated strike object is represented using thin wires and the ground is generally assumed to be perfectly conducting. Very recently, the ground finite conductivity and the buried grounding structure of the tower were included in the analysis [56-57]. The lightning return-stroke channel is modelled as a vertical wire antenna and the lightning return-stroke current is injected by a voltage source at the tip of the tower. The current distribution along the channel and along the tower is found by solving an electric field integral equation [17].

2.2.2.1 Influence of the finite ground conductivity and the buried structure of the tower

Petrache et al. [56-57] employed the Numerical Electromagnetics Code NEC-4 [58], a well-known and widely used computer code based on the Method of Moments for analyzing the

electromagnetic response of antennas and scatterers. Compared to previous NEC versions, such as NEC-2 used by Baba and Ishii [16], NEC-4 is numerically more efficient and can also model wires buried in the ground or penetrating from the air into the ground. Fig. 2.4b illustrates a wire model for the CN tower adopted by Petrache et al. [56]. Compared to previous models used by Podgorski and Landt [14] and by Kordi et al. [17], structural discontinuities are better reproduced in the present model and furthermore, the grounding structure of the tower is also taken into account as it can be seen in the inset of Fig. 2.4b. The buried part is composed of 6 vertical wires, each 15-m long. The ground is characterized by its conductivity σ_g and its relative permittivity ϵ_{rg} , assumed to be constant and frequency-independent. In order to reproduce a return-stroke speed along the lightning channel lower than the speed of light, distributed series inductances and resistances are added to the modeled channel [16]. The adopted values are those suggested by Baba and Ishii [16], namely $3 \mu\text{H/m}$, and $1 \Omega/\text{m}$, respectively. These values correspond to an equivalent return-stroke speed of about half the speed of light. The wire structure representing the tower and the lightning channel were divided into 10-m length segments, whereas the underground structure was divided into 1-m length segments. The voltage source at the top of the strike object is determined by the desired current waveform at the channel-base and by the input impedances of the lightning channel and the tower. The detailed procedure is explained in [59] and [17].

Fig. 2.5 presents two current waveforms associated with return-strokes to the CN Tower, which occurred, respectively, on April 7th and April 11th, 1999 [57]. The currents were measured at a height of 509 m. In the same figures, simulation results for the current obtained using NEC-4.

For computations, the source current waveform was specified using Heidler's functions according to the procedure described by Kordi et al. [17]. Comparisons presented in Fig. 2.8 reveal good agreement between calculated and measured waveforms, especially when the finite ground conductivity is taken into account. In that figure, P.G. stands for perfect ground.

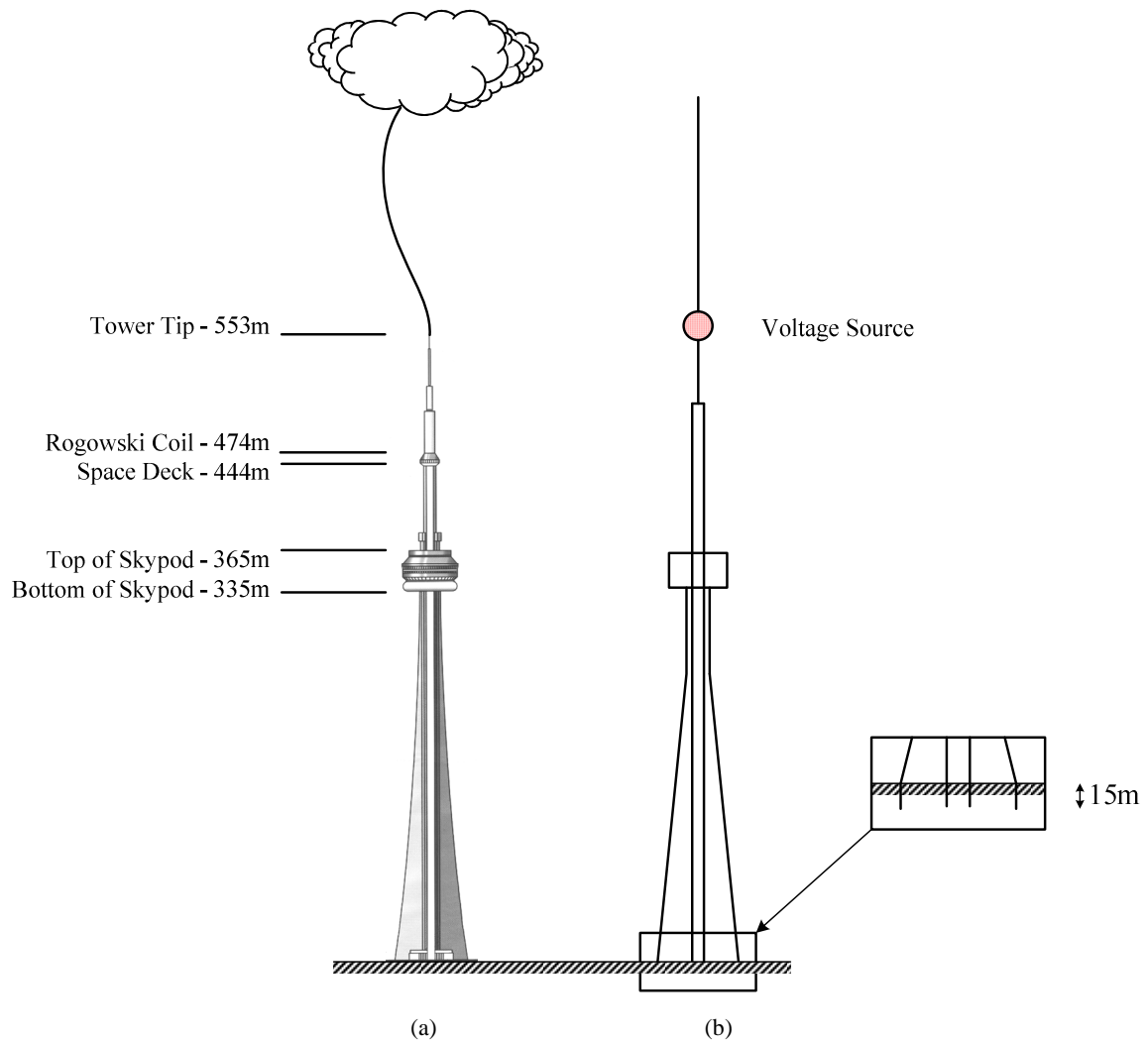


Fig. 2.4 (a) The CN Tower, (b) its wire model including its grounding system. (Adapted from [56])

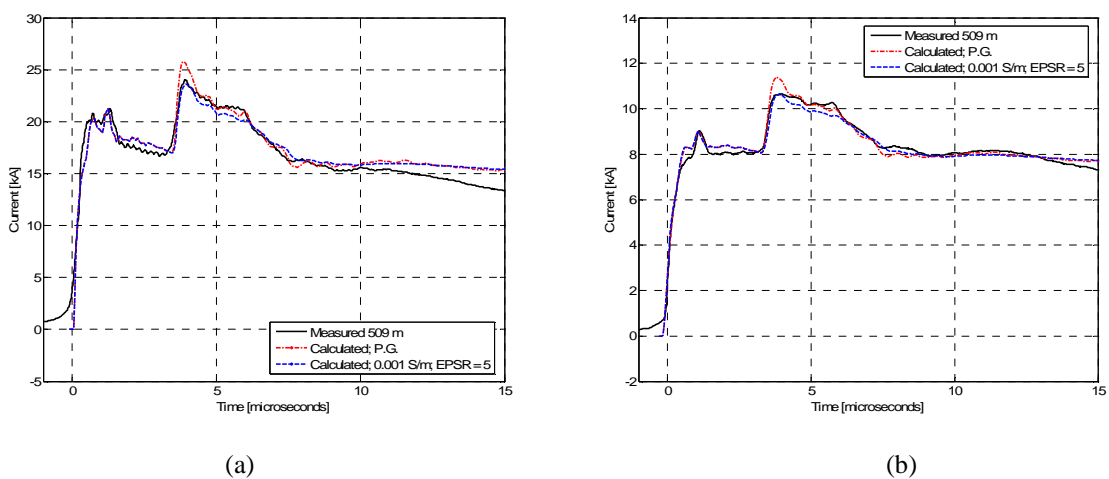


Fig. 2.5 Lightning return-stroke currents at a height of 509 m above ground. The measured current waveforms correspond to events recorded at the CN Tower on: (a) April 7th, 1999, first return-stroke; (b) April 11th, 1999, second return-stroke. P.G. stands for perfect ground. (Adapted from [57])

2.2.2.2 Reflections from the ground and their dependence on ground conductivity

To analyze the influence of the ground conductivity upon the reflection coefficient at ground level, Petrache et al. [57] considered a simpler tower configuration which is shown in Fig. 2.6.

They also considered a narrow-width pulse for the incident current (see Fig. 2.7), so as to determine the reflection coefficient in a straightforward way as proposed by Bermudez et al. [33].

Fig. 2.8 shows the simulations for the current at 509 m above ground level and at ground level [57]. The simulations were carried out for different ground conductivities, namely ∞ (perfect ground), 0.01 S/m and 0.001 S/m. The ground's relative permittivity ϵ_{rg} was assumed to be constant and equal to 10.

From Fig. 2.8, it can be seen that the reflection coefficient at ground level, nearly equal to 1 for a perfectly conducting ground, drops to 0.75 for a ground conductivity of 0.01 S/m and 0.52 for a ground conductivity of 0.001 S/m.

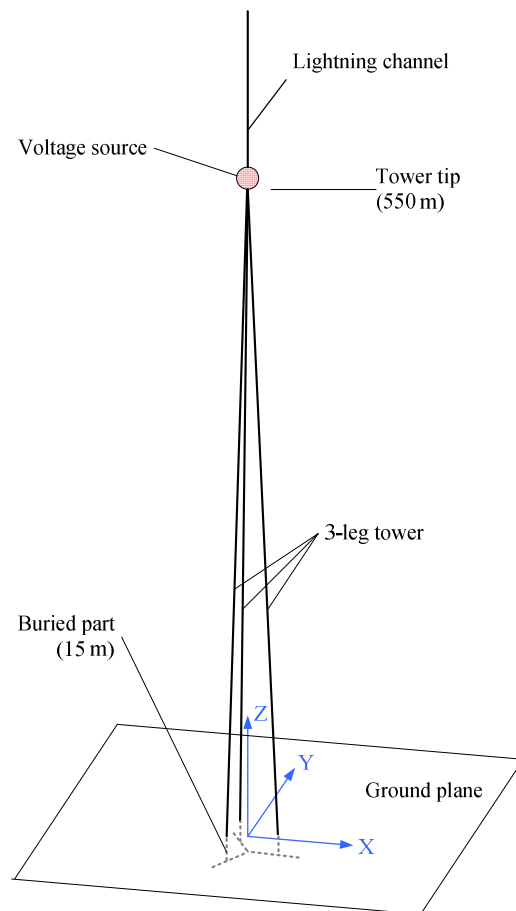


Fig. 2.6 Model of the tower used for the analysis of ground reflections. (Adapted from [57])

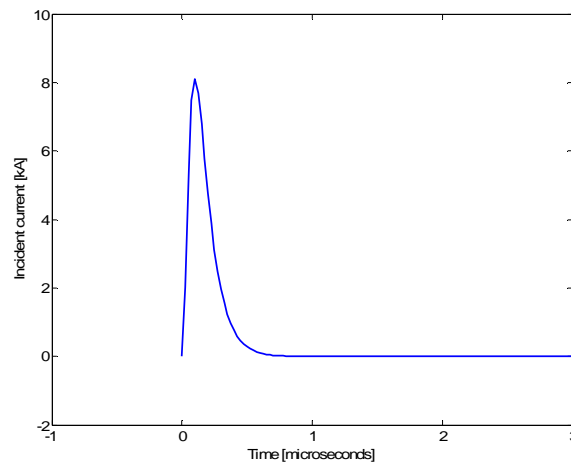


Fig. 2.7 Narrow-width pulse incident current. (Adapted from [57])

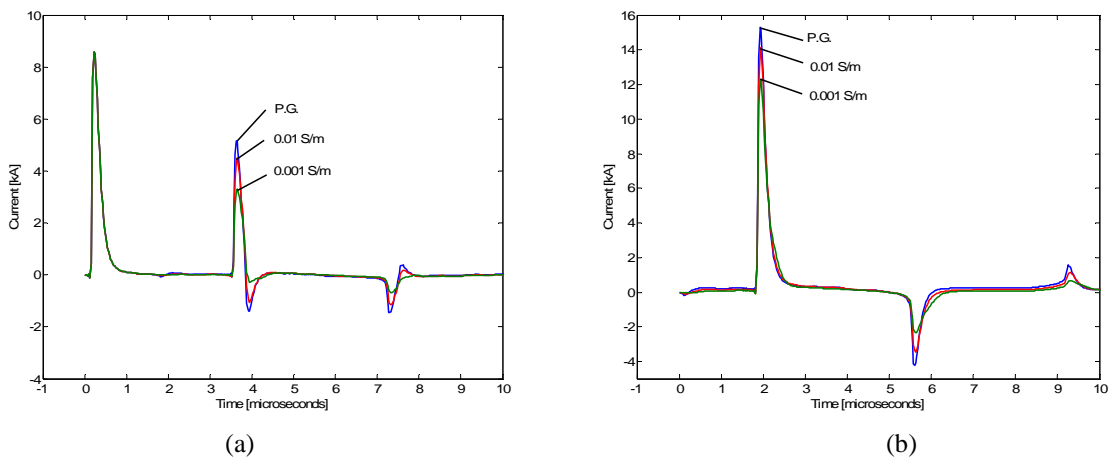


Fig. 2.8 Current at two heights along the tower as a function of the ground conductivity: (a) 509 m, and (b) 0 m (ground level). The incident current is represented in Fig. 2.7. (Adapted from [57])

2.2.3 Hybrid Electromagnetic Circuit Model (HECM)

The so-called Hybrid Electromagnetic Circuit Model (HECM) (e.g. [19-20]) is a combination of electromagnetic and circuit theory models. In this model, the electric scalar and the magnetic vector potentials are employed to take into account electromagnetic coupling, which is represented in terms of circuit quantities, voltages, and currents.

2.3 Electromagnetic field computation

In contrast with electromagnetic models for which the electromagnetic fields are computed simultaneously with the distribution of the current along the radiating structure (strike object and lightning channel), the use of engineering models (which specify the spatial-temporal distribution of the current along the channel and the struck object) require the evaluation of

the associated electromagnetic fields. The calculation procedure essentially depends on the ground electromagnetic properties. When the ground is assumed to be a perfectly conducting plane, image theory can be adopted for the evaluation of the electromagnetic fields. For distances not exceeding several kilometres, the perfect ground assumption is considered to be a reasonable approximation for the vertical component of the electric field and for the azimuthal component of the magnetic field (e.g. [60-61]). Indeed, even for a finitely conducting ground, contributions of the source dipole and of its image (see Fig. 2.9) to these field components add constructively and, consequently, relatively small variations in the image field due to the finite ground conductivity will have little effect on the total field. However, the horizontal (radial) component of the electric field radiated by lightning is appreciably affected by the finite ground conductivity. Indeed, for this field component, the effects of the two contributions subtract, and small changes in the image field may lead to appreciable changes in the total horizontal field. Although the intensity of the horizontal field component is generally much smaller than that of the vertical one, within the context of certain field-to-transmission line coupling models (e.g. [62]), this component plays an important role and thus, its calculation requires the use of the rigorous expressions or at least reasonable approximations of those.

2.3.1 Electromagnetic field expressions for a perfectly conducting ground

According to Eq. (2.1), at a generic height z' along the channel, the current results from the contribution of a series of time-delayed current components. The first one, moving upward at a constant speed v , represents the return-stroke wave front which progressively turns on the distributed current sources [13] by way of which the channel is modeled.

Assuming that no current flow is possible above the return-stroke wave front, the current distribution has to be abruptly cut off at this front [48, 63]. This is mathematically expressed by the Heaviside function present in Eq. (2.1).

All other contributions resulting from multiple reflections at the two ends of the tall structure, are supposed to travel at the speed of light. Because of their higher speed, they catch up with the return-stroke wave front providing a nonzero contribution which leads to a discontinuity if no current is admitted above the front. Notice that this truncation already produces a discontinuity at time $t = 0^+$ since the contribution of the very first distributed

current source in the channel is reflected from the tower top and propagates upward at the speed of light [48].

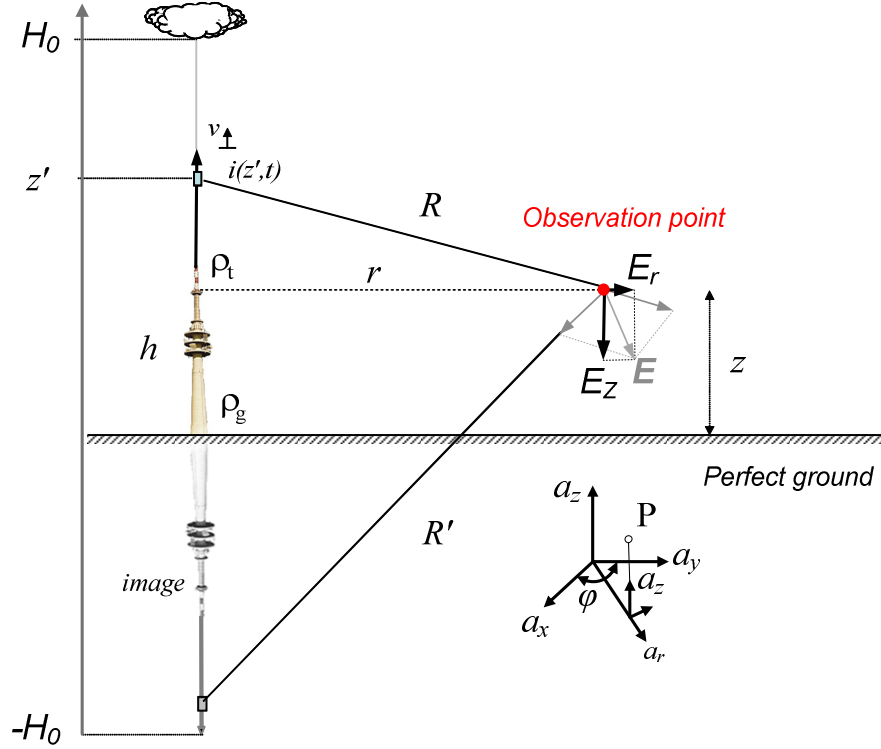


Fig. 2.9 Adopted geometry for field computation [63]

Although such a discontinuity may not be conceivable from a physical point of view, it must still be considered in the analysis for the sake of consistency with the adopted engineering models.

The electromagnetic field contributions from an elemental dipole of current $i(z', t)$ of length dz' located along the vertical axis at z' (see Fig. 2.9) are calculated with the usual expressions valid for a perfectly conducting ground (e.g. [64]):

$$dE_z(r, z, z', t) = \frac{dz'}{4\pi\epsilon_0} \left[\frac{2(z-z')^2 - r^2}{R^5} \int_{R/c}^t i(z', \tau - R/c) d\tau + \frac{2(z-z')^2 - r^2}{cR^4} i(z', t - R/c) - \frac{r^2}{c^2 R^3} \frac{\partial i(z', t - R/c)}{\partial t} \right] \quad (2.7)$$

$$dE_r(r, z, z', t) = \frac{dz'}{4\pi\epsilon_0} \left[\frac{3r(z-z')}{R^5} \int_{R/c}^t i(z', \tau - R/c) d\tau + \frac{3r(z-z')}{cR^4} i(z', t - R/c) + \frac{r(z-z')}{c^2 R^3} \frac{\partial i(z', t - R/c)}{\partial t} \right] \quad (2.8)$$

$$dH_{\varphi}(r, z, z', t) = \frac{dz'}{4\pi} \left[\frac{r}{R^3} i(z', t - R/c) + \frac{r}{cR^2} \frac{\partial i(z', t - R/c)}{\partial t} \right] \quad (2.9)$$

in which

- r, z are the cylindrical coordinates of the observation point,
- R is the distance between the dipole and the observation point, $R = \sqrt{r^2 + (z' - z)^2}$,
- $i(z', t)$ is the dipole current,
- c is the speed of light, and,
- ϵ_0 is the permittivity of free space.

The total electromagnetic fields are calculated by integrating the above equations along the tower-channel and its image, assuming a perfectly-conducting ground.

In the presence of a current discontinuity, the radiation term, namely the last term in each equation, which is proportional to the current time-derivative, introduces a singularity that needs to be treated separately [64-69].

2.3.1.1 Turn-on term

The complete expression of the electromagnetic field is obtained by integrating (2.7) through (2.9) along z' from ground level to the wave front and then by adding the corrective turn-on term across the discontinuity in H , expressed as

$$\int_H f(z', z, r) \frac{\partial i(z', t - R/c)}{\partial t} dz' \quad (2.10)$$

where $f(z', z, r)$ can be r^2/c^2R^3 , $r(z-z)/c^2R^3$ or r/cR^2 , depending on which component of the field is being calculated [48].

The reason why an additional turn-on term must be introduced in the field equations is that the presence of the Heaviside function in Eq. (2.1) cannot be disregarded when the time-derivative of the current is calculated. Its derivative, namely, a delta function, multiplied by the amplitude of the current at the wave front, needs to be added to the radiation term. In the case in which the current distribution presents no discontinuity at the return-stroke wave front, this turn-on term contribution vanishes. The discontinuity can be treated considering a nondiscontinuous current wave front of length $\Delta z''$ which reaches the level I_{front} linearly in a time Δt , and expressing the radiation integral across H taking the limit when the front duration tends to zero [64].

The final expressions for the turn-on term fields, in which the apparent front speed appears as the reciprocal of the term between brackets are given by [48]:

$$H_{\Phi/\text{turn-on}} = \frac{I_{\text{front}}(H) \cdot r}{4\pi cR^2} \cdot \frac{1}{\left[\frac{1}{v} - \frac{(z-H)}{cR} \right]} + \frac{I_{\text{front}}(H') \cdot r}{4\pi cR'^2} \cdot \frac{1}{\left[\frac{1}{v} - \frac{(z-H')}{cR'} \right]} \quad (2.11)$$

$$E_{r/\text{turn-on}} = \frac{I_{\text{front}}(H) \cdot r \cdot (z-H)}{4\pi\epsilon_0 c^2 R^3} \cdot \frac{1}{\left[\frac{1}{v} - \frac{(z-H)}{cR} \right]} - \frac{I_{\text{front}}(H') \cdot r \cdot (z-H')}{4\pi\epsilon_0 c^2 R'^3} \cdot \frac{1}{\left[\frac{1}{v} - \frac{(z-H')}{cR'} \right]} \quad (2.12)$$

$$E_{z/\text{turn-on}} = -\frac{I_{\text{front}}(H) \cdot r^2}{4\pi\epsilon_0 c^2 R^3} \cdot \frac{1}{\left[\frac{1}{v} - \frac{(z-H)}{cR} \right]} - \frac{I_{\text{front}}(H') \cdot r^2}{4\pi\epsilon_0 c^2 R'^3} \cdot \frac{1}{\left[\frac{1}{v} - \frac{(z-H')}{cR'} \right]} \quad (2.13)$$

In equations (2.11)-(2.13), the two terms on the right-hand side represent the turn-on term due to the discontinuity at the wavefront and at its image, respectively.

The general expression for the current at the wavefront is simply obtained from Eq. (2.1) in which the time variable t appears implicitly through H [48]:

$$\begin{aligned} I_{\text{front}}(H) = & P(H-h) i_0 \left(h, \frac{H-h}{v} + \frac{1}{c} \sqrt{r^2 + (H-z)^2} - \frac{H-h}{v^*} \right) \\ & - \rho_i i_0 \left(h, \frac{H-h}{v} + \frac{1}{c} \sqrt{r^2 + (H-z)^2} - \frac{H-h}{c} \right) \\ & + (1-\rho_t)(1+\rho_t) \sum_{n=0}^{\infty} \rho_g^{n+1} \rho_t^n i_0 \left(h, \frac{H-h}{v} + \frac{1}{c} \sqrt{r^2 + (H-z)^2} - \frac{H+h}{c} - \frac{2nh}{c} \right) \end{aligned} \quad (2.14)$$

It is worth to observe that the first term on the right-hand side of Eq. (2.14) is nonzero only for the BG and TCS models, and it corresponds to the inherent discontinuity predicted by these two models. This means, by consequence, that the turn-on term has the same expression for the TL, MTLL and MTLE models [48].

The contribution of the turn-on term to the total field depends on many factors such as the height of the tower, the reflection coefficients at its extremities, the return-stroke speed and the position of the observation point (distance and elevation). Pavanello et al. [48] found that the contribution of the turn on term to the total electric and magnetic fields is negligible at close distances (below 100 m) and increases rapidly to reach an asymptotic value of about 12% at a distance of 5 km and beyond. At these distances, the field peak is essentially due to the radiation term.

2.3.1.2 Comparison between different engineering models

Pavanello et al. [46] compared five engineering models (BG, TCS, TL, MTLL and MTLE) employing the same undisturbed current $i_o(t)$, presented in Fig. 2.1. The elevated strike object was assumed to have a height $h = 168$ m, corresponding to the Peissenberg tower in Germany. The reflection coefficients were set respectively to $\rho_t = -0.53$ and $\rho_g = 0.7$ [8].

Fig. 2.10 presents electric and magnetic fields calculated at a distance of 50 m from the tower base [46]. At this distance, the electric field is dominated (at later times) by its electrostatic term. The model- predicted electric fields are very similar for the first 5 μ s, beyond which the BG, TCS and MTLL models predict the flattening of the field, typically observed at close distances, while the TL model predicts a field decay. The late-time E-field predicted by the MTLE model exhibits a ramp, as in the case of a ground-initiated return-stroke [46]. Note, however, that a judicious choice of the attenuation factor would result in the flattening of the late-time E-field at close range [70].

Fig. 2.10b shows that the predicted magnetic field is nearly model-independent. At this distance, the magnetic field is dominated by its induction term, and its waveshape is similar to the current at the base of the tower shown in Fig. 2.3b.

Fig. 2.11 presents calculated electric and magnetic fields at a distance of 5 km [46]. The electric and magnetic field waveshapes for the first 5 μ s are dominated by the radiation term and hence they are very similar. No significant differences are found between the various models in this early-time region. The differences between the model predictions become more pronounced at late times, $t > 5$ μ s or so, although they are unremarkable. Note that all the models predict a flattening of the electric field at later times at a value that is significantly smaller than the initial peak, in contrast with calculated electric fields for ground-initiated return-strokes (see, for example, Fig. 12 of [47]).

The electric and magnetic fields at a distance of 100 km are plotted in Fig. 2.12 [46]. At this distance, the fields are essentially radiation fields, and electric and magnetic fields have the same waveshape. The fields associated with ground-initiated return-strokes at such distances exhibit a zero-crossing which is only reproduced by the MTLE and MTLL models [12, 47]. As seen in Fig. 2.12, for the considered case of a 168-m tower-initiated return-stroke, none of the models predicts a zero-crossing. The absence of zero-crossing, in particular for the MTLE and MTLL models, can be explained by the contribution of the turn-on term [48].

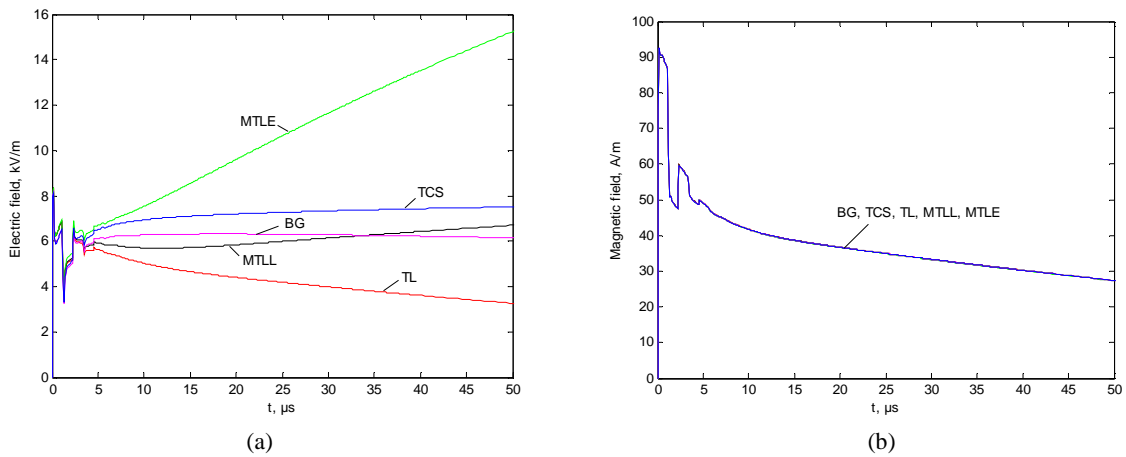


Fig. 2.10 Electric (a) and magnetic (b) fields calculated at a distance of 50 m from a lightning return-stroke to a 168-m tower. (Adapted from [46])

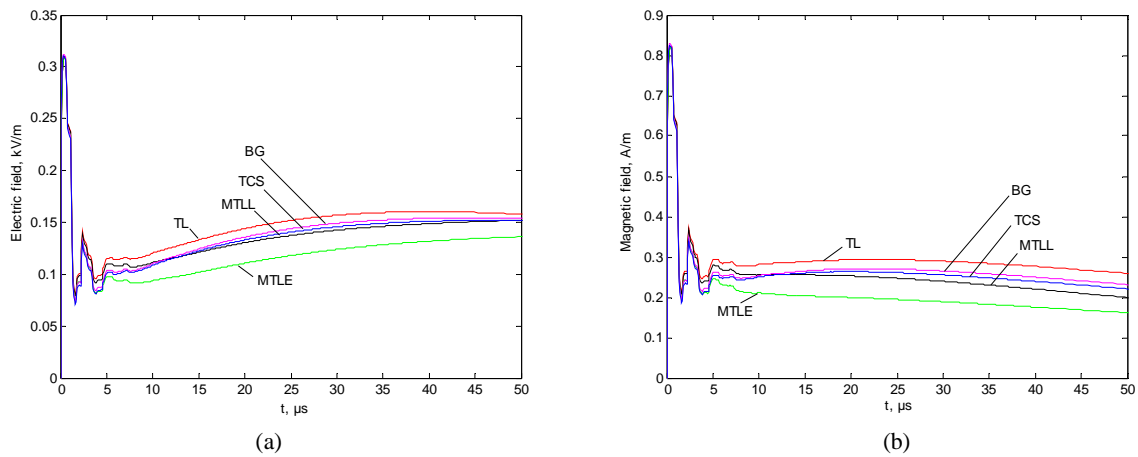


Fig. 2.11 Electric (a) and magnetic (b) fields calculated at a distance of 5 km from a lightning return-stroke to a 168-m tower. (Adapted from [46])

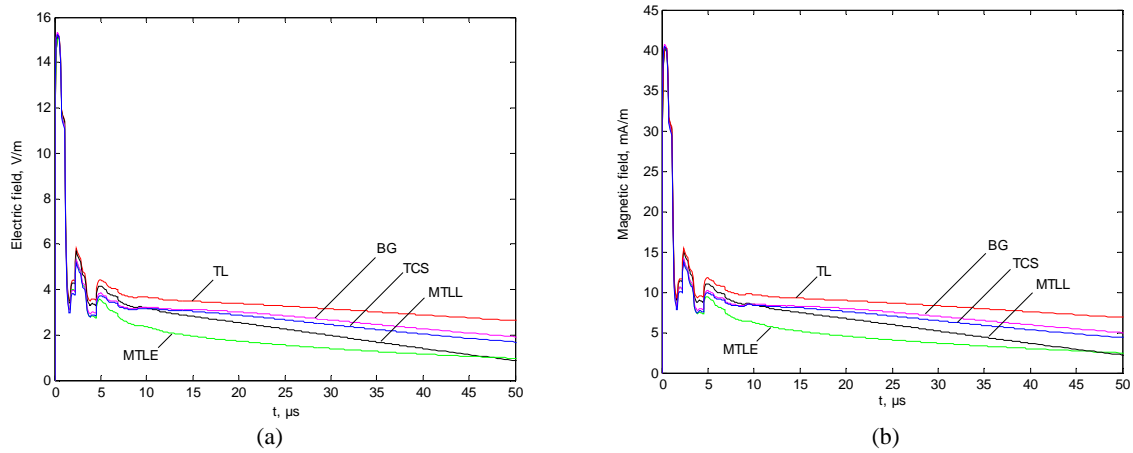


Fig. 2.12 Electric (a) and magnetic (b) fields calculated at a distance of 100 km from a lightning return-stroke to a 168-m tower. (Adapted from [46])

2.3.1.3 Propagation effects

The effect of the finite conductivity of the ground on the amplitude and waveshape of electromagnetic fields radiated by lightning return-strokes to tall towers was recently investigated in [71]. The study was based on the engineering return-stroke models extended to take into account the presence of a vertically-extended strike object. In [71], the propagation along a finitely-conducting ground is taken into account using Cooray's approach [72]. Simulations were presented for a homogeneous ground and considering three cases: (1) a return-stroke initiated at ground level, (2) a return-stroke to a 168-m tall tower corresponding to the Peissenberg tower, and (3) a return-stroke to a 553-m tall tower corresponding to the CN Tower. It is shown that the propagation along an imperfectly conducting ground causes the amplitude of the field to decrease and its risetime to increase with decreasing ground conductivity. In addition, it was found that some of the fine structure of the electromagnetic field associated with transient processes along the struck tower vanishes due to propagation effects. Simulations presented in [71] revealed also that the enhancement effect of the tower (with respect to a ground-initiated return-stroke) on the peak field, which is considerable for a perfectly conducting ground, tends to become less significant for a lossy ground.

2.3.1.4 Effect of the tower

Based on theoretical modeling and experimental observations, it is well established that the presence of a tower could result in a substantial increase (a factor of 3 or so) of the electric and magnetic field peaks and their derivatives (e.g. [27, 34-35]) for observation points located at distances exceeding the height of the tower.

Interestingly, the effect of the tower at distances of about the height or the tower or less, could result in a significant decrease of the electric field (e.g. [35, 73-74]).

2.3.2 Electromagnetic field computation for a finitely conducting ground

Assuming the lightning channel as a lossless vertical antenna above a finitely conducting ground the associated electromagnetic fields could be basically calculated using three different approaches: 1) use of dedicated algorithms; 2) use of simplified approaches; and 3) use of numerical methods (MoM or FDTD) [21].

2.3.2.1 Dedicated Algorithms

The exact solution of Maxwell's equations due to a vertical dipole located above a finitely conducting ground as discussed in [75] result in the so-called Sommerfeld integral equations [76]. The high oscillatory nature of the Sommerfeld integrals makes it difficult to get the resulting expressions numerically evaluated. Some efforts have been recently made to find an efficient algorithm that could numerically evaluate the resulting expressions. A dedicated algorithm [77-80] has been developed by Delfino and co-workers that could be applied to the both air-ground expressions generated by a lightning discharge.

2.3.2.2 Simplified Approaches

A Cooray-Rubinstein formula (above-ground horizontal electric field)

Several studies have shown that the Cooray-Rubinstein formula [81-82] yields a satisfactory approximation of the above-ground horizontal electric field at close (one hundred meters), intermediate (some kilometers), and far (tens of kilometers) distances (e.g. [61, 81]). In the Cooray-Rubinstein formula the horizontal electric field at a given height, h , is expressed as the sum of two terms. The first term is the horizontal electric field for a perfectly conducting ground and the second term accounts for the effect of a finitely-conducting ground. This formula reads

$$E_r(z=h, r) = E_{rp}(z=h, r) - H_{\phi p}(z=0, r) \frac{\sqrt{\mu_0}}{\sqrt{\epsilon + \sigma/j\omega}} \quad (2.15)$$

where, E_{rp} is the radial electric field calculated at the height, h , and $H_{\phi p}$ the azimuthal magnetic field computed at the ground level, both computed assuming the ground to be a perfect conductor.

Delfino et al. [79] showed that only for very low conductivities, does the Cooray-Rubinstein formula exhibit some deviations from the reference one, but it still gives a conservative estimate of the radial field component, since it behaves as an upper bound for the exact curve. General limits of validity of the Cooray-Rubinstein approximation were theoretically examined by Wait [83]. Shoory et al. [84] presented a general equation for the horizontal electric field, from which the Cooray-Rubinstein formula can be derived as a special case. Cooray [85] further proposed a simple modification of (2.15) that provides a better early time response. Barbosa and Paulino [86] proposed an approximate time-domain formula for the horizontal electric field whose range of validity was stated to be equivalent to that of the

Cooray-Rubinstein formula (which is in the frequency domain). Caligaris et al. [87] mathematically derived the time-domain counterpart of the Cooray-Rubinstein formula.

B Cooray formula (under-ground electric fields)

Use of modern underground power and communication systems over the past few years has resulted in increasing attention to the study of penetrating lightning electromagnetic fields into a finitely conducting ground. The direct use of equations for radiated electromagnetic fields inside the ground [75] from a simple dipole as for the case of above-ground fields, can be very costly in terms of computation time. In [88], Cooray has proposed a simplified formula for the evaluation of underground vertical and horizontal electric fields from lightning. The accuracy of Cooray simplified expression has been further evaluated by Petrache et al. [89] by taking as reference the exact solutions published by Zeddami [90]. Petrache et al. reported a good agreement between the exact and predicted horizontal electric field penetrating the ground at distances as close as 100 m [89]. The predictions of the Cooray's formula were found to be in good agreement with exact solutions for large values of ground conductivity (about 0.01 S/m) [77]. For poor ground conductivities (0.001 S/m or so), Cooray's expression yields less satisfactory results, especially for the late time response [77].

2.3.2.3 Numerical Methods

A Finite Difference Time Domain (FDTD)

Compared with traditional approaches for the evaluation of electromagnetic fields in the vicinity of the lightning channel, the FDTD method has the advantage of being easily implemented in computer codes [91], and, further, the finite ground conductivity is taken into account in a straightforward way. The one-dimensional FDTD method has been widely applied to the analysis of the induced overvoltages on overhead transmission lines by nearby lightning return strokes (e.g., [92]). It is only recently that the method has also been applied to the analysis of lightning electromagnetic fields. Sartori et al. [93] have proposed a hybrid method based partially on the FDTD technique for the near electric field calculation. The magnetic field was first determined analytically, assuming the spatial-temporal distribution of the current in each radiating dipole to be a step function. In 2004, Yang et al. [94] also used FDTD to compute electromagnetic fields in the vicinity of a return stroke. Their FDTD

approach has been used as a reference to test the validity of the quasi-image method and the Cooray-Rubinstein formula.

More recently Mimouni et al. [95-96] calculated the underground electric and magnetic fields for strikes to both flat ground and tall towers, using engineering return-stroke models and the FDTD method. Fig. 2.13 and Fig. 2.14 show simulation results obtained by Mimouni et al. for the evaluation of the underground horizontal electric field which have been compared with those of Delfino et al. [80] as well as the results obtained using the Cooray simplified formula [88].

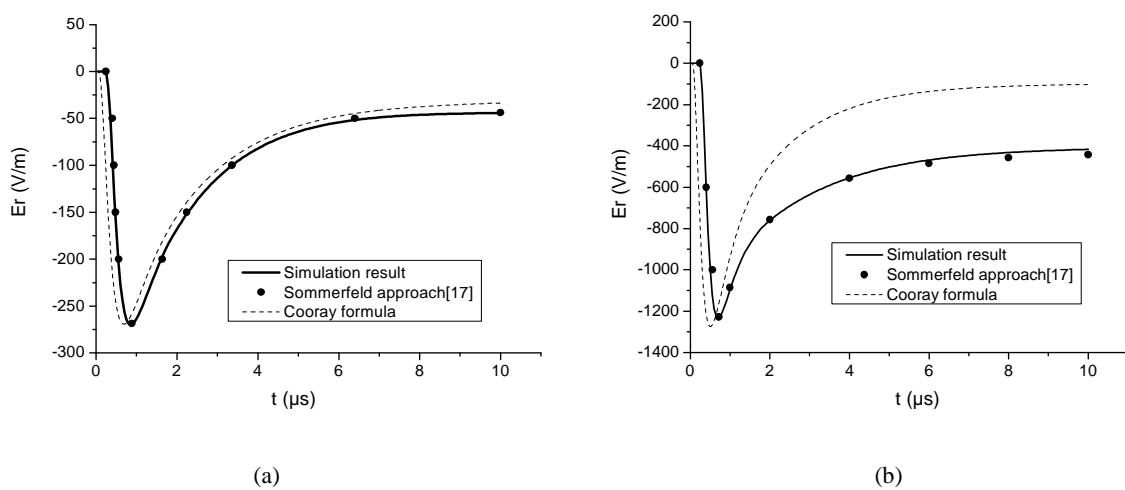


Fig. 2.13 Underground radial electric field ($r = 50$ m, depth $d = 5$ m) for (a) $\sigma = 0.01$ S/m, and (b) $\sigma = 0.001$ S/m lossy ground, compared with Sommerfeld approach and Cooray formula (Adapted from [95]). The results using Sommerfeld approach are from [80].

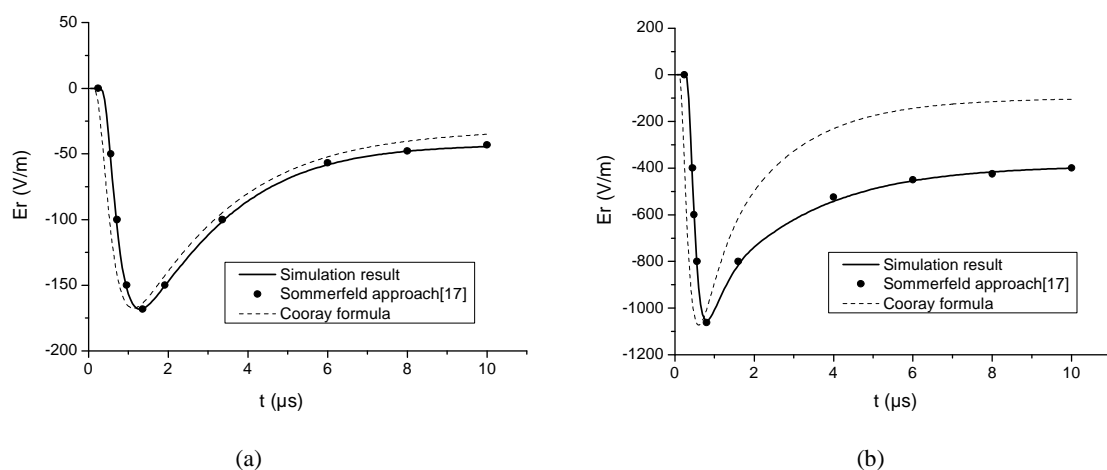


Fig. 2.14 Underground radial electric field ($r = 50$ m, depth $d = 10$ m) for (a) $\sigma = 0.01$ S/m, and (b) $\sigma = 0.001$ S/m lossy ground, compared with Sommerfeld approach and Cooray formula (Adapted from [95]). The results using Sommerfeld approach are from [80].

It can be seen that the FDTD results are in excellent agreement with the exact evaluation of Delfino et al. [80]. The comparisons also show that the results obtained using the Cooray formula are in general in good agreement with more exact solutions, although some discrepancies can be observed for the late-time response of the field and for poor ground conductivities. Similar conclusions have been reported in [80].

Baba and Rakov [44, 97] also used the FDTD method to study the mechanisms of current wave propagation along vertical conductors [97], to reproduce small-scale experiments [44], and to study the enhancement of electromagnetic fields measured on the top of buildings [98].

B Method of Moments (MoM)

The method of moments has also been extensively applied to compute electromagnetic fields radiated by a lightning discharge, within the so-called antenna theory (AT) models, which belong to the class of electromagnetic models and in which the return-stroke channel is represented using thin wires (e.g., [15-17, 54-56, 59, 84]). Most of the MoM solutions are implemented in the frequency domain, which allows taking into account the presence of a lossy ground in a straightforward way.

2.4 Experiments

Two types of lightning observations are reviewed here: (a) recent current measurements on instrumented towers and (b) measurements of radiated electric and magnetic fields from tall towers.

2.4.1 Measurements of lightning current

Traditional lightning parameters needed in engineering applications include lightning peak current, maximum current derivative (di/dt), average current rate of rise, current risetime, current duration, charge transfer, and action integral, all derivable from direct current measurements. Distributions of these parameters presently adopted by most lightning protection standards are based on measurements by K. Berger and co-workers in Switzerland [99]. More recently direct current measurements on instrumented towers were made in Russia, South Africa, Canada, Germany, Brazil, Japan, and Austria. Important results from

the Brazilian, Japanese, and Austrian studies were published during the last decade and will be briefly reviewed³.

2.4.1.1 The Morro do Cachimbo tower, Brazil

Visacro et al. [100] reported statistical parameters of lightning current measurements on the 60-m Morro do Cachimbo tower near Belo Horizonte, Brazil. A total of 31 negative downward flashes containing 80 strokes were recorded during a period of 13 years. Median peak currents for first and subsequent strokes were found to be 45 and 16 kA, respectively, higher than the corresponding values, 30 and 12 kA, reported for 101 flashes containing 236 strokes by Berger et al. [99]. Possible reasons for the discrepancy include a relatively small sample size in Brazil, the dependence of lightning parameters on geographical location (Brazil vs. Switzerland), and different positions of current sensors on the tower at the two locations (bottom of 60-m tower in Brazil vs. top of 70-m tower in Switzerland). For typical first strokes (longer risetimes) the towers in question are expected to behave as electrically short objects, so that the position of current sensor should not influence measurements. On the other hand, for subsequent strokes (shorter risetimes) the towers may exhibit a distributed-circuit behaviour, in which case the peak current measured at the bottom of tower might be influenced in a higher degree by the transient process in the tower compared to the peak current at the top [4, 101-102]. Visacro and Silveira [103], using a hybrid electromagnetic model and assuming a 100-m long upward connecting leader, showed that, for typical subsequent-stroke current risetimes, however, peak currents at the top and bottom of the Morro do Cachimbo tower should be essentially the same.

2.4.1.2 Transmission-line towers, Japan

Takami and Okabe [104] presented measurements of lightning return-stroke currents on 60 transmission-line towers (at the top) whose heights ranged from 40 to 140 m. A total of 120 current waveforms for negative first strokes were obtained from 1994 to 2004. This is the largest sample size for negative first strokes as of today. The median peak current was 29 kA, which is similar to that reported by Berger et al. [99], although the trigger threshold in Japan (9 kA) was higher than in Switzerland. Interestingly, initial data from this Japanese study (for

³ This Section is heavily drawn from [21].

35 negative first strokes recorded in 1994-1997) yielded the median peak current of 39 kA [10].

2.4.1.3 The Gaisberg tower, Austria

Diendorfer et al. [105] analyzed parameters of 457 upward negative flashes initiated from the 100-m Gaisberg tower in 2000-2007. Upward flashes contain only strokes that are similar to subsequent strokes in downward flashes; that is, they do not contain first strokes initiated by downward stepped leaders. Some upward flashes contain no strokes at all, only the so-called initial-stage current. The median return-stroke peak current was 9.2 kA ($n = 615$, the largest sample size as of today).

2.4.1.4 The CN tower, Canada

Studies on lightning striking the 553-m tall Toronto Canadian National (CN) Tower have been performed and reported by the “CN Tower Lightning Studies Group (CNT-LSG)” since 1978 (e.g. [27, 106-108]). Hussein et al. [108] reported the median value of the initial peak of current pulses measured in 1992-2001 at the top of the tower to be 5.1 kA, which is considerably lower than for the Gaisberg-tower return strokes, as well as for subsequent strokes in downward lightning and for strokes in rocket-triggered lightning (e.g., [4]). The discrepancy may be due to inclusion in the Canadian sample of events with current peaks smaller than 1 kA, some of which could be associated with the so-called initial-stage pulses, not with return strokes. Miki et al. [109] presented a detailed characterization of initial-stage pulses in object-initiated (100-m Gaisberg tower, 160-m Peissenberg tower, and 200-m Fukui chimney) and rocket-triggered lightning. The Peissenberg-tower data were further examined by Flache et al. [110].

2.4.2 Measurements of lightning electromagnetic fields from tall towers

Knowledge of the characteristics of electromagnetic fields produced by lightning discharges is needed for studying the coupling of lightning fields to various electrical circuits and systems, as well as sensitive electronic circuits. On the other hand, measured electric and magnetic fields can be used for the indirect estimation of lightning parameters and for testing lightning models.

Bermudez et al. [34] made simultaneous records, gathered during the summers of 2000 and 2001, of the return-stroke current and its associated electric and magnetic fields measured at two distances, namely, 2 km and 16.8 km, related with lightning strikes to the CN Tower.

During the summer of 2005, Pavanello et al. [111] measured the vertical component of the electric field and the azimuthal component of the magnetic field produced by lightning strikes to the CN Tower at three distances, 2.0, 16.8, and 50.9 km, from the tower.

A representative set of simultaneously measured return-stroke current and associated electric and magnetic fields at 2.0 km, 16.8 km, and 50.9 km, respectively, related to the second stroke of a CNT flash on Aug. 19th (14:13:13, Toronto time) is shown in Fig. 2.15 [111]. The current waveform is characterized by an initial peak, considered as the actual value of the return-stroke current injected by lightning on the tower top, followed by a second, higher, peak, due to reflection from ground of the current wave. At 2 km, the electric field is characterized by its initial peak followed by an increasing ramp, and the magnetic field is characterized by an initial peak followed by a hump. These features are in agreement with characteristics of fields at this distance range for direct strikes to ground as reported in [112], although fields associated with strikes to tall structures have a more pronounced initial peak [27, 34]. At 16.8 km and 50.9 km, the electric and magnetic fields are characterized by similar waveforms, typical of distant fields [111]. The waveforms of the electric and magnetic fields at 16.8 km and 50.9 km exhibit a first zero crossing accompanying a narrow undershoot about 5 microseconds after the onset of the return-stroke. For fields at 50.9 km, the expected zero crossing at about 40 microseconds [112] is also observed. The observed early undershoot has been attributed by Pavanello et al. [111] to the transient processes along the tower.

Pavanello et al. [111] compared the measured waveforms with predictions of the five engineering return-stroke models extended to include the presence of the strike object. A reasonable agreement is found for all the models for the magnetic field waveforms at the three considered distances, although the peak values of the computed fields were systematically about 25% lower than measured values [111]. None of the models, however, was able to reproduce the early zero crossing and the narrow undershoot seen in the measured field waveforms. As far as the electric field was concerned, larger differences have been observed between simulations and measurements. These differences were attributed to the enhancement effect of the metallic structures of the buildings on which measuring sensors were located [111].

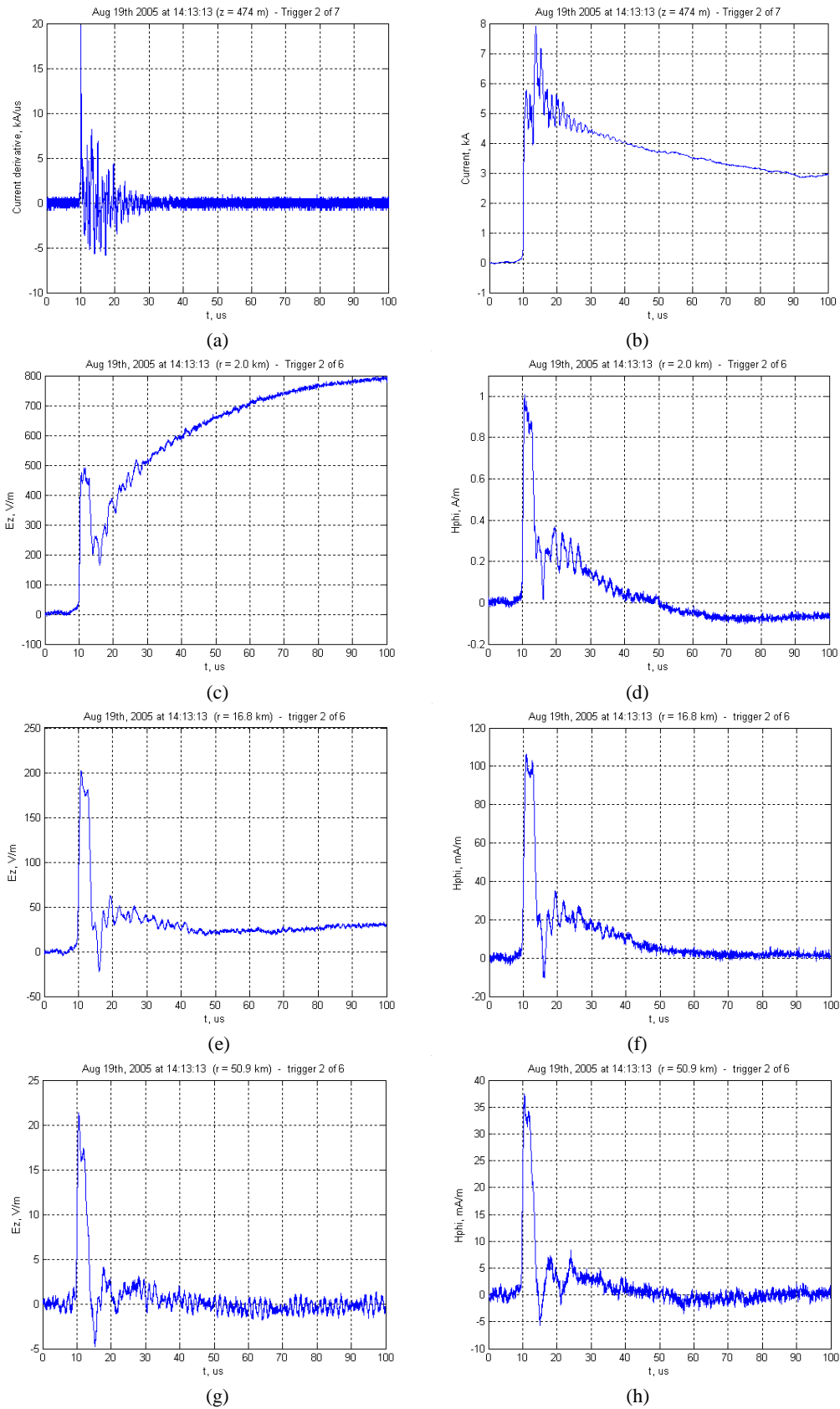


Fig. 2.15 Simultaneous records of (a) return-stroke current derivative, (b) return-stroke current (numerically integrated), (c) electric and (d) magnetic fields at 2 km, (e) electric and (f) magnetic fields at 16.8 km, and (g) electric and (h) magnetic fields at 50.9 km. 2nd stroke of the flash striking the CN Tower tip at 14:13:13 on August 19th, 2005. (Adapted from [111])

2.5 Conclusions

Recent progress in the modeling of lightning strikes to tall towers and associated experimental data obtained during the last decade or so were reviewed. Two types of return stroke models namely the Engineering Models, and the Electromagnetic or Antenna-Theory (AT) models, extended to take into account the presence of a tall strike object were discussed.

The engineering models are characterized by a discontinuity at the return stroke wavefront which requires special care when calculating the electromagnetic fields. In addition, this discontinuity cannot be considered as physically plausible.

Neither the two classes of models was able to reproduce the far field zero crossing of the electromagnetic fields, nor was it able to predict the narrow undershoot observed in the waveforms of the electromagnetic fields associated with lightning strikes to the Toronto CN Tower.

The research performed by different research groups in the last decade has raised some important questions that need to be elucidated by further theoretical investigations and experimental measurements. Some of these issues are the following

- Why do lightning return stroke models not reproduce the far-field zero crossing associated with lightning to tall structures? How should these models be revised to be able to reproduce such an effect?
- How should the engineering models be revised in order to remove the associated current discontinuity at the return stroke wavefront?
- No systematic theoretical analysis nor experimental data are available for electromagnetic fields in the immediate vicinity of a tall structure struck by lightning. The characterization of nearby electromagnetic fields is particularly important in the analysis of the interaction to nearby electrical and electronics systems.
- It is well-known that the measurements of electromagnetic fields from lightning are affected by the presence of nearby buildings and metallic structures. However, no systematic and quantitative analysis of such an effect is presently available in the literature.

The above issues will be dealt with in the following chapters of this thesis.

Chapter 3

Characteristics of Very Close Electromagnetic Fields in the Vicinity of a Tall Struck Object

3.1 Introduction

Lightning interaction with tall structures has been a subject of interest among lightning researchers in the last decade or so (e.g. [3-5]). Towers have been used for decades to record lightning current waveforms. The data obtained by Berger and co-workers (e.g. [99]) in the 1970's represents still today the most complete statistical characterization of lightning current parameters. More recently, experimental observations on both current and electromagnetic fields have been obtained on tall telecommunication towers (e.g. CN Tower in Canada [113], Peissenberg Tower in Germany [8], Gaisberg Tower in Austria [114]). On the one hand, the experimental data on towers, as well as theoretical analyses (e.g. [4-5]), have provided evidence that the lightning current and current-derivative data obtained by means of instrumented tall towers might be affected ('contaminated') by transient processes occurring along the tower. On the other hand, based on theoretical modeling and experimental observations, it is a well established fact that the presence of a tower may result in a substantial increase (a factor of 3 or so) of the electric and magnetic field peaks and their derivatives (e.g. [27, 34-35]) for observation points located at distances exceeding the height of the tower.

Interestingly, the effect of the tower at distances of about the height or the tower or less could result in a significant decrease of the electric field (e.g. [35, 73-74]).

In this chapter, we discuss the signature of electric and magnetic fields at very close distance, within the tower height, to a tower struck by lightning [115].

3.2 Theory and adopted model

In this study, we make use of the engineering models extended to take into account the presence of an elevated strike object [13]. The expression for the current distribution along the lightning channel, $h < z < H$, is [13]

$$i(z,t) = \left[P(z-h) i_o \left(h, t - \frac{z-h}{v^*} \right) - \rho_t i_o \left(h, t - \frac{z-h}{c} \right) + (1-\rho_t)(1+\rho_t) \sum_{n=0}^{\infty} \rho_g^{n+1} \rho_t^n i_o \left(h, t - \frac{h+z}{c} - \frac{2nh}{c} \right) \right] u \left(t - \frac{z-h}{v} \right) \quad (3.1)$$

and, for the current distribution along the strike object, $0 < z < h$,

$$i(z,t) = (1-\rho_t) \sum_{n=0}^{\infty} \left[\rho_t^n \rho_g^n i_o \left(h, t - \frac{h-z}{c} - \frac{2nh}{c} \right) + \rho_t^n \rho_g^{n+1} i_o \left(h, t - \frac{h+z}{c} - \frac{2nh}{c} \right) \right] u \left(t - \frac{h+z}{c} - \frac{2nh}{c} \right) \quad (3.2)$$

In (3.1) and (3.2), h is the height of the tower, ρ_t and ρ_g are the top and bottom current reflection coefficients for upward and downward propagating waves, respectively, c is the speed of light, $P(z)$ is a model-dependent function, $u(t)$ the Heaviside unit-step function, v is the return-stroke front speed, and v^* is the current-wave speed. Expressions for $P(z)$ and v^* for some of the most commonly used return-stroke models can be found in [12]. Furthermore, $i_o(t)$ is the so-called ‘undisturbed current’, which represents the ‘ideal’ current that would be measured at the tower top if the current reflection coefficients at both of its extremities were equal to zero. Equations (3.1) and (3.2) can be represented equivalently in terms of the short-circuit current [4], which is simply twice the undisturbed current, $i_{sc} = 2i_o$.

It is also assumed that the current reflection coefficients ρ_t and ρ_g are constant. In addition, any upward connecting leader and any reflections at the return stroke wavefront [30] are disregarded in the analysis presented in this chapter. These effects will be considered and included in the analysis in the next Chapter.

3.3 Considered configurations, channel-base current and return-stroke model

Two elevated strike objects are considered in this study: (1) a 168-m tall tower corresponding to the Peissenberg tower in Germany, with reflection coefficients set, respectively, to $\rho_t = -0.53$ and $\rho_g = 0.7$ [8], and, (2) a 553-m tall tower corresponding to the CN tower in Canada, with reflection coefficients set, respectively, to $\rho_t = -0.366$ and $\rho_g = 0.8$ [53].

The above values for the reflection coefficients have been determined by analyzing the current waveforms measured at the two considered towers. It is worth noting that, as suggested by Baba and Rakov [44], the waveguide properties of a conical tower above ground seem to depend on the direction of propagation. In particular, while the current pulses suffer no attenuation while traveling from the tower apex to its base, the attenuation is significant when pulses propagate from the base to the apex. As a result, the value for the reflection coefficient at ground level inferred from the measurements of the current near the top of the tower, as done by Janischewskyj et al. [53] for the CN Tower, might be somewhat underestimated. However, Heidler et al. [8] used simultaneous records of current waveforms measured near the top and near the base of the Peissenberg Tower. Therefore, their estimation for the reflection coefficient should not suffer from this effect.

In our computations, the short-circuit current $i_{sc}(t)$ and the undisturbed current $i_o(t)$ are represented by a Heidler's function and characterized by a risetime of 1.2 μs and a pulse duration at half peak of 50 μs . The peak of the short circuit current is 20 kA:

$$i_o(t) = \frac{i_{sc}(t)}{2} = \frac{I_o}{\eta} \frac{(t/\tau_1)^2}{1+(t/\tau_1)^2} \exp(-t/\tau_2) \quad (3.3)$$

the values of the parameters are: $I_o = 9.5$ kA, $\eta = 0.882$, $\tau_1 = 0.5$ μs , $\tau_2 = 63$ μs . The value for the return-stroke speed is assumed to be 120 m/ μs ([116]).

The adopted return-stroke model is the TL model ($P(z) = 1$, $v^* = v$). Other return stroke models will also be considered later in Section 3.5.

The electromagnetic fields are computed using the expressions derived by Uman et al. [117] assuming a perfectly conducting ground. It is worth shortly discussing the apparent inconsistency of engineering models in which, on the one hand, the ground reflection coefficient can be set to a value inferior to 1, corresponding to an imperfect ground, and on the other hand, the electromagnetic fields are generally computed based on a perfect ground

assumption. Indeed, a value for the ground reflection coefficient of about 0.7 to 0.8 would correspond to a ground conductivity of 0.01 S/m for the CN Tower (and its grounding) geometry, as inferred by Petrache et al. [57], who used a wire-model to represent the tower and applied in their analysis the Numerical Electromagnetics Code NEC-4. Since the vertical electric and azimuthal magnetic field components are very weakly affected by a finite conductivity of 0.01 S/m, especially at the considered very close distance ranges [118], considering a perfect ground when calculating electromagnetic fields appears to be a reasonable assumption.

Note that, throughout this chapter, we will adopt the atmospheric electricity sign convention for the electric field sign.

3.4 Simulation results and discussion

3.4.1 168-m tall tower

Fig. 3.1 presents vertical electric and azimuthal magnetic fields calculated at the horizontal distances of 5 m, 10 m, 15 m, 20 m, 25 m and 50 m from the struck tower. The observation point is at ground level.

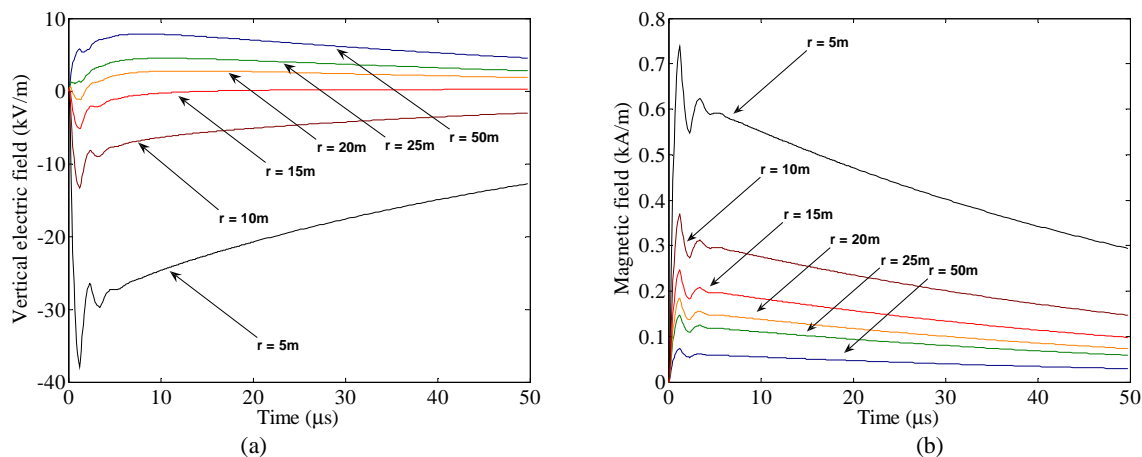


Fig. 3.1 Electric (a) and magnetic field (b) at different distances from the 168-m tall struck tower. $\rho_t = -0.53$ and $\rho_g = 0.7$, $v = 120$ m/μs.

It can be seen that, as expected, the magnetic field, dominated at these distances by the induction term, is characterized by a wavelshape similar to that of the current (at the base of the channel) and it has a $1/r$ dependence. On the other hand, it can be seen, interestingly and

in contrast with waveforms associated with strikes to ground, that the electric field at very close range (within 15 m) exhibits a negative polarity. Beyond 25 m, the field becomes positive. Note that in all the considered cases, the very initial excursion of the electric field is positive. At very close distance ranges, this initial positive excursion lasts only some tens of nanoseconds and is not discernible in the plots. Fig. 3.2 shows the first 50 nanoseconds of the electric field at a distance of 5 m from the tower base during which a slight positive excursion prior to the negative's is clearly distinguishable.

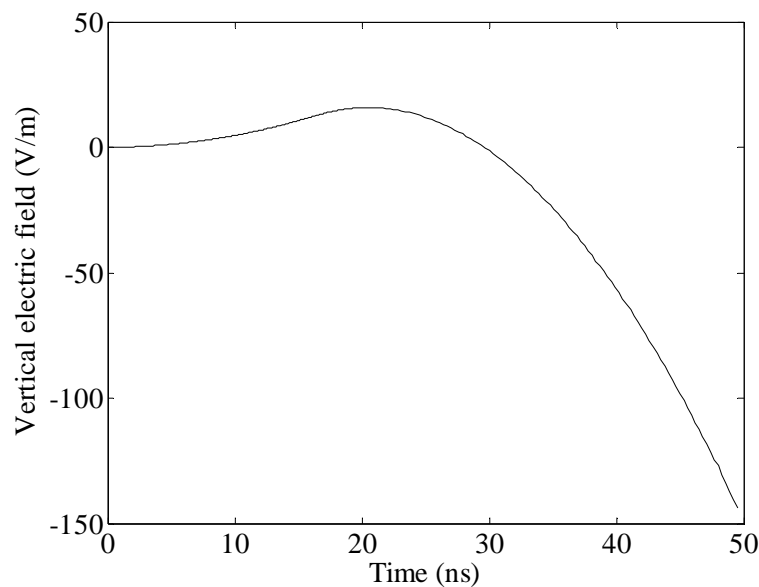


Fig. 3.2 The initial positive excursion of the electric field at a distance of 5 m from the 168-m tall struck tower.
 $\rho_t = -0.53$ and $\rho_g = 0.7$, $v = 120$ m/ μ s.

3.4.2 553-m tall tower

Fig. 3.3 presents similar results for the vertical electric and azimuthal magnetic fields calculated at the horizontal distances of 20 m, 30 m, 50 m, 60 m and 100 m from the struck tower. The observation point is at ground level.

As with the 168-m tall tower, it can be seen from the simulations that the electric field at very close range (this time within 30 m) exhibits a negative polarity. At the distance of about 40 m, the field has a bipolar waveshape. Beyond 50 m, the field becomes positive. As for the case of the shorter 168-m tall tower, the magnetic field is positive at all the considered distances and the electric field has an initial positive excursion which is not clearly visible in the figure.

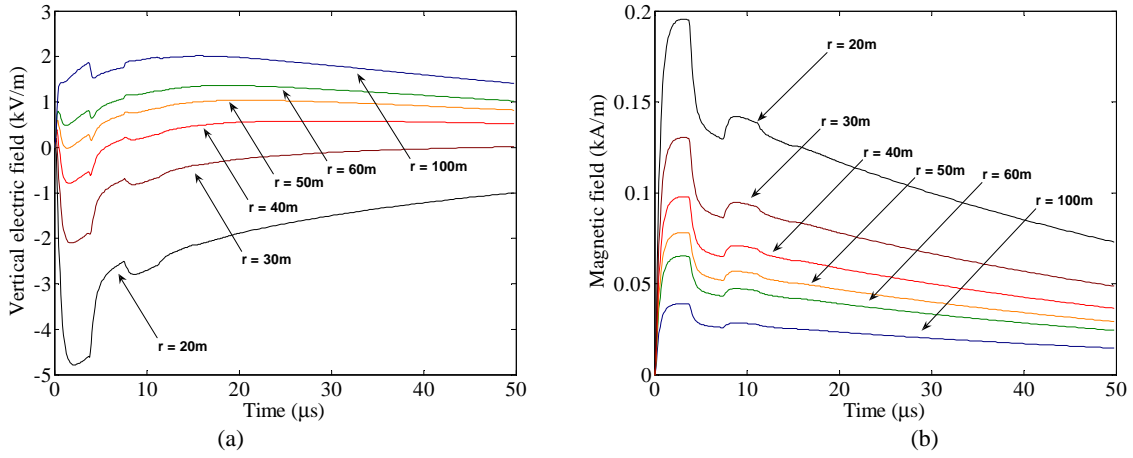


Fig. 3.3 Electric (a) and magnetic field (b) at different distances from the 553-m tall struck tower.
 $\rho_l = -0.366$ and $\rho_g = 0.8$, $v = 120$ m/ μ s.

3.5 Theoretical explanation for the inversion of polarity

Two different theoretical explanations are provided. The first is based on the general expressions of the electromagnetic field implemented in this study, and the second, using the equation derived by Baba and Rakov [35].

3.5.1 Explanation using general field equations

The general expressions for the vertical component of the electric field and the azimuthal component of the magnetic field from a vertical antenna above a perfectly conducting ground, given by [117] for an observation point at ground level, are given by

$$E_z(r, t) = -\frac{1}{2\pi\epsilon_o} \left[\int_0^H \frac{2z^2 - r^2}{R^5} \int_{R/c}^t i(z, \tau - R/c) d\tau dz + \int_0^H \frac{2z^2 - r^2}{cR^4} i(z, t - R/c) dz - \int_0^H \frac{r^2}{c^2 R^3} \frac{\partial i(z, t - R/c)}{\partial t} dz \right] \quad (3.4)$$

$$H_\phi(r, t) = \frac{1}{2\pi} \left[\int_0^H \frac{r}{R^3} i(z, t - R/c) dz + \int_0^H \frac{r}{cR^2} \frac{\partial i(z, t - R/c)}{\partial t} dz \right] \quad (3.5)$$

where H is the height of the return stroke wavefront as seen by the observer, r is the horizontal distance between the channel and the observation point, and R is the distance

between a single dipole located at a height z above ground and the observation point ($R = \sqrt{r^2 + z^2}$) (see Fig. 3.4).

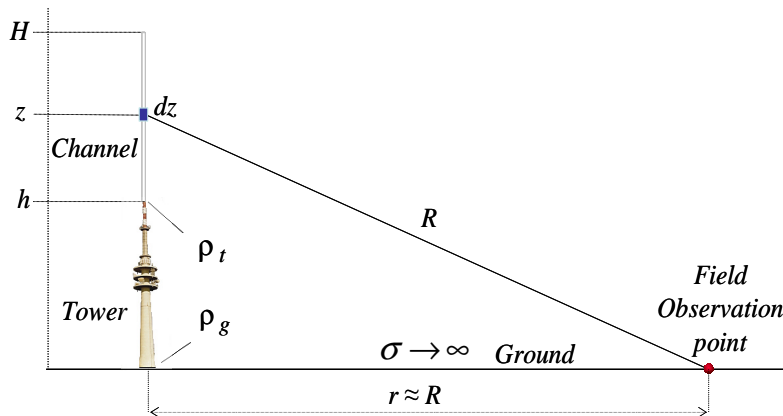


Fig. 3.4 Geometry for the calculation of electric and magnetic fields generated by a lightning return stroke initiated at the top of an elevated strike object.

Considering very close observation points such that $r \ll h$, at early times, when the height of the active dipoles is located near the top of the struck object, the multiplicative term $2z^2 - r^2$ in the static and induction components of the electric field is positive. This is in contrast with the case of a return stroke to ground, for which $2z^2 - r^2$ is negative at early times. Therefore, at the considered very close distance ranges, where the static and induction⁴ terms are predominant, these two terms start by giving a negative contribution to the overall field. Note, however, that the magnitude of the negative excursion of the field is mainly due to the induction term which depends on the current; since the static term is dependent on the time-integral of the current, it remains very small at the early times and yields a positive contribution at later times.

Note that the above phenomenon occurs solely for the vertical electric field component and only at distances lower than the height of the tower.

Fig. 3.5 and Fig. 3.6 illustrate the above observation. In these figures, we have plotted the vertical electric field, for the case of the 168-m tall tower, at distances of 10 m and 50 m. In the same figures, we have also plotted the contributions of the static, induction and radiation terms.

⁴ Note that, as shown by Thottappillil and Rakov [67], the three field components are not uniquely defined.

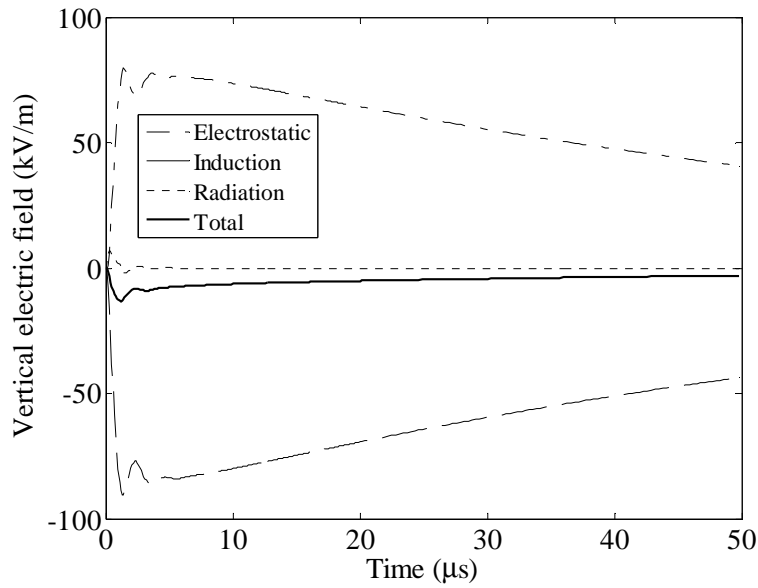


Fig. 3.5 Electric field at a distance of 10 m from the 168-m tall struck tower. Contribution of static, induction and radiation terms. $\rho_t = -0.53$ and $\rho_g = 0.7$, $v = 120$ m/ μ s.

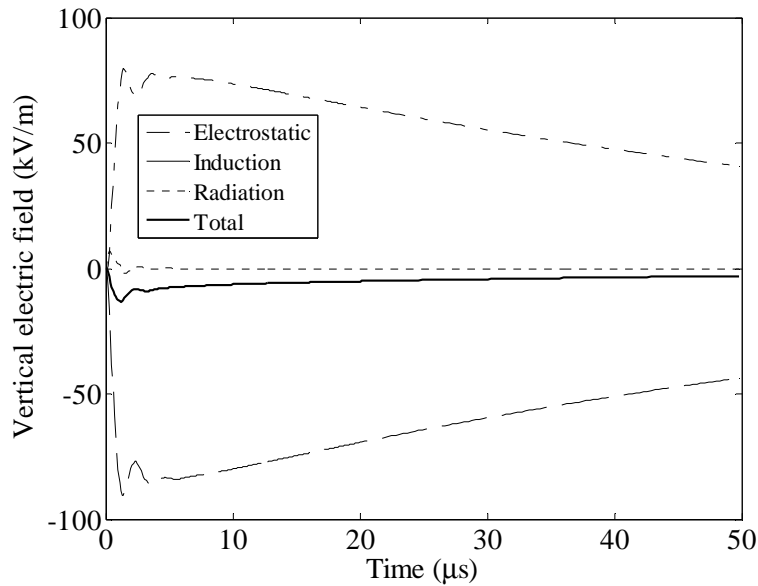


Fig. 3.6 Electric field at a distance of 50 m from the 168-m tall struck tower. Contribution of static, induction and radiation terms. $\rho_t = -0.53$ and $\rho_g = 0.7$, $v = 120$ m/ μ s.

At a distance of 10 m (Fig. 3.5), it can be seen that the contribution of the induction term is negative and greater, in absolute value, than that of the static and radiation terms. At 50 m (Fig. 3.6), the induction term is still negative; however, the positive contributions of the static and radiation terms are more significant at this distance.

3.5.2 Explanation using the formula derived by Baba and Rakov [35]

In [35], Baba and Rakov decomposed the total electric field due to a lightning strike to a tower into its incident- and reflected-wave components. Doing so, and based on the theory developed by Thottappillil et al. [119], they derived analytical expressions for the electric and magnetic fields for the special case of a return stroke speed $v = c$ and $\rho_t = 0$ (inferences below are not significantly influenced by these simplifying assumptions) at a horizontal distance r from the tower base. These equations read [35]

$$E_z(r,t) = \frac{1}{2\pi\epsilon_0 c \sqrt{r^2 + h^2}} i_{sc} \left(h, t - \frac{\sqrt{r^2 + h^2}}{c} \right) - \frac{1}{2\pi\epsilon_0 cr} 0.5 i_{sc} \left(h, t - \frac{h}{c} - \frac{r}{c} \right) + \frac{1}{2\pi\epsilon_0 cr} 0.5 \rho_g i_{sc} \left(h, t - \frac{h}{c} - \frac{r}{c} \right) \quad (3.6)$$

$$H_\phi(r,t) = \frac{1}{2\pi r} i_{sc} \left(h, t - \frac{\sqrt{r^2 + h^2}}{c} \right) - \frac{1}{2\pi r} 0.5 i_{sc} \left(h, t - \frac{h}{c} - \frac{r}{c} \right) + \frac{1}{2\pi r} 0.5 \rho_g i_{sc} \left(h, t - \frac{h}{c} - \frac{r}{c} \right) \quad (3.7)$$

A careful examination of equations (3.6) and (3.7) allows making the following observations:

- The magnetic field has always a positive polarity, regardless of the value for the reflection coefficient and the distance to the observation point.
- The initial electric field excursion (determined by the first term of (3.6), before the second and third terms start giving their contributions) is positive, regardless of the distance to the observation point. However, at very close distances such that $r \ll h$, the electric field could exhibit a change of polarity in the form of a negative excursion following the initial positive excursion when the reflection coefficient $\rho_g < 1$. For the ideal case when $\rho_g = 1$, the second and third terms in (3.6) cancel each other and the electric field would become positive and unipolar.

A rough estimation of the distance up to which the electric field exhibits a change of polarity can be made by simplifying (3.6) for $r \ll h$, namely

$$E_z(r,t) \cong \frac{1}{2\pi\epsilon_0 ch} i_{sc} \left(h, t - \frac{h}{c} \right) - \frac{1}{2\pi\epsilon_0 cr} 0.5 i_{sc} \left(h, t - \frac{h}{c} \right) + \frac{1}{2\pi\epsilon_0 cr} 0.5 \rho_g i_{sc} \left(h, t - \frac{h}{c} \right) \quad (3.8)$$

The critical distance r_c up to which the electric field exhibits the negative excursion can be therefore estimated as

$$r_c = (1 - \rho_g) \frac{h}{2} \quad (3.9)$$

For the considered 168-m and 553-m tall towers, the estimated values for r_c are respectively 25 m and 55 m. These values correspond very well to the simulation results presented in the previous Section.

3.6 Sensitivity of the polarity inversion to different parameters

3.6.1 Return-stroke speed

Fig. 3.7 presents for the case of a strike to the 168-m tower, the vertical electric field at a distance of 10 m, considering different values for the return stroke speed, namely, 100 m/ μ s, 150 m/ μ s and 200 m/ μ s. It can be seen that the field inversion of polarity at very close distances is not sensitive to the value of the return stroke speed.

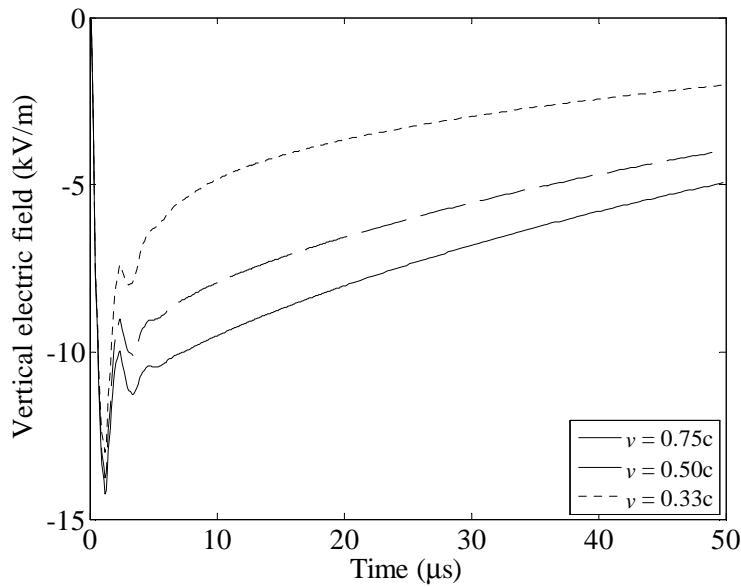


Fig. 3.7 Electric field at a distance of 10 m from the 168-m tall struck tower calculated assuming three different values for the return stroke speed: 100 m/ μ s, 150 m/ μ s and 200 m/ μ s. $\rho_t = -0.53$ and $\rho_g = 0.7$

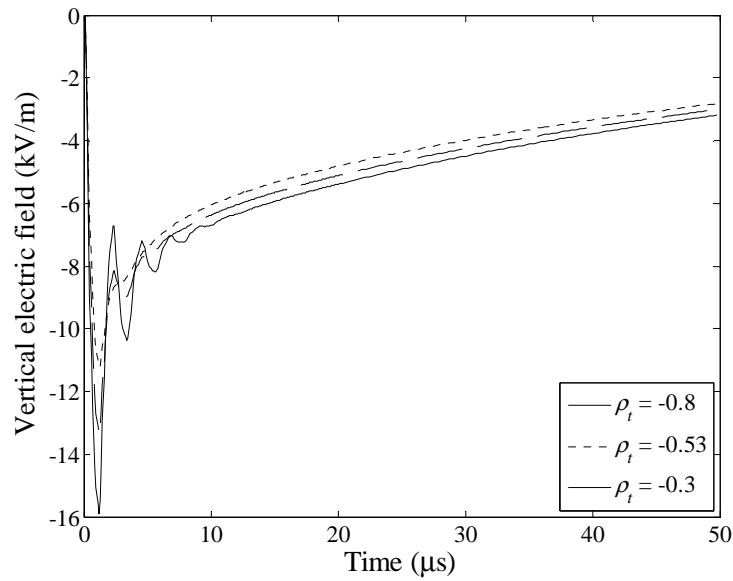


Fig. 3.8 Electric field at a distance of 10 m from the 168-m tall struck tower calculated assuming three different values for the top reflection coefficient: $\rho_t = -0.3$, $\rho_t = -0.53$, $\rho_t = -0.8$. $\rho_g = 0.7$, $v = 120$ m/ μ s.

3.6.2 Reflection coefficients

Fig. 3.8 presents the same case (168-m tall tower, distance $r = 10$ m), considering different values for the top reflection coefficients: $\rho_t = -0.3$, -0.53 , and -0.8 . Again, the polarity and the overall waveshape of the electric field is not significantly affected by the value of the top reflection coefficient.

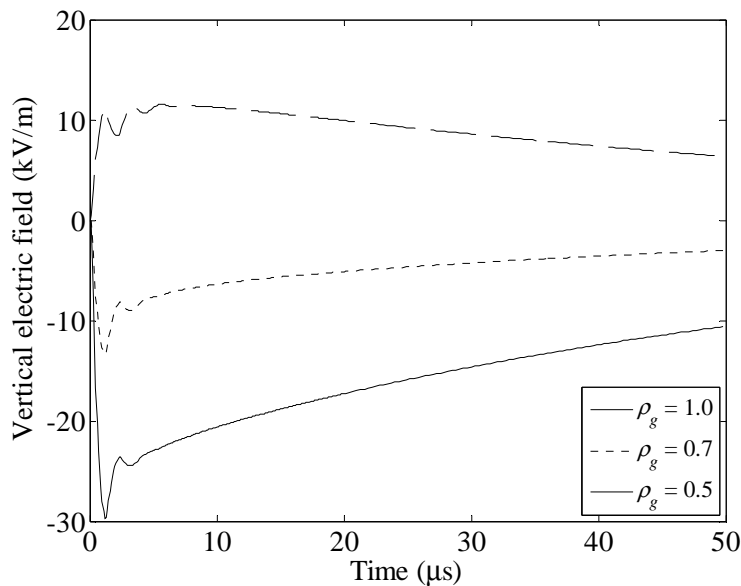


Fig. 3.9 Electric field at a distance of 10 m from the 168-m tall struck tower calculated assuming three different values for the ground reflection coefficient: $\rho_g = 0.5$, $\rho_g = 0.7$, $\rho_g = 1$. $\rho_t = -0.53$, $v = 120$ m/ μ s.

Fig. 3.9 presents the effect of the reflection coefficient at ground, ρ_g . The electric field at a distance of 10 m from a 168-m tall tower is calculated for three different values for ρ_g , namely 0.5, 0.7 and 1.

Interestingly, it can be seen that the polarity of the electric field at very close range depends on the ground reflection coefficient. The peak of the negative excursion of the electric field decreases when increasing the ground reflection coefficient. And for the large values of the coefficient ($\rho_g = 1$), the field becomes positive and unipolar, as theoretically predicted by Equation (3.6).

In order to illustrate the vertical electric and azimuthal magnetic fields polarity dependence on the tower's grounding properties, the field peak values are selected and plotted as a function of distance to the tower in Fig. 3.10. Taking the 553-m tall tower as the study case, two cases have been considered: (1) the same configuration and parameters described in section 3.3, and, (2) same as (1) but considering a perfect tower grounding, $\rho_g = 1$ [120].

It can be seen that when the ground reflection coefficient is about 0.8 or lower, the maximum E-field peak at very close distance range is of negative polarity. However, no considerable change is found in the azimuthal magnetic field when the ground reflection coefficient becomes less than unity.

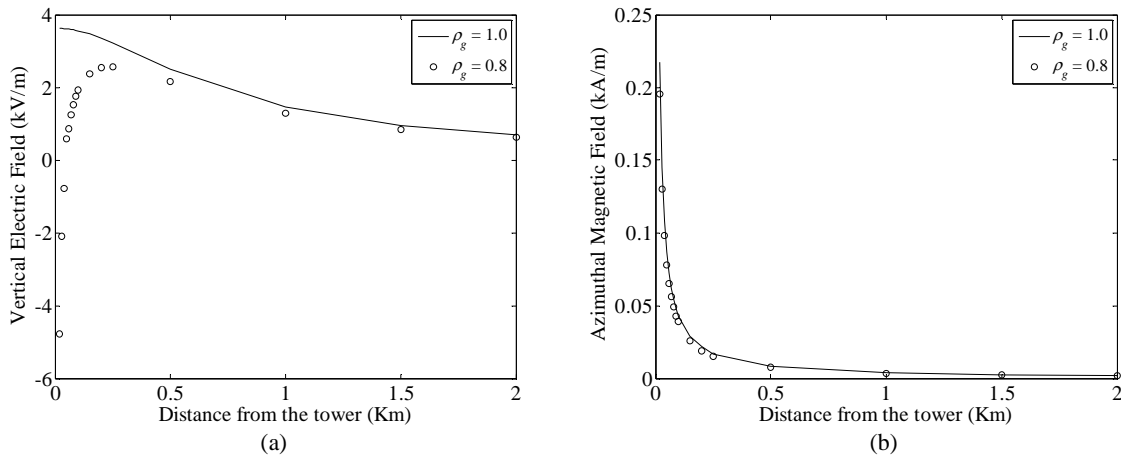


Fig. 3.10 Electric (a) and magnetic field (b) peaks at different distances from the 553-m tall struck tower. $\rho_t = -0.366$, $v = 120$ m/ μ s. Two different values for the ground reflection coefficient are considered: $\rho_g = 0.8$ and $\rho_g = 1$.

3.6.3 Shadowing effect of the tower

In order to analyze the effect of the strike tower on nearby fields, the variation of the electric field and magnetic field peaks are calculated as a function of the horizontal distance to the

observation point and shown in Fig. 3.11. The ground has been assumed to be a perfectly-conducting plane. Two cases have been considered: (i) a lightning strike to ground, and (ii) the same strike to a 100-m tall object [121].

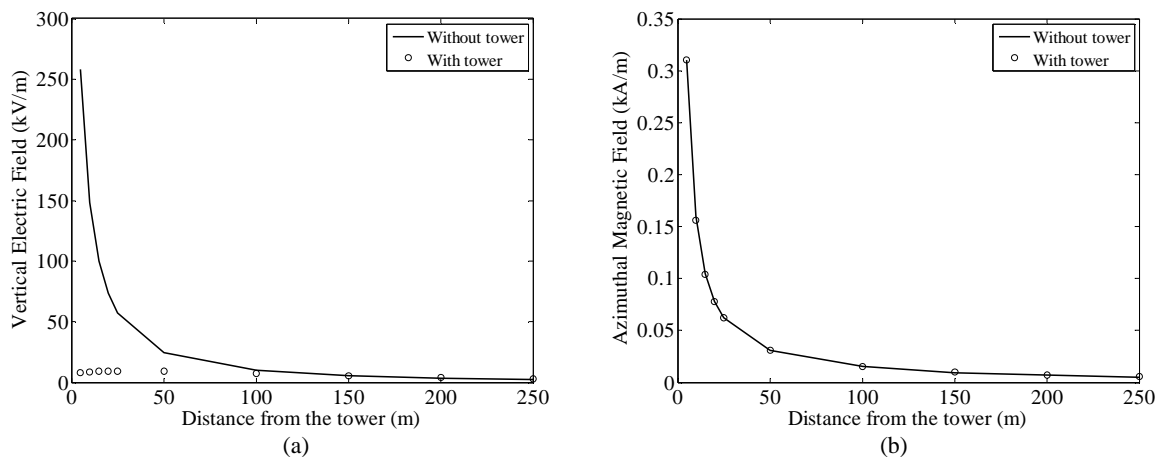


Fig. 3.11 Electric (a) and magnetic field (b) peaks at different distances in the presence and absence of the 100-m struck tower. Solid line: strike to ground. o: strike to a 100-m tall tower

It can be seen that the electric field peak at distances beyond the height of the tower or so exhibits the typical $1/r$ dependence. At closer distances, however, the E-field peak features a saturation, due to the so-called tower shadowing effect [35, 73-74]. This shadowing effect results in a substantial decrease of the nearby electric field.

On the other hand, the magnetic field peak varies inversely proportional to the horizontal distance and does not depend significantly on the presence of an elevated strike object.

3.6.4 Return-stroke models

Fig. 3.12 presents the electric field at a distance of 10 m from the 168-m tower, adopting 5 engineering return stroke models (TL, MTLL, MTLE, BG and TCS) [12], extended to take into account the presence of a tall structure [13]. The value for the decay constant λ in MTLE is assumed to be 2 km.

It can be seen that all the models predict the initial negative excursion of the field. At early times, the considered models predict a similar response for the electric field, although the BG and TCS models produce sharper initial peaks than do the TL, MTLL and MTLE models. At later times, however, the models predictions deviate significantly one from another.

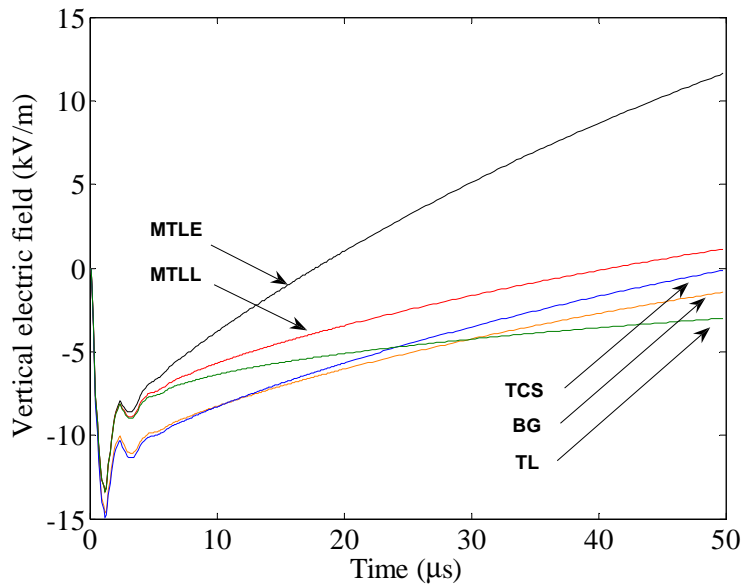


Fig. 3.12 Electric field at a distance of 10 m from the 168-m tall struck tower calculated assuming five different return stroke models (TL, MTL, MTLE, BG and TCS). $\rho_i = -0.53$ and $\rho_g = 0.7$, $v = 120$ m/ μ s.

3.7 Summary and conclusions

We have shown in this chapter that the electric field generated by a lightning return stroke to a tall structure can change polarity at very close distance range, typically at distances of about one tenth the height of the struck object or so. This change in the polarity appearing as a negative excursion preceded by a short (some tens of nanoseconds) initial positive excursion, seems to be a specific signature of very close vertical electric fields. Two different theoretical explanations of such an inversion of polarity are given, the first based on general field equations for a perfectly-conducting ground, and the second based on the equation derived by Baba and Rakov for the case when the return stroke wave front speed is assumed to be equal to the speed of light and the reflection coefficient at the top of the tall structure is zero. A simple equation is derived which provides an estimate of the critical distance below which such an inversion of polarity might occur. We also showed that the inversion of polarity depends on the value for the reflection coefficient at the base of the tower and might disappear for reflection coefficients close to 1. On the other hand, other parameters such as the return stroke speed, the reflection coefficient at the top of the tower, and the adopted return stroke model seem not to have an impact on the inversion of polarity. Experimental data on electromagnetic fields at very close range to a tower struck by lightning are needed in order to confirm the theoretical finding. This finding, if experimentally confirmed, would

have implications on the interaction of electromagnetic fields to nearby electrical and electronics systems.

Chapter 4

Radiated Fields from Lightning Strikes to Tall Structures: Effect of Upward Connecting Leader and Reflections at the Return Stroke Wavefront

4.1 Introduction

Recently, Pavanello et al. [111] presented measurements of the electric and magnetic fields at three distances from the return stroke current associated with lightning strikes to the Toronto CN Tower (553 m). The vertical component of the electric field and the azimuthal component of the magnetic field were measured simultaneously at distances of 2.0 km, 16.8 km, and 50.9 km from the CN Tower. The waveforms of the electric and magnetic fields at 16.8 km and 50.9 km exhibited a narrow undershoot and a first zero crossing about 5 microseconds after the onset of the return stroke. Moreover, most of the field records exhibited a double-peak initial response. For fields at 50.9 km, the expected zero crossing at about 40 microseconds was also observed. A representative measured waveform exhibiting all four features (double-peak, narrow undershoot, early zero-crossing and standard zero-crossing) can be seen in Fig. 4.1.

Pavanello et al. [111, 122] presented also calculations of the electric and magnetic fields using six engineering models (TL, MTLL, MTLE, BG, TCS), extended to take into account the presence of a tall structure using a distributed-source approach [13], and the model

proposed by Baba and Rakov [39], based on a lumped-source approach). It was shown that the six considered engineering models produce very similar results, especially as far as the initial peak of the fields is concerned. While a reasonable agreement between simulations and measurements was found for the magnetic fields, the measured electric fields appeared to be significantly affected by the structures on which the sensors were installed (see Chapter 6 for a detailed discussion on this effect). The electric field peaks, in particular, were found to be considerably larger than the theoretical predictions [98, 123-124]. For this reason, we limit ourselves to magnetic fields in this study.

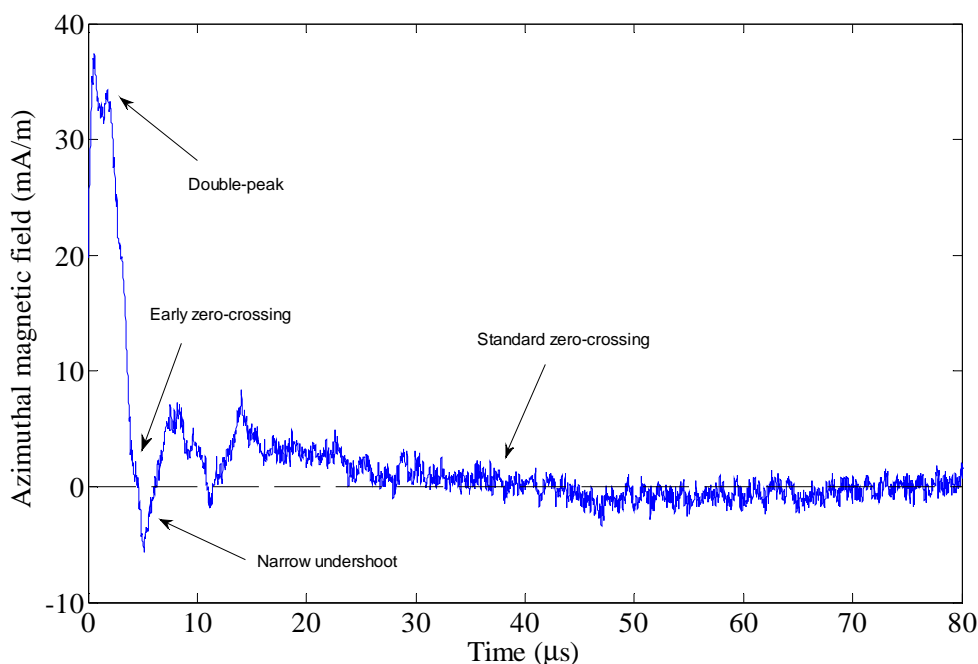


Fig. 4.1 A representative waveform of the azimuthal magnetic field at 50.9km showing three features: Double-peak, narrow undershoot, early zero-crossing and standard zero-crossing of azimuthal magnetic field.

The model proposed by Baba and Rakov reproduced better than the others the narrow undershoot that can be observed right after the first peak because its formulation does not imply the presence of the ‘turn-on’ term, which must be taken into account for the other five models, in which a current discontinuity appears at the return stroke wavefront [48]. None of the six considered models was able to reproduce either the typical zero-crossing of the far field, or the initial double-peak.

In this chapter, we propose an improved version of the engineering models for return strokes to tall structures that takes into account the presence of possible reflections at the return stroke wavefront and an upward connecting leader [125-126]. To do this, we apply the procedure

proposed by Shostak et al. [30]. The present approach is based on the so-called distributed-source representation of the lightning channel [13] featuring a self-consistent treatment of the impedance discontinuity at the tower top. In addition, we propose an elegant iterative solution which can be easily implemented into computer simulation programs to take into account in a straightforward way multiple reflections occurring at the discontinuities at the tower ends and at the return stroke wavefront.

The chapter is organized as follows: in Section 4.2, an improved version of the engineering models is presented, in which the presence of an upward-connecting leader and reflections at the return stroke wavefront are accounted for. Section 4.3 presents a comparison between simulations and measured data of Pavanello et al. [111]. The data consist of magnetic field waveforms at three different distances (2 km, 16.8 km and 50.9 km) associated with lightning strikes to the CN Tower. Conclusions are given in Section 4.4.

4.2 Proposed Model

In this study, we make use of the engineering models extended to take into account the presence of an elevated strike object [13]. The tall object is represented as an ideal, uniform transmission line characterized by constant and frequency independent current reflection coefficients at its top and bottom (see Fig. 4.2). The expression for the current distribution along the lightning channel, $h < z < H$ reads

$$i(z, t) = \left[P(z-h) i_0 \left(h, t - \frac{z-h}{v^*} \right) - \rho_t i_0 \left(h, t - \frac{z-h}{c} \right) + (1-\rho_t)(1+\rho_t) \sum_{n=0}^{\infty} \rho_g^{n+1} \rho_t^n i_0 \left(h, t - \frac{h+z}{c} - \frac{2nh}{c} \right) \right] \times u \left(t - \frac{z-h}{v} \right) \quad (4.1)$$

and, for the current distribution along the strike object, $0 < z \leq h$,

$$i(z, t) = (1-\rho_t) \sum_{n=0}^{\infty} \left[\rho_t^n \rho_g^n i_0 \left(h, t - \frac{h-z}{c} - \frac{2nh}{c} \right) + \rho_t^n \rho_g^{n+1} i_0 \left(h, t - \frac{h+z}{c} - \frac{2nh}{c} \right) \right] \times u \left(t - \frac{h+z}{c} - \frac{2nh}{c} \right) \quad (4.2)$$

where h is the height of the tower, ρ_t and ρ_g are the tower top and bottom (ground) current reflection coefficients for upward and downward propagating waves, respectively, c is the speed of light, $i_o(t)$ is the so-called undisturbed current [13], $P(z)$ is a model-dependent function, $u(t)$ the Heaviside unit-step function, v is the return-stroke front speed, and v^* is the current-wave speed [12].

Note that the undisturbed current can be equivalently expressed in terms of the ‘short-circuit current’ $i_{sc}(t) = 2i_o(h,t)$ [4, 39], or the ‘reference current’ [40]. The two latter (the reference current and the short-circuit current) coincide when the reflection coefficient at ground is equal to 1.

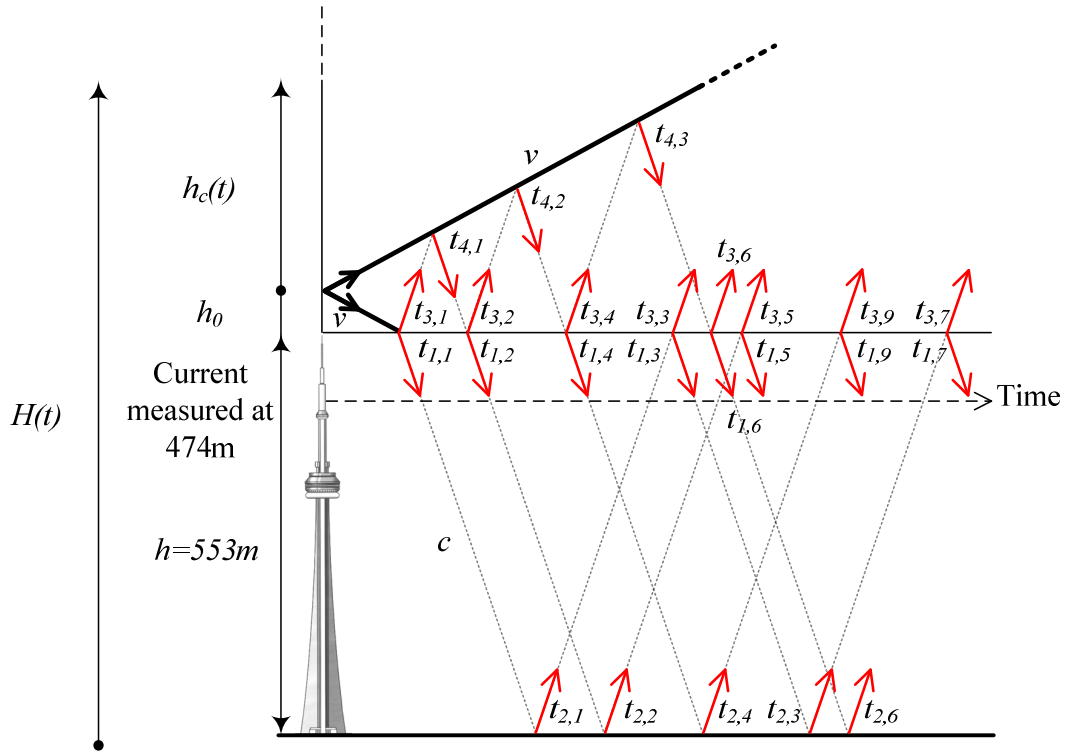


Fig. 4.2 Lattice diagram of the return stroke current multiple reflections along the tower and the channel. The expressions for the time and magnitude of current reflections are given in Tables Table 4.1 and Table 4.2.

In the proposed model we suppose that the return stroke channel is initiated at a height of h_0 above the tower. The time dependent wavefront level $H(t)$ and the channel length above the RS initiation point $h_c(t)$ are simply given as

$$\begin{aligned} H(t) &= h + h_0 + h_c(t) \\ h_c(t) &= vt \end{aligned} \quad (4.3)$$

In Fig. 4.2, the multiple reflections are illustrated using a lattice diagram. Starting at the level of h_0 where the downward and upward connecting leaders meet, the return stroke channel is

assumed to be initiated, moving vertically in opposite directions at the speed of the return stroke v . The current injected into the tower from its top is reflected back and forth at its ends, and portions of it are transmitted into the channel; these transmitted pulses, which are assumed to travel at the speed of light c , catch up with the return stroke wavefront travelling at a lower speed v . Assuming that the current vanishes abruptly at the return stroke wavefront results in a discontinuity at the wavefront [48]. It is worth noting that, strictly speaking, the lattice diagram used in this study is an approximation in the sense that it is implicitly assumed that all the time components of the current pulse ‘see’ the same wavefront, an approximation which is valid for early times.

In this study, we developed an iterative approach (with a similar algorithm used in [127]) to obtain closed-form expressions for the current distribution along the tower and along the channel, taking into account the reflection coefficient at the return stroke wavefront and the initiation of the return stroke above the tower ($h + h_0$).

The new expression for the current in the channel reads [125-126]

$$i(z, t) = \left[P(z - h - h_0) i_0 \left(h + h_0, t - \frac{z - h - h_0}{v^*} \right) + i_0 \left(h + h_0, t - \frac{h + h_0 - z}{v} \right) + \sum_{n=1}^{\infty} i_{3,n} i_0 \left(h + h_0, t - \frac{z - h}{c} - t_{3,n} \right) + \sum_{n=1}^{\infty} i_{4,n} i_0 \left(h + h_0, t - \frac{H(t_{4,n}) - z}{c} - t_{4,n} \right) \right] \times u \left(t - \frac{z - h - h_0}{v} \right) \quad (4.4)$$

and the corresponding expression for the current in the tower is

$$i(z, t) = \sum_{n=1}^{\infty} i_{1,n} i_0 \left(h + h_0, t - \frac{h - z}{c} - t_{1,n} \right) + \sum_{n=1}^{\infty} i_{2,n} i_0 \left(h + h_0, t - \frac{z}{c} - t_{2,n} \right) \quad (4.5)$$

The times and magnitudes of successive current terms in (4.4) and (4.5) have been determined and their expressions are given in Table 4.1 and Table 4.2.

The validity of the proposed expressions has been carefully checked through analysis and numerical simulations. It can be easily seen that (4.4) and (4.5) reduce to (4.1) and (4.2), simply by substituting $h_0 = 0$ and $\rho_c = 0$ (see ρ_c in $i_{4,n}$).

It is worth noting that Baba and Rakov [128] have included the presence of an upward connecting leader in their model – which is in terms of a lumped voltage source excitation – and analyzed its effects. Note also that according to Baba and Rakov’s model, no reflections

could occur at the return stroke wavefront since current pulses in the channel are assumed to travel at the return stroke speed.

Table 4.1 Current reflection times associated with the lattice diagram of Fig. 4.2.

Iteration No.	$t_{1,l..k}$	$t_{2,l..k}$	$t_{3,l..k}$	$t_{4,l..k}$
0	$t_{1,1} = \frac{h_0}{v}$		$t_{3,1} = \frac{h_0}{v}$	
1	$t_{1,2} = 2t_{4,1} - t_{3,1}$ $t_{1,3} = \frac{h}{c} + t_{2,1}$	$t_{2,1} = \frac{h}{c} + t_{1,1}$	$t_{3,2} = 2t_{4,1} - t_{3,1}$ $t_{3,3} = \frac{h}{c} + t_{2,1}$	$t_{4,1} = \frac{\left(t_{3,1} + \frac{h_0}{c}\right)}{\left(1 - \frac{v}{c}\right)}$
2	$t_{1,4} = 2t_{4,2} - t_{3,2}$ $t_{1,5} = \frac{h}{c} + t_{2,2}$	$t_{2,2} = \frac{h}{c} + t_{1,2}$	$t_{3,4} = 2t_{4,2} - t_{3,2}$ $t_{3,5} = \frac{h}{c} + t_{2,2}$	$t_{4,2} = \frac{\left(t_{3,2} + \frac{h_0}{c}\right)}{\left(1 - \frac{v}{c}\right)}$
k	$t_{1,2k} = 2t_{4,k} - t_{3,k}$ $t_{1,2k+1} = \frac{h}{c} + t_{2,k}$	$t_{2,k} = \frac{h}{c} + t_{1,k}$	$t_{3,2k} = 2t_{4,k} - t_{3,k}$ $t_{3,2k+1} = \frac{h}{c} + t_{2,k}$	$t_{4,k} = \frac{\left(t_{3,k} + \frac{h_0}{c}\right)}{\left(1 - \frac{v}{c}\right)}$

Table 4.2 Current reflections magnitude corresponding to the terms listed in Table 4.1

Iteration No.	$i_{1,l..k}$	$i_{2,l..k}$	$i_{3,l..k}$	$i_{4,l..k}$
0	$i_{1,1} = (1 - \rho_t)$		$i_{1,1} = -\rho_t$	
1	$i_{1,2} = (1 - \rho_t)i_{4,1}$ $i_{3,1} = \rho_t i_{2,1}$	$i_{2,1} = \rho_g i_{1,1}$	$i_{3,2} = -\rho_t i_{4,1}$ $i_{3,3} = (1 + \rho_t)i_{2,1}$	$i_{4,1} = \rho_c i_{3,1}$
2	$i_{1,4} = (1 - \rho_t)i_{4,2}$ $i_{1,5} = \rho_t i_{2,2}$	$i_{2,2} = \rho_g i_{1,2}$	$i_{3,4} = -\rho_t i_{4,2}$ $i_{3,5} = (1 + \rho_t)i_{2,2}$	$i_{4,2} = \rho_c i_{3,2}$
k	$i_{1,2k} = (1 - \rho_t)i_{4,k}$ $i_{1,2k+1} = \rho_t i_{2,k}$	$i_{2,k} = \rho_g i_{1,k}$	$i_{3,2k} = -\rho_t i_{4,k}$ $i_{3,2k+1} = (1 + \rho_t)i_{2,k}$	$i_{4,k} = \rho_c i_{3,k}$

4.3 Simulation and comparison with experimental data of Pavanello et al. [111]

Pavanello et al. [111] reported on simultaneous measurements of the return-stroke current and electric and magnetic fields at three distances associated with lightning strikes to the Toronto CN Tower (553 m), obtained during the summer of 2005. The lightning return-stroke current

was measured using a 40-MHz Rogowski coil installed at a height of 474 m AGL (above ground level). The vertical component of the electric field and the azimuthal component of the magnetic field were simultaneously measured at distances of 2.0 km, 16.8 km, and 50.9 km from the CN Tower. The magnetic field sensor at 2 km was a loop antenna (697 Hz – 150 MHz) located on the roof of the four-floor Pratt building of the University of Toronto. The magnetic field sensors at the two other locations were loop antenna sensors (TSN 245-H30, Thomson CSF, 4 kHz – 150 MHz), which were also located on the roof of buildings. The details of the experimental setup and the measuring equipment can be found in [111]. In this chapter, we have selected three sets of data comprising the return-stroke current and the associated magnetic fields at the three distances (see Table 4.3). Measured electric field waveforms are not used in the present study because they were significantly affected by the enhancement effect of the buildings on which the sensors were located [111, 124].

Table 4.3 Selected return strokes for the analysis (events occurred on August 19, 2005)

Event	Hour, Stroke	I_{Peak} (kA)	10-90% Risetime (μ s)
#1	14:13:13, Stroke 2/6	5.5	0.4
#2	14:13:13, Stroke 3/6	11.7	1.0
#3	14:11:41, Stroke 1/9	7.9	0.8

The return stroke speed is assumed to be $v = 120$ m/ μ s. The total length of the lightning channel is assumed to be 12 km. Two models were adopted in the analysis:

(1) The MTLE model [37, 129], including the presence of the tower [13]. The corresponding function $P(z)$ is given by [12]

$$P(z) = \exp(-z / \lambda) \quad (4.6)$$

A value of 2 km was assumed for the current decay constant λ [27].

(2) The proposed improvement of the MTLE model, taking into account the presence of an upward connecting leader and reflections at the return stroke wavefront.

The reflection coefficient at the return stroke wavefront was determined using the following equation [130-131]

$$\rho_c = \frac{v - c}{v + c} \quad (4.7)$$

4.3.1 Current

For each event, the undisturbed current is represented using the sum of two Heidler's functions:

$$i_0(h+h_0, t) = \begin{cases} \frac{I_{o1}}{\eta_1} \frac{(t/\tau_{11})^{N_1}}{1+(t/\tau_{11})^{N_1}} \exp(-t/\tau_{21}) + \frac{I_{o2}}{\eta_2} \frac{(t/\tau_{12})^{N_2}}{1+(t/\tau_{12})^{N_2}} \exp(-t/\tau_{22}) & t \geq 0 \\ 0 & t < 0 \end{cases} \quad (4.8)$$

The parameters of the Heidler's functions representing the current in (4.8) were determined using a trial-and-error approach to obtain the best match with the current recorded experimentally. The parameters are presented in Table 4.4, for the original MTLE model (in which the presence of an upward connecting leader and reflections at the return stroke wavefront are not considered) and in Table 4.5 for the proposed improved model. The currents at 474 m calculated using the two models and the parameters of Table 4.4 and Table 4.5 are shown in Fig. 4.3a, 3b and 3c, for which the effect of different reflections on the current waveforms are highlighted and quantified in Table 4.6. In Fig. 4.4a, 4b and 4c, the computed currents are compared with the actual current waveforms measured at the same height on the CN Tower. It can be seen that the fine structure of the measured current is better reproduced with the improved model. However, it is likely that some of the fine structure of the measured current waveforms is also due to structural discontinuities of the CN Tower. Some studies (e.g. [132]) have attempted to take into account these effects by modeling the tower as a cascaded multisection transmission line.

Table 4.4 Parameters for the undisturbed current, tower reflection coefficients, return-stroke speed, for the MTLE model

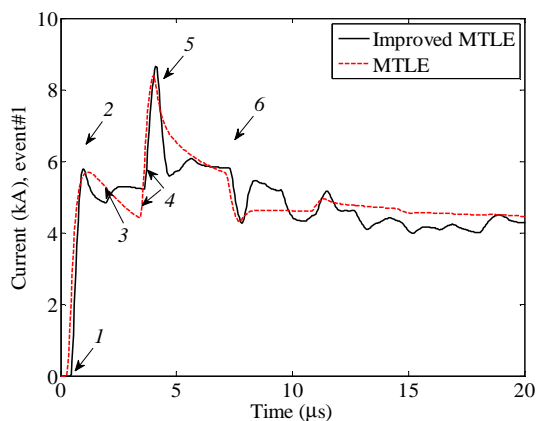
Event	$v(\times 10^8 \text{ m/s})$	ρ_g	ρ_t	η_l	$I_{o1} \text{ (kA)}$	$\tau_{11} \text{ (}\mu\text{s)}$	$\tau_{21} \text{ (}\mu\text{s)}$	N_1	η_2	$I_{o2} \text{ (kA)}$	$\tau_{12} \text{ (}\mu\text{s)}$	$\tau_{22} \text{ (}\mu\text{s)}$	N_2
#1	1.2	0.8	-0.36	0.57	1.8	0.3	2.0	2	0.94	2.5	0.3	150	2
#2	1.2	0.8	-0.36	0.46	4.48	0.3	1.0	2	0.94	6.05	0.3	140	2
#3	1.2	0.8	-0.36	0.49	5.42	0.3	1.2	2	0.89	4.03	1.0	150	2

Table 4.5 Parameters for the undisturbed current, reflection coefficients, return-stroke speed, height of the return-stroke initiation for the proposed improved MTLE model

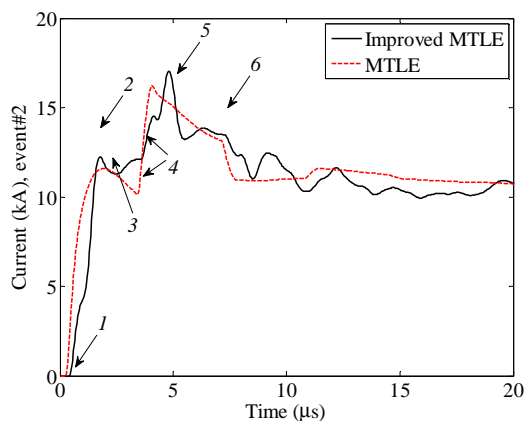
Event	$v(\times 10^8 \text{ m/s})$	$h_0 \text{ (m)}$	ρ_g	ρ_t	ρ_c	η_l	$I_{o1} \text{ (kA)}$	$\tau_{11} \text{ (}\mu\text{s)}$	$\tau_{21} \text{ (}\mu\text{s)}$	N_1	$I_{o2} \text{ (kA)}$	η_2	$\tau_{12} \text{ (}\mu\text{s)}$	$\tau_{22} \text{ (}\mu\text{s)}$	N_2
#1	1.2	20	0.6	-0.7	-0.43	0.74	3.71	0.3	7.0	2	2.7	0.77	6.0	170	2
#2	1.2	20	0.6	-0.7	-0.43	0.006	4.5	4.0	0.3	2	9.03	0.97	1.0	120	6
#3	1.2	15	0.6	-0.7	-0.43	0.77	5.7	0.3	9.0	2	4.5	0.74	7.0	150	2

Table 4.6 Reflections in the current waveform as shown in Fig. 4.3a,b and c

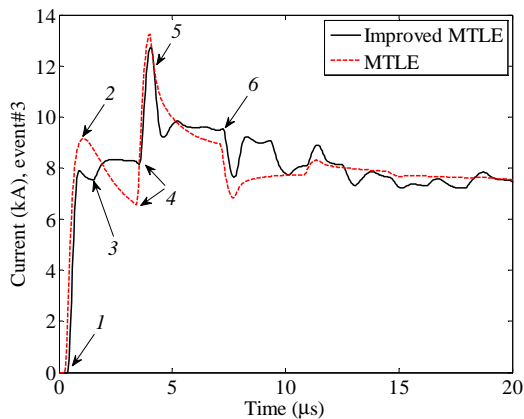
Reflections		Reflection Time General	Event #1,2	Event #3
			Reflection Time (μs)	Reflection Time (μs)
1	Current arrival $h = 474$ m	$t = t_{1,1} + \frac{h-474}{c}$	0.43	0.39
2	First reflection from the channel top seen at $h = 474$ m	$t = t_{1,2} + \frac{h-474}{c}$	0.87	0.72
3	Second reflection from the channel top seen at $h = 474$ m	$t = t_{1,4} + \frac{h-474}{c}$	1.91	1.5
4	First reflection from the ground seen at $h = 474$ m	$t = t_{2,1} + \frac{474}{c}$	3.59	3.55
5	Third reflection from the channel top seen at $h = 474$ m	$t = t_{1,6} + \frac{h-474}{c}$	4.1	4.07
6	Ground-tower-ground reflection seen at $h = 474$ m	$t = t_{2,3} + \frac{474}{c}$	7.27	7.23



(a)



(b)



(c)

Fig. 4.3 Computed current $h = 474$ m using the original MTLE and the proposed improved MTLE: 1 – current arrival; 2 – first reflection from the channel top; 3 – second reflection from the channel top; 4 – first reflection from the ground; 5 – third reflection from the channel top; 6 – ground-tower-ground reflection. See also Table 4.4 – (a) Event #1, (b) Event#2, and (c) Event#3.

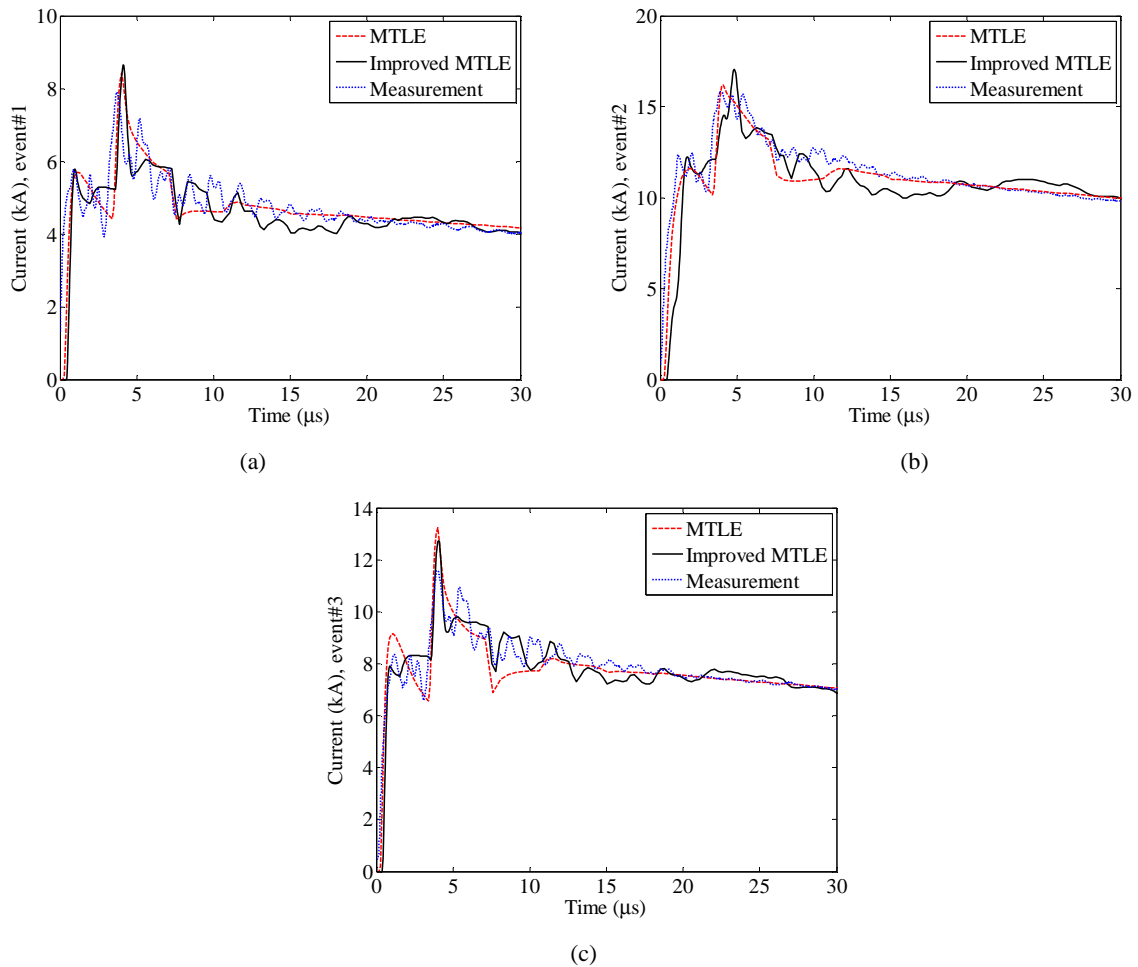


Fig. 4.4 Comparison of predicted currents using the original MTLE model and the proposed improved version at the height 474 m with the measured waveform on the CN Tower. (a) Event #1, (b) Event #2, (c) Event #3.

4.3.2 Magnetic Field

Fig. 4.5, Fig. 4.6 and Fig. 4.7 present, for the three considered events, the magnetic field computed for the three considered distances (2 km, 16.8 km and 50.9 km) by using the original MTLE model and the proposed improved version of it. On the same figures, measured waveforms of Pavanello et al. [111] are also shown for comparison.

The measured magnetic field waveforms at 2 km feature an unexpected zero-crossing at about 40 microseconds, which is due to the value of the time constant of the H-field sensor of the University of Toronto used at that location [111]. As mentioned in Section 4.1, the magnetic field waveforms at 16.8 km and 50.9 km feature a first zero crossing about 5 microseconds after the onset of the return-stroke, which is part of a narrow undershoot. Such an early undershoot, which occurs at a time given approximately by twice the propagation time along the tower, was attributed to the transient processes along the tower [111].

Measured fields at 50.9 km exhibit the expected zero-crossing at about 40 microseconds [112].

It can be seen that the computed results using the proposed improved version of the MTLE model are in better agreement with experimental observations than those obtained disregarding possible reflections at the return-stroke wavefront. Namely, the initial double peak, the early narrow undershoot typical of measured fields from lightning strikes to the CN Tower, and the far-field zero-crossing are all well reproduced by the improved model. None of these features were predicted by the original model. It is worth noting that the presence of the undershoot was found to be responsible for detection anomalies of the North American Lightning Detection Network (NALDN) which misclassified some of the return strokes to the CN Tower as cloud flashes ([133]).

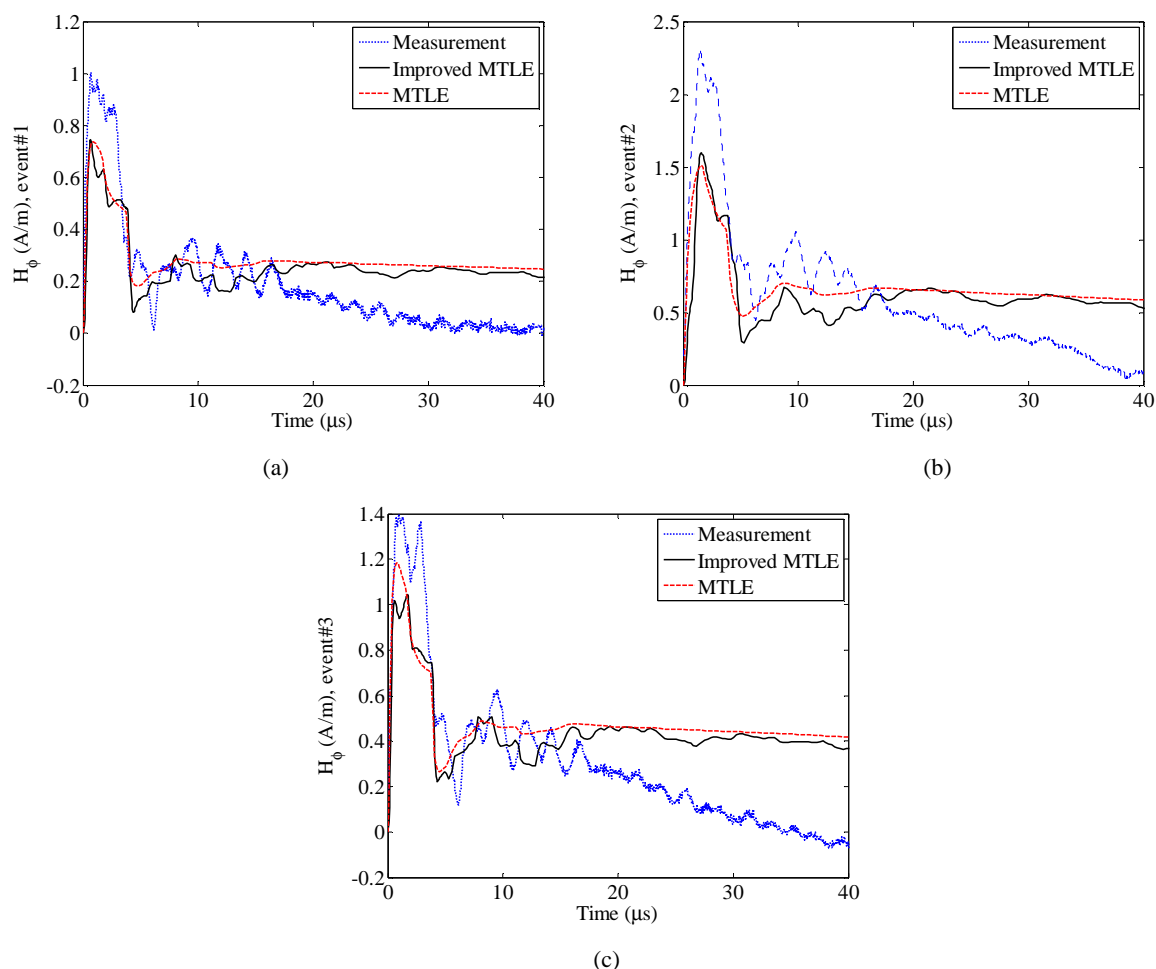


Fig. 4.5 Comparison of simulated azimuthal magnetic fields at 2 km using the original MTLE model and the proposed improved version with the measured waveform: (a) Event #1, (b) Event #2, (c) Event #3.

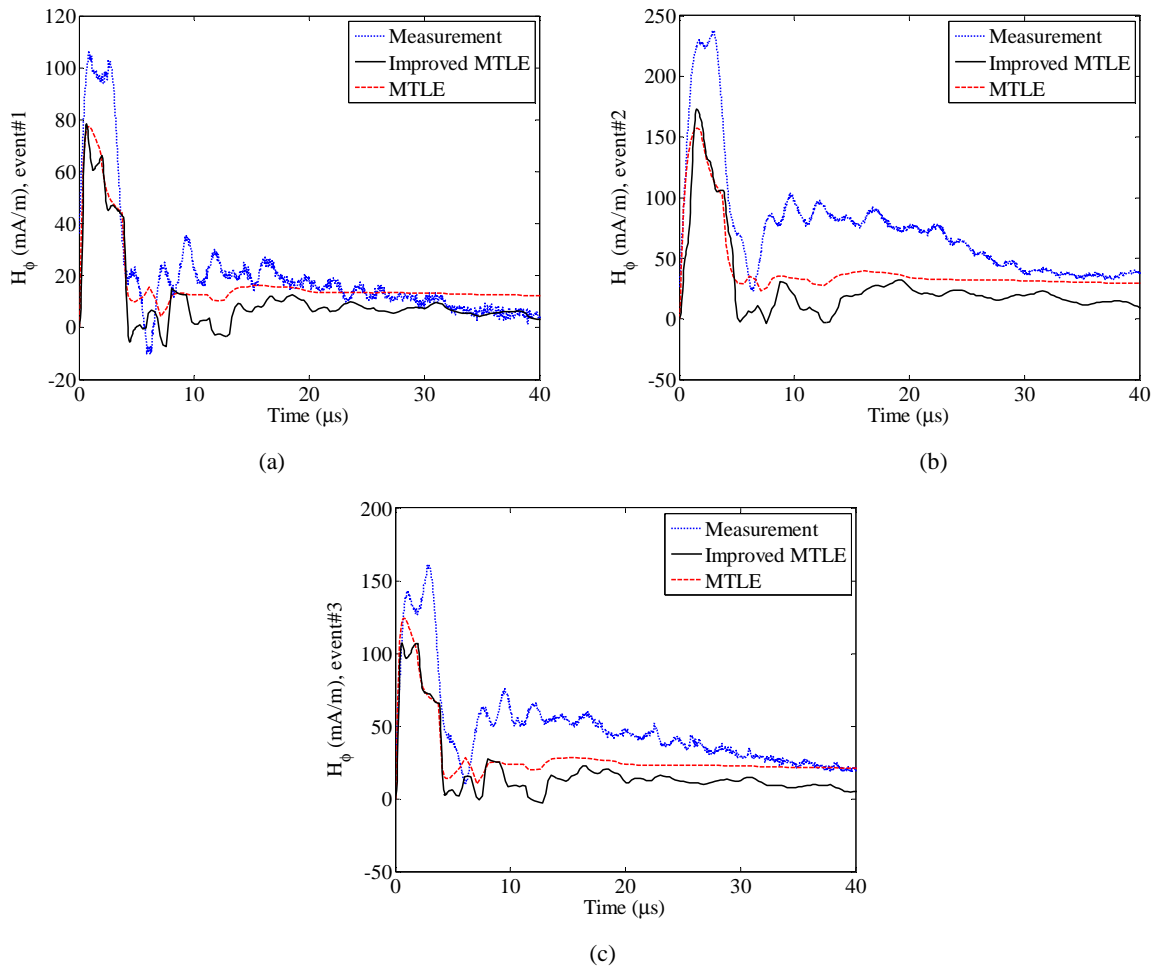


Fig. 4.6 Comparison of simulated azimuthal magnetic fields at 16.8 km using the original MTLE model and the proposed improved version with the measured waveform: (a) Event #1, (b) Event #2, (c) Event #3.

The computed magnetic field peaks are systematically about 25% lower than measured values. Reasons for this discrepancy are discussed in [111] and can be partially attributed to the geometrical and electrical characteristics of objects in the vicinity of the sensors.

It is also worth mentioning that other reasons for the observed differences between simulations and measurements can be the influence of channel inclination (e.g. [55, 134]) and the complexity of the tower structure (e.g. [135]).

Fig. 4.8 presents the influence of the height of the upward connecting leader on the computed magnetic field. The reported results refer to event #1 (see Table 4.3), and the fields are computed at a distance of 50.9 km. The considered values for the length of the upward leader are 10, 20, 30 and 100 m. It can be seen that the height of the upward-connecting leader mostly affects the early-time response of the field, namely the two initial peaks. Interestingly, the double-peak field response is reproduced considering a length of the upward leader of about 10-30 m, which is in the order of typical values for subsequent strokes ([1]). The

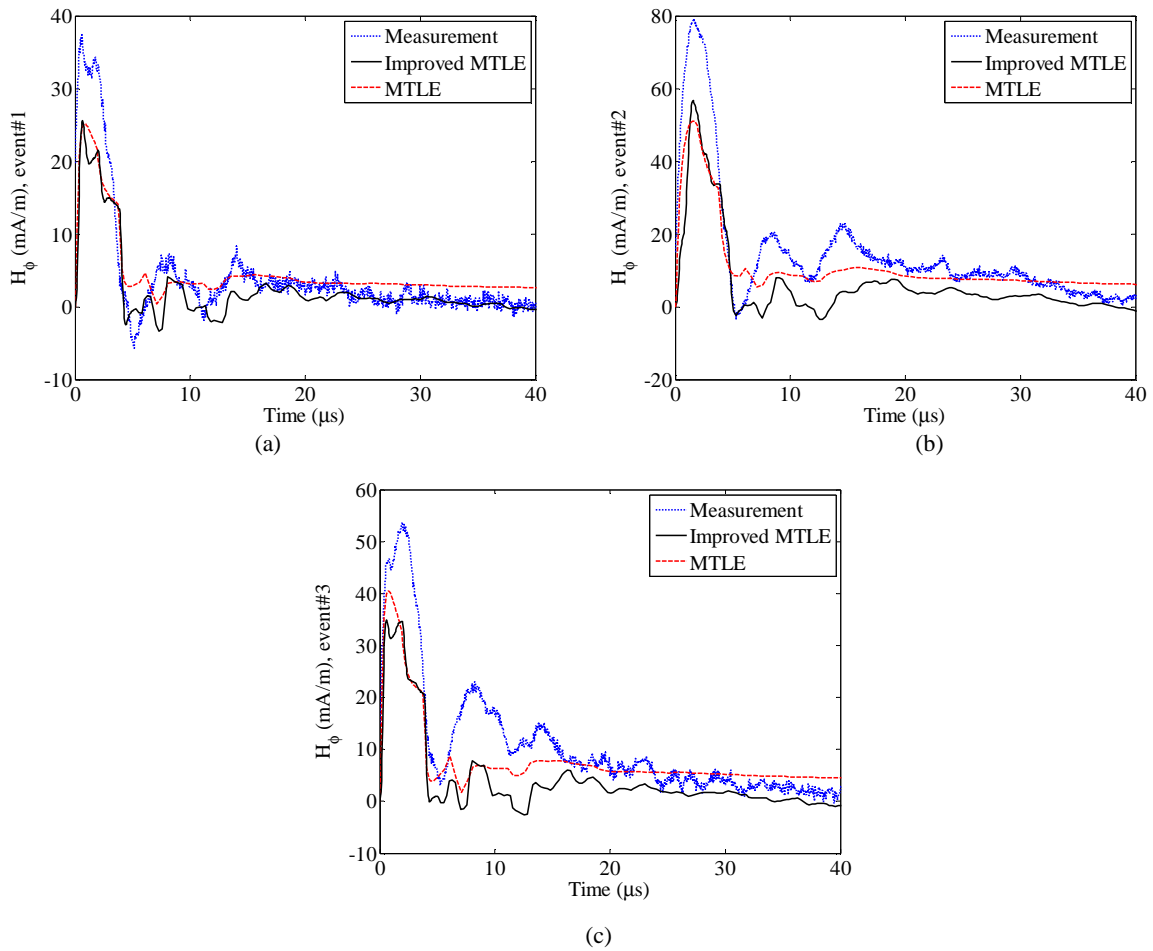


Fig. 4.7 Comparison of simulated azimuthal magnetic fields at 50.9 km using the original MTLE model and the proposed improved version with the measured waveform: (a) Event #1, (b) Event #2, (c) Event #3.

response for larger values of the upward connecting leader length (100 m) does not show this double-peak feature. The field's narrow undershoot and zero crossing are not significantly affected by the height of the upward connecting leader.

Fig. 4.9 presents the effect of the return stroke speed on the computed magnetic field for the same configuration as that of Fig. 4.8. It can be seen that the return stroke speed does not significantly affect the magnetic field for strikes to tall tower.

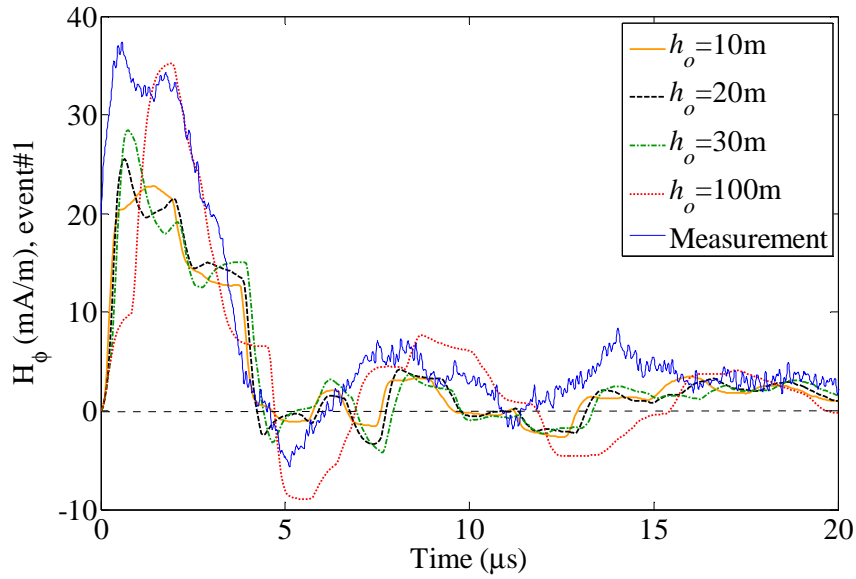


Fig. 4.8 Effect of the height of the upward connecting leader on the computed magnetic field at 50.9 km using the proposed improved version model (event #1).

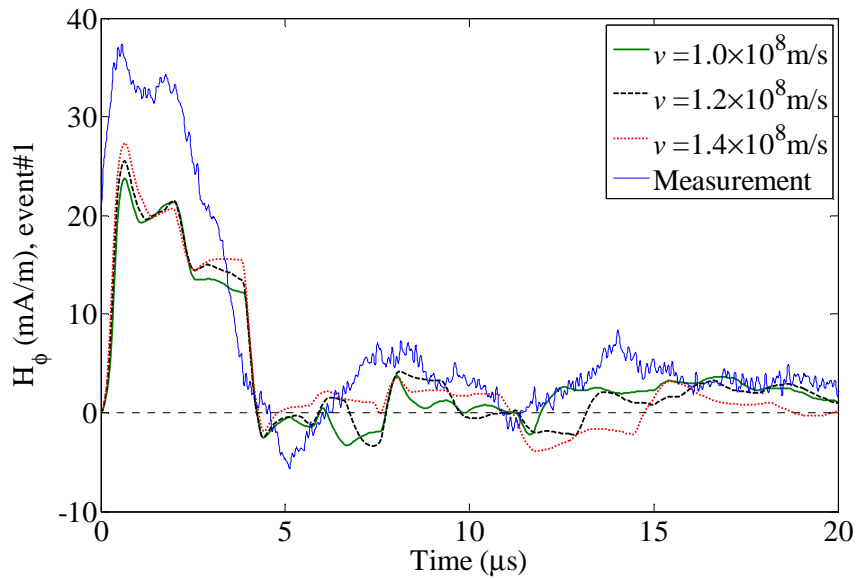


Fig. 4.9 Effect of return stroke speed on the computed magnetic field at 50.9 km using the proposed improved version model (event #1).

4.4 Conclusions

In this chapter, we proposed an improved version of the engineering models for return-strokes to tall structures that takes into account the presence of possible reflections at the return stroke wavefront and a return stroke initiation above the structure due to an upward connecting leader. Based on the approach proposed by Shostak et al. [30], we derived closed-form iterative solutions for the current distribution along the channel and the strike object.

Simulation results for the magnetic fields are compared with experimental waveforms associated with lightning strikes to the CN Tower (553 m). It is shown that taking into account the reflections at the return-stroke wavefront results in better reproducing the fine structure of the magnetic field waveforms, including the double-peak, the early narrow undershoot and the far-field zero crossing. The results also suggest that the typical double-peak response of the radiated fields from tall structures might be due to the combined effect of upward-connecting leaders and reflections at the return stroke wavefront.

Chapter 5

Lightning Electromagnetic Fields at Very Close Distances Associated with Lightning Strikes to the Gaisberg Tower in Austria

5.1 Introduction

As we have seen in Chapters 2 and 3, the effect of the presence of a strike object on the radiated electric and magnetic field depends essentially on the height of the strike object and on the distance to the observation point. For observation points located at distances exceeding the height of the tower, the presence of the tower results in a substantial increase of the electric and magnetic field peaks (e.g., [27, 34-35]). On the other hand, theoretical analyses suggest that the presence of the tower at distances of about the height of the tower or less could result in a significant decrease of the electric field peak (e.g., [35, 73-74]), and sometimes in an inversion of polarity [115, 128]. Pavanello et al. [111, 136] have also shown that measured distant electric and magnetic fields associated with lightning return-strokes to the Toronto CN Tower (553 m tall) exhibit a first zero crossing about 5 microseconds after the onset of the return-stroke. This early zero crossing is part of a narrow undershoot, which is due to the transient processes along the tower (the undershoot occurs at a time given approximately by twice the propagation time along the tower) [136].

Signatures of close electric field of dart leader/return stroke sequences in rocket-triggered lightning have been studied e.g., in [137-140]. Rubinstein et al. [137] analyzed vertical

electric field waveforms for 31 leader/return-stroke sequences at 500 m and two leader/return-stroke sequences at 30 m from the lightning channel. The data were obtained at the Kennedy Space Center, Florida, in 1986 and 1991, respectively, using the classical rocket-and-wire technique (Chapter 7 of [1]). Specifically, they found, that at tens to hundreds of meters from the lightning channel the leader/return-stroke vertical electric field sequences exhibit a characteristic asymmetric V-shaped waveform with an initial negative transition being associated with the descending leader and the following positive transition with the return stroke. Note that the atmospheric electricity sign convention is used throughout this chapter, according to which a downward directed field is defined as positive [141]. For the radial electric field, the same convention used by Baba and Rakov [128] is used, according to which an outward directed field is defined as positive (see also Fig. 5.1). The bottom of the V corresponds to the transition from the leader stage to the return stroke stage [137].

Assuming a uniform charge distribution model for the leader, Rubinstein et al. [137] found that about 90 % of the leader electric field change measured at 30 m was determined by the charge on the channel below around 280 m, while at 500 m the corresponding contributing channel length was 2.5 km.

Multiple-station measurements of triggered lightning electric fields were first performed in 1993 at Camp Blanding, Florida [142] and in the same year at Fort McClellan, Alabama [143]. Electric fields were measured at 30, 50, and 110 m from the lightning channel at Camp Blanding and at 9.3 and 19.3 m at Fort McClellan. Rakov et al. [144] provided a detailed analysis of these experimental data showing that the variation of the close leader electric field change with distance was slower than the inverse proportionality (r^{-1}) predicted by a uniformly charged leader model. In 2001, Crawford et al. [138] reported multiple-station measurements of the leader electric field change for strokes in triggered lightning flashes in 1997, 1998, and 1999 at Camp Blanding, Florida. The fields were measured at distances from the lightning channel ranging from 10 to 621 m. In contrast with the 1993 data analyzed by Rakov et al. [144], Crawford et al. found that most of the 1997-1999 data indicate a distance dependence of the leader electric field change close to an inverse proportionality, consistent with a uniform distribution of leader charge.

In this chapter, we present and discuss measurements of electric (vertical and radial) and azimuthal magnetic fields from leaders and return strokes associated with lightning strikes to the 100-m tall Gaisberg tower in Austria obtained in 2007 and 2008. The fields were

measured at a distance of about 20 m from the tower's vertical axis. Simultaneously with the fields, return-stroke currents were also measured at the top of the tower.

The measured data will be used to test engineering models and antenna-theory (or electromagnetic) models for the return stroke.

5.2 Experimental setup

5.2.1 Gaisberg Tower

The Gaisberg tower is a 100-m tall radio tower located 1287 m above sea level on the top of a mountain 5 km east of the city of Salzburg, Austria. On average, the tower is exposed to about 60 upward initiated flashes per year [105]. The tower dimensions at ground level are 10.5 m × 10.5 m.

5.2.2 Current Measurement System

The current at the tower top is measured with a current viewing shunt with 0.25 mΩ and a total bandwidth of 0 Hz to 3.2 MHz. The electrical signal is split into two channels with a measuring range of ± 2 kA and ± 40 kA respectively. The signals of these two channels are routed to the bottom of the tower via fiber optic links (Isobe 3000, bandwidth 0 Hz – 15 MHz) to the recording system consisting of a two-channel 20 MS/s, 8-bit digitizer. The recording time for each event is 800 ms with a 15-ms pre-trigger.

5.2.3 Electromagnetic Field Measurement

Radial electric fields at 20 m distance from the tower center axis were measured using an active spherical electric field sensor (TSN 245-E30, Thomson CSF, 1 kHz – 150 MHz). A similar sensor but with a different sensitivity (TSN 245-E31, Thomson CSF, 1 kHz – 150 MHz) was used to measure the vertical electric field at 22 m. The azimuthal magnetic field at 20 m was measured using a loop-antenna magnetic field sensor (TSN 245-H31, Thomson CSF, 2 kHz – 150 MHz). All the sensors were located on the metallic roof of a one-storey building at a height of about 3 meters above ground. The measured signals from the sensors were relayed via fiber optic links to the recording system, which consisted of a 50-MS/s, 8-bit digitizer with 1 MB memory per channel and a computer controller with local clock. The time scale of the digitizer was set to 20-ns resolution and segmented for recording up to twenty

200- μ s-long EM field pulses per lightning flash. A 40-MHz low pass filtering was applied to both electric and magnetic field signals to reduce high frequency noise and to minimize aliasing.

It is worth noting that the electric field sensors being located on the top of metallic structures could result in a local enhancement of the electric field of a factor typically ranging from 1.5 to 2.5 [98, 123, 145-146], see Chapter 6. However, a calibration campaign aiming at evaluating such an enhancement effect was carried out in the summer of 2008, measuring waveforms associated with distant lightning return strokes using as reference a flat plate antenna located on the surface of the ground [147] The campaign revealed that the enhancement effect of the metallic structures on the measured electric fields was minimal (about 1.1).

5.3 Presentation of experimental data

The whole measurement campaign includes three different measurement setups. All the data are associated with lightning strikes to the Gaisberg tower and each setup includes records of lightning current waveforms measured on the top of the tower. In the first setup (from May 1st, 2007 to September 10th, 2007), we measured the vertical electric field and the azimuthal magnetic field, respectively at 22 m and 20 m from the center of the tower. In the second setup (from September 11th, 2007 to June 31st, 2008), we obtained records of the radial electric field and azimuthal magnetic field, respectively at 22 m and 20 m from the center of the tower. Finally, for the third setup (from July 1st, 2008 to August 1st, 2008), we measured the vertical and radial components of the electric field at 22 m and 20 m from the tower, respectively. The three setups are illustrated in Fig. 5.1.

Representative sets of simultaneously measured return-stroke current and associated fields for each setup are shown in Fig. 5.2, Fig. 5.3, and Fig. 5.4, respectively. Note that a high frequency noise is superimposed on the first peak of the return-stroke current whose origin is unknown and currently under investigation [148]. The statistical data on lightning current peak presented in this work are obtained by applying a 650-kHz filter to the measured current waveforms. The filtered waveforms are shown in Fig. 5.2b, Fig. 5.3b, and Fig. 5.4b. Note that, unlike Diendorfer et al. [105] who applied in their analysis a 250-kHz filter, we chose a 650-kHz filter because the resulting current waveforms have similar early-time waveshapes to those of the corresponding magnetic fields measured at 20 m.

It is worth noting that this is the first time that recorded waveforms of the vertical and radial electric fields are obtained at such close distances. As discussed in [149], there is an inherent difficulty in measuring the distant radial electric field component of lightning above the ground because of the overshadowing effect of the vertical electric field component that results even from a small tilt in the measuring antenna. Indeed, for observation points located on the ground or a few meters above the ground, the vertical electric field magnitude is much larger than that of the radial component (typically two orders of magnitude). This may explain the fact that data on radial electric fields are very rare. To the best of the authors' knowledge, there are only four sets of available data: (1) The data obtained by Thomson et al. [150], who reported on the first ever simultaneous measurements of both the radial and the vertical E-Field components for distant strokes. (2) The data by Michishita et al. [151] consisting of vertical and radial fields at distances beyond 16 km, (3) the data by Miki et al. [152] who measured simultaneously both vertical and horizontal electric fields at distances from the triggered lightning channel attachment point ranging from 0.1 to 1.6 m, and (4) the recent data on current and radial electric fields associated to return strokes of triggered lightning presented by Barbosa et al. [153]. Note that model-predicted vertical and radial electric field waveforms were presented in [128].

For lightning strikes to tall structures and at very close distances (within 50 m or so), the two electric field components (vertical and radial) become comparable in magnitude, as shown by simulations [128] [149] and verified by experimental data associated with lightning strikes to the Austrian Gaisberg tower which will be presented in this chapter. The obtained data will be analyzed in the next section.

5.4 Data analysis

A total of 13 upward initiated flashes containing 40 ICC pulses (pulses superimposed on the ICC, the initial continuing current typical for upward initiated flashes) and 44 return-strokes were recorded during the whole measuring campaign, although the sample size was different depending on the studied quantities and examined features for each data set.

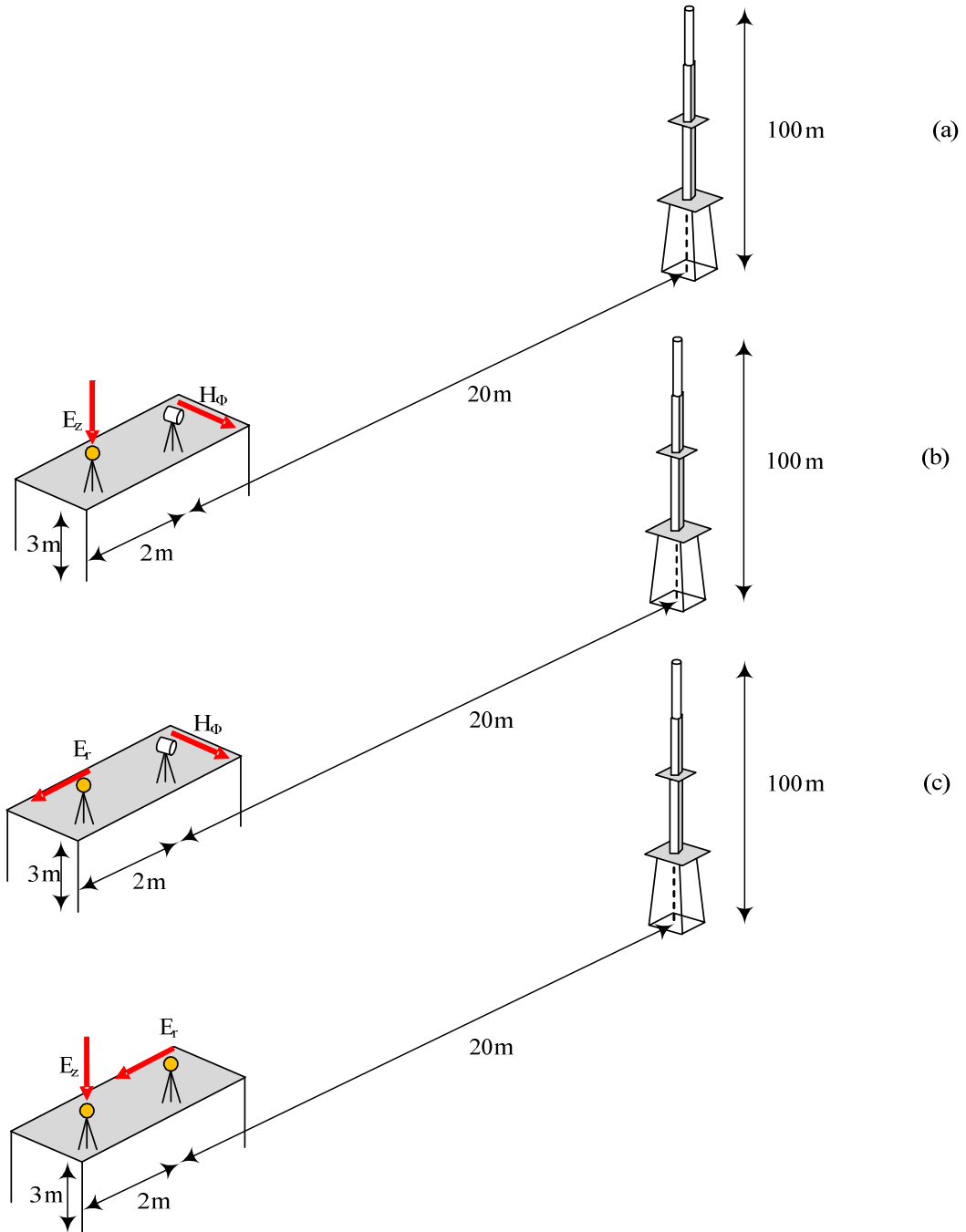


Fig. 5.1 3D schematic view of the tower and the near field measuring campaign (a) first, (b) second, and (c) third setup (not in scale).

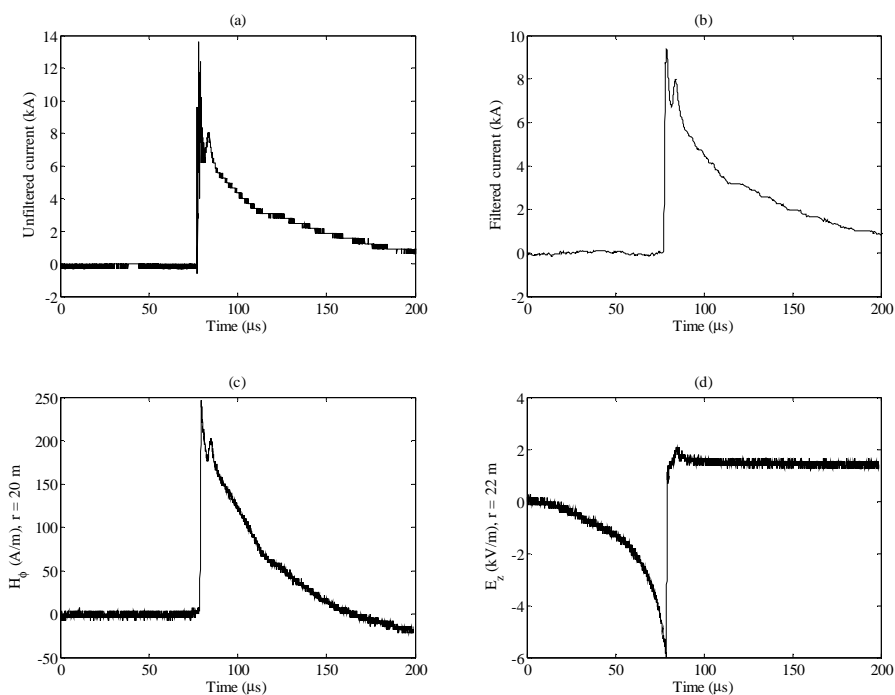


Fig. 5.2 Representative waveforms of the data recorded during first setup on 2007-10-18, (a) tower top unfiltered current, (b) tower top 650 kHz filtered current, (c) azimuthal magnetic field at $r = 20$ m, (d) vertical electric field at $r = 22$ m (flash 574, stroke 1 of 5). Note that the faster decay of the magnetic field waveforms at late times and their unexpected zero crossing are presumably due to the value of the time constant of the H-field sensor which is in the order of 100 microseconds.

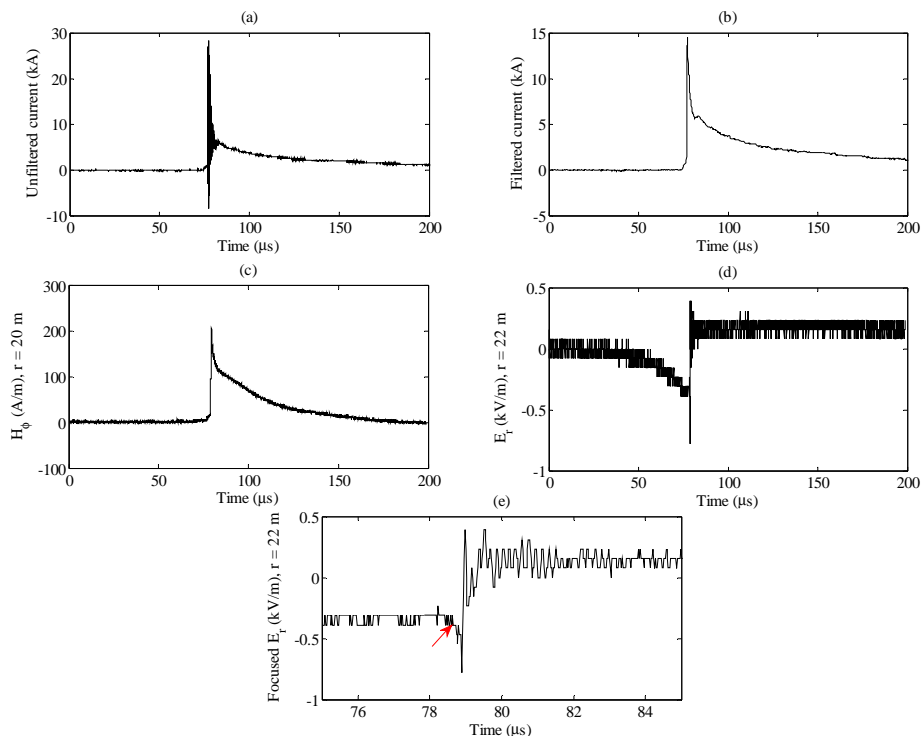


Fig. 5.3 Representative waveforms of the data recorded during second setup on 2008-03-12, (a) tower top unfiltered current, (b) tower top 650 kHz filtered current, (c) azimuthal magnetic field at $r = 20$ m, (d), and radial electric field at $r = 22$ m. Expanded waveform of the radial electric field is shown in (e). Note that the faster decay of the magnetic field waveforms at late times and their unexpected zero crossing are presumably due to the value of the time constant of the H-field sensor which is in the order of 100 microseconds (flash 644, stroke 2 of 2). The arrow represents the transition between the leader and the return stroke.

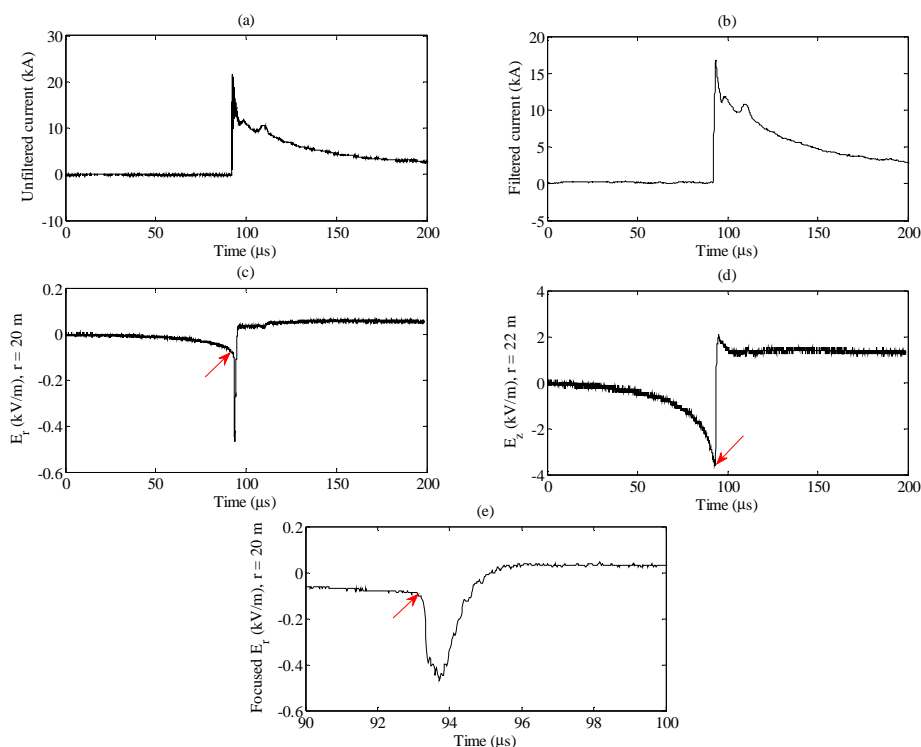


Fig. 5.4 Representative waveforms of the data recorded during third setup on 2008-07-20, (a) tower top unfiltered current, (b) tower top 650 KHz filtered current, (c) radial electric field at $r = 20$ m, and (d) vertical electric field at $r = 22$ m (flash 682, stroke 1 of 3). Expanded waveform of the radial electric field is shown in (e). The arrow represents the transition between the leader and the return stroke.

5.4.1 Magnetic fields

Table 5.1 summarizes the peak values of the magnetic fields and associated return stroke currents measured at the top of the Gaisberg tower. The corresponding minimum, mean, standard deviation, and maximum values are also summarized in Table 5.2. From Fig. 5.2 and Fig. 5.3, it can be observed, as expected at these distances [154], that the magnetic field waveforms are characterized by waveshapes similar to those of the incident currents. The faster decay of the magnetic field waveforms at late times and their unexpected zero crossing are presumably due to the value of the time constant of the H-field sensor which is in the order of 100 microseconds. Fig. 5.5 presents a histogram of the magnetic field peak at 20 m for the first and second data sets recorded in the periods from 2007-05-01 to 2007-09-10 and 2008-07-01 to 2008-08-01. The mean value of the magnetic field is 158.9 A/m and its standard deviation is 94.5 A/m. Fig. 5.6 presents a scatter plot of the measured magnetic field peaks as a function of the measured current peaks. The regression curve in the scatter plot shows a linear relationship between peak magnetic fields and the corresponding peak currents. The correlation coefficient indicated in the figure as $R = 0.92$ confirms the presence of a strong linear relationship between the measured peak magnetic field and the peak current. In

the same figure, we have plotted the prediction of Ampere's law. Note, however, that Ampere's law should be applied to the current at the tower base. Numerical simulations indicate that the peak current for a typical subsequent stroke at the bottom of a 100-m tall structure is about 1.25 times larger than the current at the top as a result of current reflections at the tower top and tower bottom. Such a value is still not large enough to explain the measured levels of magnetic field peaks. The observed discrepancy could also be due to the filtering applied to the measured current waveforms which might have resulted in an underestimation of the peak current. Other reasons could partially explain this enhancement, such as the proximity to the tower base and other close-by metallic structures, and also to the presence of a radial ground wire connected to the base of the tower which runs close to the magnetic field sensor and might give a non-negligible contribution to the overall magnetic field at the sensor location.

Note, finally, that the used magnetic field sensor was checked and re-calibrated after the experimental campaign in the EMC Laboratory of the Swiss Federal Institute of Technology (EPFL) and found to be working properly.

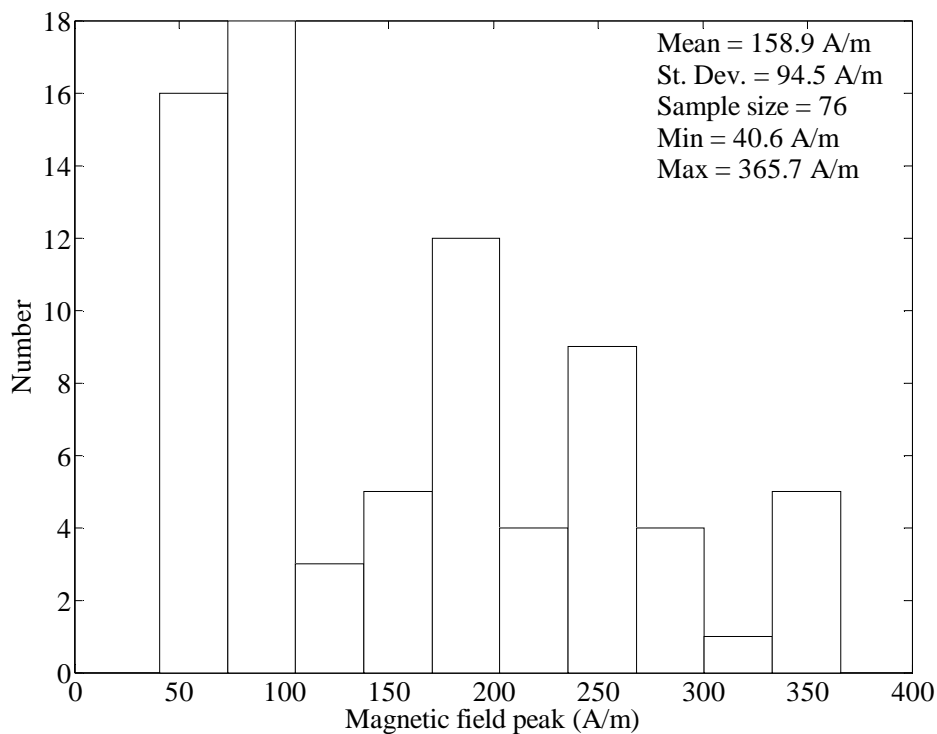


Fig. 5.5 Histogram of the magnetic field peak at $r = 20$ m for the first and second data set recorded in the period from 2007-05-01 to 2007-09-10 and 2008-07-01 to 2008-08-01.

Table 5.1 Summary of the magnetic field and current peaks

Date	Hour	Flash #	Event	Current peak (kA)	Magnetic field peak (A/m)
2007-10-18	16:11:54	568	1	13.8	364.4
			2	22.7	Saturated at 483.7
2007-10-18	19:28:42	569	1*	2.6	48.9
			2*	2.5	47.9
			3*	7.6	175.9
			4*	4	105
			5*	7.6	192.5
			6*	2.2	57.2
			7*	5.3	135.1
			8*	6.6	165.4
			9*	11.6	293.2
			10*	4.1	101.9
			11*	2.6	75.1
			12*	3.3	88.6
			13*	3.1	83.5
2007-10-18	19:31:59	570	1*	2.5	63.9
			2*	1.8	46
			3*	1.8	43
			4*	1.8	46.8
			5*	2.6	63
			6*	1.8	45.1
			7*	1.8	40.6
S2007-10-18	19:34:29	571	2*	2.8	72.5
			3*	2.9	75
			4*	5.4	149.9
			6*	3.6	96.7
			7*	3.4	90.6
			8*	2.5	65.2
			9*	3	77.4
			10*	4.4	107.3
			11*	10.1	247.7
			12*	1.9	46.8
			13*	9.6	241.7
			15*	2.8	70.3
			16*	3.4	92.6
2007-10-18	19:36:38	572	1	10.8	252
			2	7.6	180.9
			3	5.6	140.3
			4	2.9	68.7
			5	13.7	295.2
			6	9	234.2
			7	13.5	203.1
			8	11	235.6
2007-10-19	11:05:22	574	1	9.6	240.2
			2	3	74.5
			3	10.5	258.2
			4	7.3	175.5
			5	13.5	192.4
2007-11-06	08:19:05	576	1	22.8	277.8
			2	11	240.1
2007-11-10	17:44:33	585	1*	4.2	98
2007-11-10	17:54:54	586	1	16.7	364.3
			2	24	361.2
2007-11-10	17:57:41	587	1	2.2	51.6
			2	11.5	139.1
2007-11-10	17:59:40	588	1	27.6	Saturated at 485.4
			2	8	192.3
			3	4.1	107.6
			5	7.5	186.6
			6	20	364.1
			7	3.7	102.2
			8	15.7	238.5
			9	10.1	202.4
			10	2.9	77.4
			11	17.3	265.5
			12	11.9	248.8
			13	3.9	81.6
			14	10.4	154.2
			15	15.7	221.5
			16	14.7	192.1
			2008-12-03	16-43-27	644
			2	13.4	179.7
2008-12-03	17-15-57	645	1*	18.3	330.7
			2*	9.8	173.1
			3*	4.6	81.4
			4*	12.1	219.6
			5*	33.7	Saturated at 466.4
			6*	5.2	91.9
			7	14.8	268.3

* ICC pulse

Table 5.2 Minimum, mean, standard deviation, and maximum values of the magnetic field and current peaks presented in Table 5.1

Number of events	Magnetic field Peak (A/m)				Current Peak (kA)			
	Min	Mean	St. Dev.	Max	Min	Mean	St. Dev.	Max
76	40.6	158.9	94.5	365.7	1.8	7.9	5.7	24.0

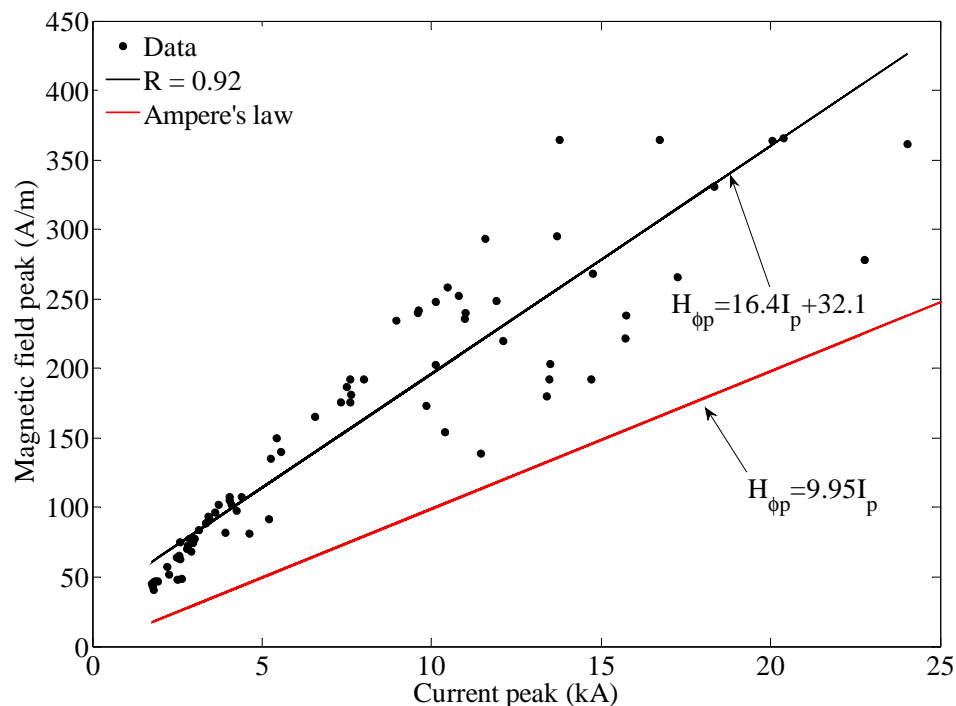


Fig. 5.6 Scatter plot and corresponding linear regression curve of the current peak and the magnetic field peak at $r = 20$ m for the first and second data set recorded in the period from 2007-05-01 to 2007-09-10 and 2008-07-01 to 2008-08-01. The curve of the Ampere's law is also included.

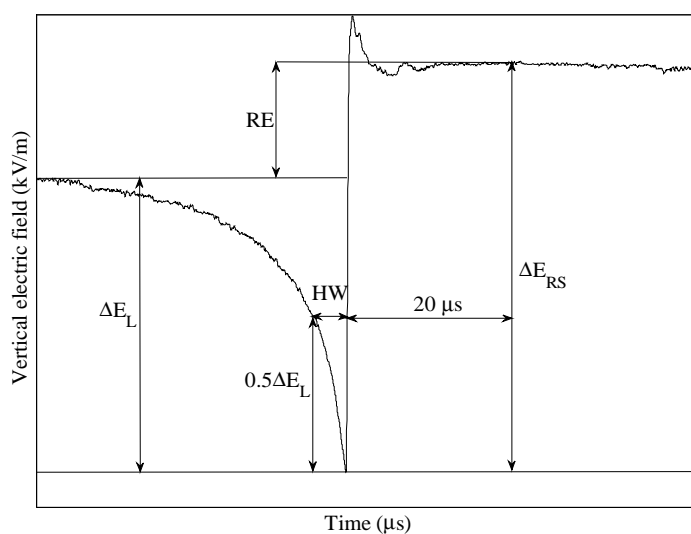
5.4.2 Vertical Electric fields

It can be seen from Fig. 5.2 and Fig. 5.4 that the overall (leader + return-stroke) vertical electric field waveforms appear as asymmetrical V-shaped pulses. The initial, relatively slow, negative electric field change is due to the downward leader and the following fast positive field change is due to the upward propagating return stroke phase of the lightning discharge [137].

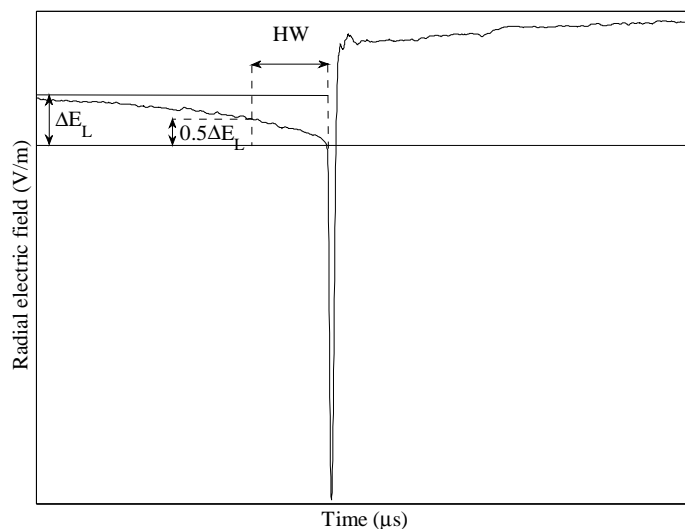
Table 5.3 and Table 5.4 summarize the parameters associated with leader-return stroke vertical electric field waveforms. ΔE_L and ΔE_{RS} are the magnitudes of the electric field changes due to the leader and the return stroke, respectively, and RE is the so-called residual electric field defined as $RE = \Delta E_L - \Delta E_{RS}$ [140]. ΔE_L , ΔE_{RS} and half peak width (HW) are defined following the same definition of Rakov et al. [140] and Rubinstein et al. [137], as

illustrated in Fig. 5.7a. Note that RE was originally defined only for the case of $\Delta E_L > \Delta E_{RS}$ [140]. In this chapter, we extend this definition to other cases as well.

Fig. 5.8 presents a histogram of the leader vertical electric field change ΔE_L at $r = 22$ m for the first and third data sets recorded in the periods from 2007-05-01 to 2007-09-10 and 2008-07-01 to 2008-08-01. Fig. 5.8 and Fig. 5.9 present, for the same data sets, the histograms of the return stroke vertical electric field change ΔE_{RS} and the residual electric field RE. The obtained histograms are, as expected, indicative of log-normal distributions. The following observations can be made on the obtained data.



(a)



(b)

Fig. 5.7 Definition of the leader electric field change, ΔE_L , return stroke electric field change, ΔE_{RS} (only for vertical), half peak width, HW, of the leader + return stroke field sequences, and residual electric field, RE (only for vertical) for (a) vertical and (b) radial electric fields.

Table 5.3 Summary of the vertical electric field at 22 m

Date	Hour	Flash #	Stroke	ΔE_L (kV/m)	ΔE_{RS} (kV/m)	RE (kV/m)	HW (μ s)
2007-10-18	19:28:42	569	1*	1.3	2.1	-0.85	18.9
			2*	1.5	1.9	-0.41	14.4
			3*	3.7	5.4	-1.7	4.9
			4*	2.4	3.2	-0.81	7
			5*	3.6	5.3	-1.65	4.7
			6*	1	2.1	-1.04	13.4
			7*	2.5	3.8	-1.33	6.7
			8*	4	4.7	-0.77	8.1
			9*	5.7	6.9	-1.24	4.6
			10*	2.4	3.3	-0.87	12.6
			11*	1.5	1.9	-0.41	11.4
			12*	2	3	-0.98	10.7
			13*	1.6	2.9	-1.32	12.9
2007-10-18	19:31:59	570	2*	1.4	1.8	-0.37	17.4
			4*	1.4	1.5	-0.16	20.2
			5*	2	2.4	-0.42	21.7
			6*	1.3	2	-0.78	22.9
			7*	0.6	1.9	-1.3	24
2007-10-18	19:34:29	571	2*	1.9	2.9	-0.94	15.8
			3*	2.2	3.1	-0.90	17.8
			4*	2.3	4.5	-2.27	5.7
			6*	1.4	3.6	-2.17	11
			7*	2.5	3.5	-1.01	18.3
			8*	2.2	3	-0.81	23.7
			9*	2.7	3.2	-0.48	17.6
			10*	3.5	4	-0.50	13
			11*	6.4	7.3	-0.92	9.7
			12*	1.3	2.2	-0.94	23.8
			13*	5.9	6.4	-0.47	6.5
			15*	1.9	2.8	-0.96	11.9
			16*	2	3.6	-1.56	7.7
2007-10-18	19:36:38	572	1	5.6	7.3	-1.67	8
			2	4.1	5.3	-1.2	14.9
			3	3.7	4.7	-1.06	17.9
			4	1.7	2.9	-1.2	19.6
			5	7.2	7.8	-0.59	6.7
			6	5.4	6.3	-0.88	7.4
			7	4.5	6.3	-1.74	15.6
			8	5.2	6.7	-1.49	12.2
2007-10-19	11:05:22	574	1	5.7	7.3	-1.56	10.9
			2	1	3.8	-2.73	31.2
			3	5.4	7.3	-1.9	6.3
			4	3.7	5.4	-1.63	14.8
			5	3.7	6.5	-2.81	16.5
2007-11-06	08:19:05	576	1	5.3	6.9	-1.65	8.9
			2	4.9	6.7	-1.84	17.5
2008-07-20	15:07:17	682	1	2.3	4.1	-1.81	18
			2	1.1	2.8	-1.67	19.4
			3	6.8	6.1	0.66	8.4
2008-08-01	21:48:31	683	1	1.8	3.5	-1.66	24.7
			2	1.3	2.1	-0.85	18.9

* ICC pulse

Table 5.4 Minimum, mean, standard deviation, and maximum values of the vertical electric field parameters (at 22 m) presented in Table 5.3

Number of events	ΔE_L (kV/m)				ΔE_{RS} (kV/m)				RE (kV/m)				HW (μ s)			
	Min	Mean	St. Dev.	Max	Min	Mean	St. Dev.	Max	Min	Mean	St. Dev.	Max	Min	Mean	St. Dev.	Max
51	0.6	3.1	1.8	7.2	1.5	4.3	1.9	7.8	-2.8	-1.2	0.7	0.7	4.6	13.9	6.3	31.2

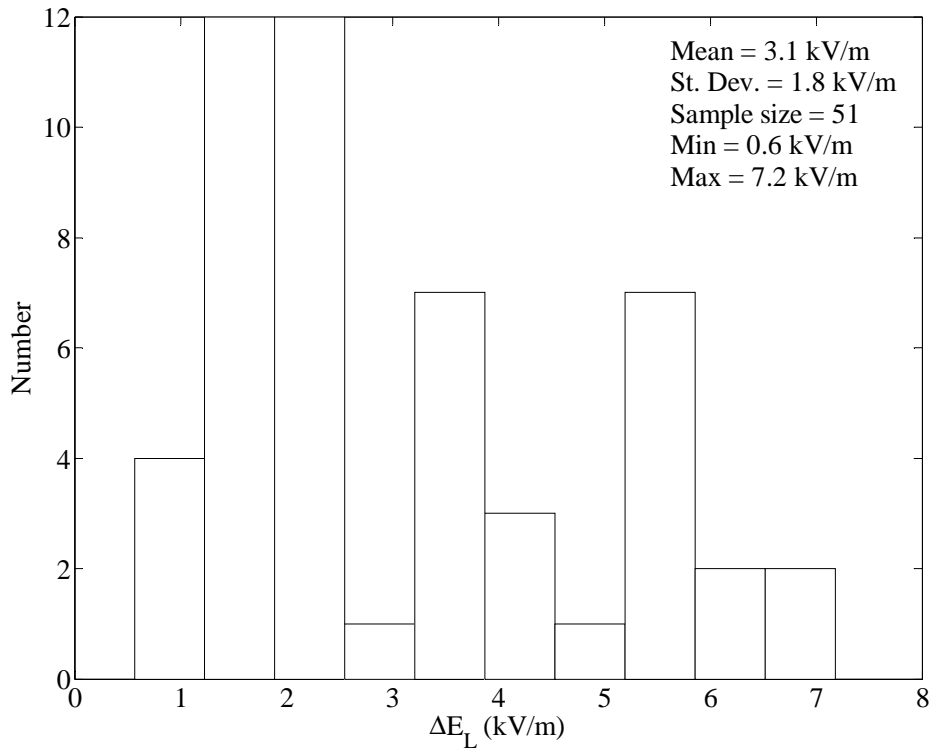


Fig. 5.8 Histograms of the vertical electric leader field change at $r = 22$ m for the first and third data sets recorded in the period from 2007-05-01 to 2007-09-10 and 2008-07-01 to 2008-08-01.

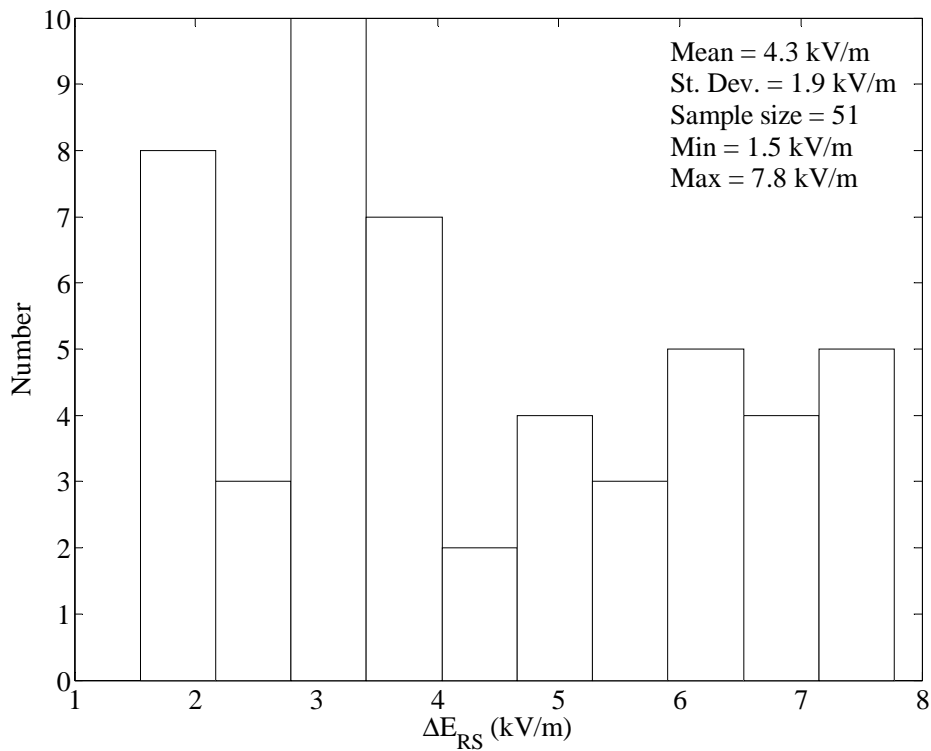


Fig. 5.9 Histograms of the vertical return stroke electric field change at $r = 22$ m for the first and third data sets recorded in the period from 2007-05-01 to 2007-09-10 and 2008-07-01 to 2008-08-01.

5.4.2.1 Magnitude of the return-stroke vertical electric field change

The return-stroke vertical electric field changes at 22 m appear to be significantly smaller than similar measurements obtained using triggered lightning (see e.g., [138]). This is presumably due to the shadowing effect of the tower, which results in a significant decrease of the electric field at distances of about the height of the tower or less (see Chapter 3, Section 3.6.3).

5.4.2.2 Ratio of leader to return stroke electric field change

The electric field change due to the return stroke is found to be larger on average than the leader electric field change. This is in agreement with the data reported by Rubinstein et al. [137] on electric fields measured at 500 m from triggered lightning. Note that the data analyzed in [140] include only selected samples with positive value for the residual electric field ($\Delta E_L > \Delta E_{RS}$).

The corresponding scatter plots versus peak currents of ΔE_L , ΔE_{RS} and RE are shown in Fig. 5.11, Fig. 5.12, and Fig. 5.13 . In accordance with the findings of Rakov et al. [140] related to triggered lightning, it can be seen that strokes having larger peak currents are associated with larger leader and the return stroke electric field changes. The corresponding correlation coefficient indicated in the figures for leader and return stroke vertical electric fields are respectively 0.73 and 0.75. The residual electric field appears to be less sensitive (correlation coefficient of 0.16) to the current peak and shows a slight decrease with increasing peak currents.

5.4.2.3 Initial peak of the return stroke field change

In a significant number of cases (33%), the vertical electric field waveform due to the return stroke is characterized by a first peak which exceeds the typical late-time flattening due to the electrostatic term (see Fig. 5.14). This is in contrast with similar measurements related to triggered lightning (e.g., [137, 140] which do not exhibit such a first peak. This first peak might be due to the radiation term of the field, which is somewhat enhanced by the presence of the tower. However, simulations made by the authors showed no such first peak at that distance. More research to better understand this behavior is underway.

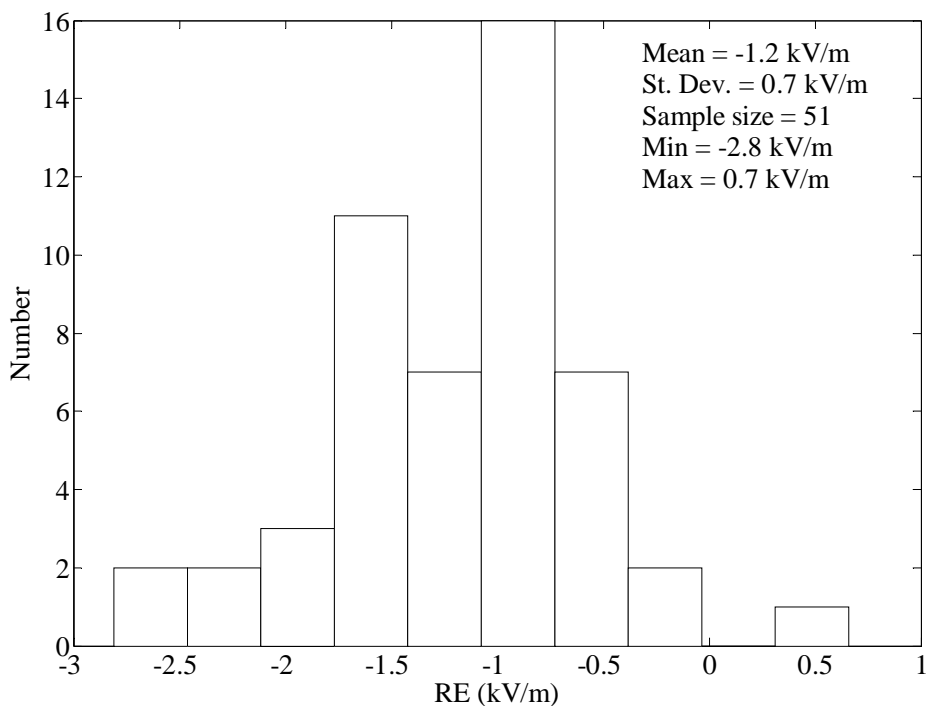


Fig. 5.10 Histograms of the vertical residual electric field change at $r = 22$ m for the first and third data sets recorded in the period from 2007-05-01 to 2007-09-10 and 2008-07-01 to 2008-08-01.

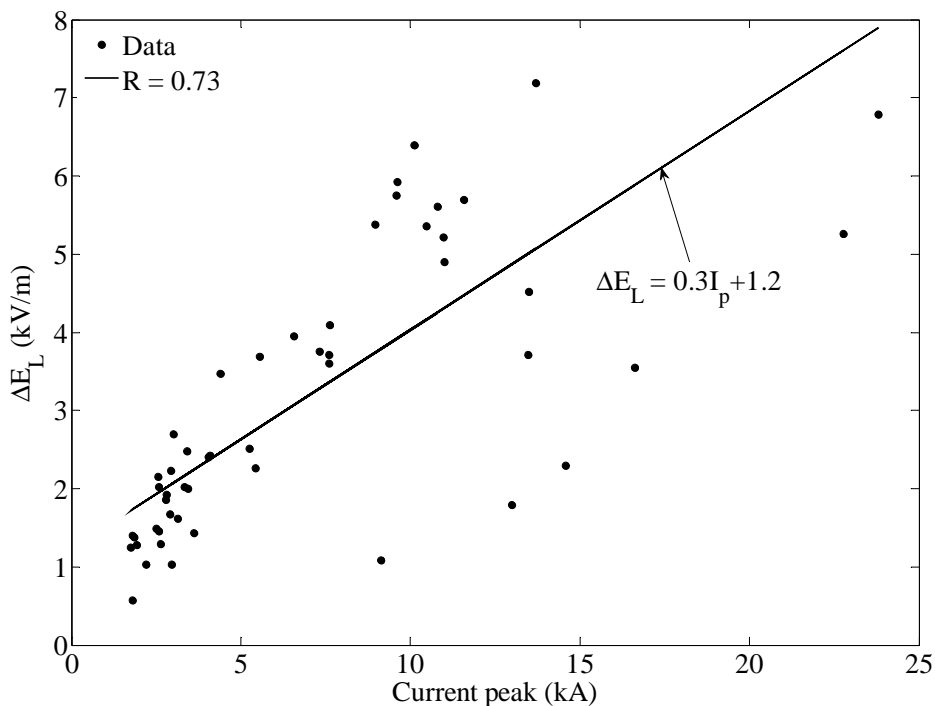


Fig. 5.11 Scatter plot and corresponding linear regression curve of the current peak and the leader vertical electric field change at $r = 22$ m for the first and third data sets recorded in the period from 2007-05-01 to 2007-09-10 and 2008-07-01 to 2008-08-01.

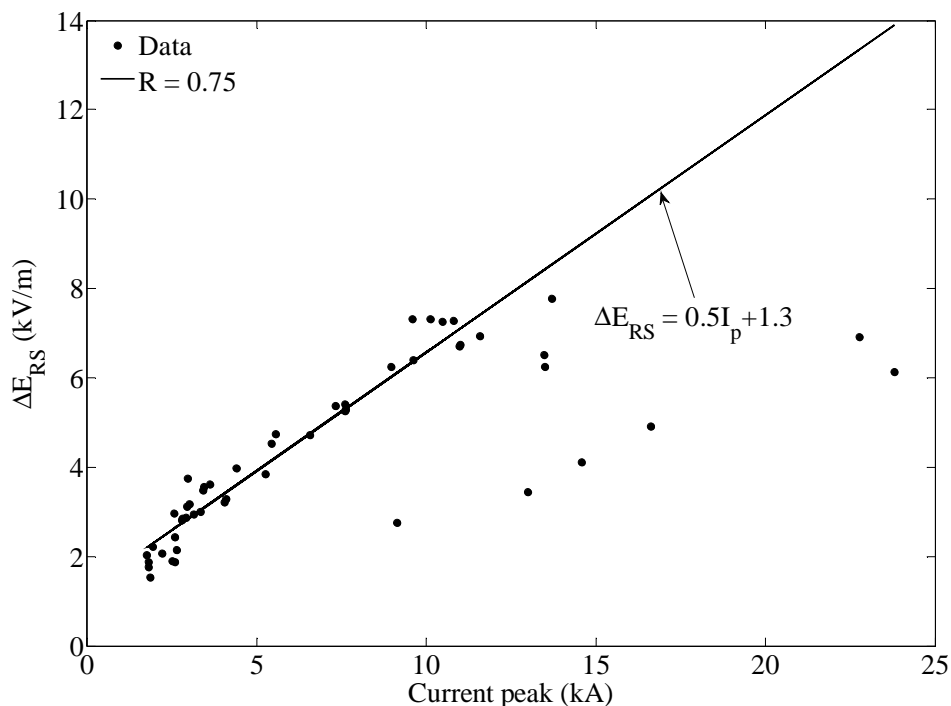


Fig. 5.12 Scatter plot and corresponding linear regression curve of the current peak and the return stroke vertical electric field change at $r = 22$ m for the first and third data set recorded in the period from 2007-05-01 to 2007-09-10 and 2008-07-01 to 2008-08-01.

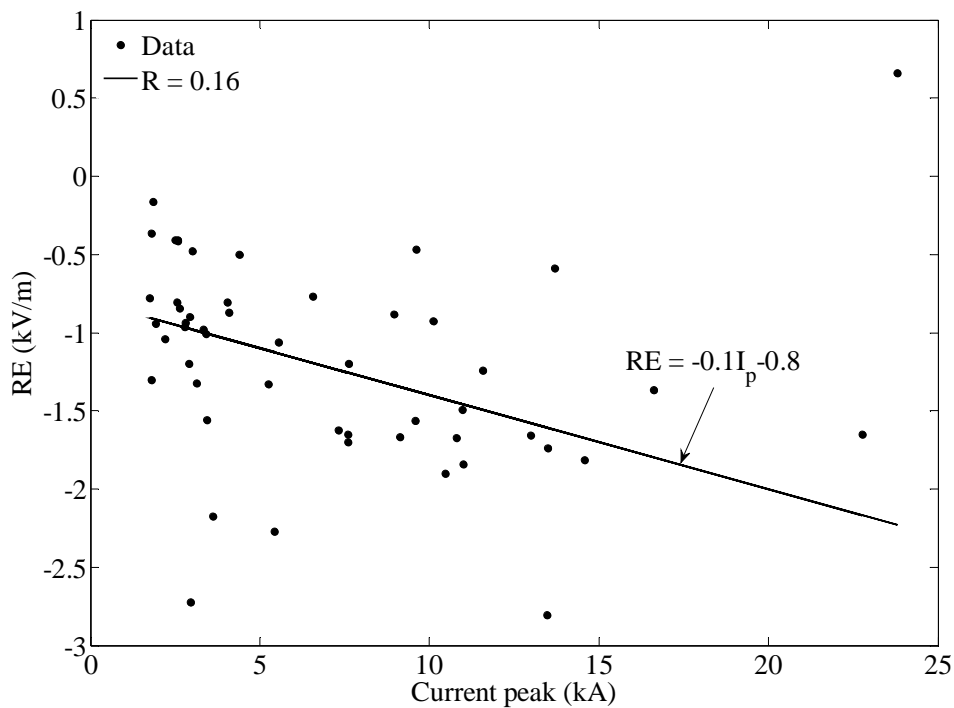


Fig. 5.13 Scatter plot and corresponding linear regression curve of the current peak and the residual vertical electric field change at $r = 22$ m for the first and third data sets recorded in the period from 2007-05-01 to 2007-09-10 and 2008-07-01 to 2008-08-01.

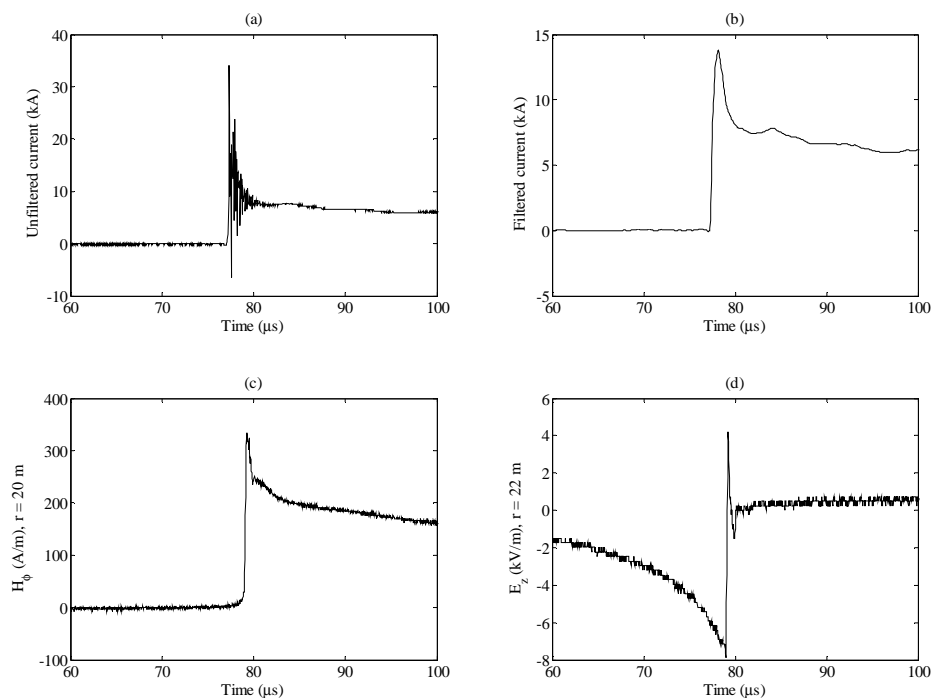


Fig. 5.14 Expanded waveforms of a representative data recorded during first setup on 2007-10-18 featuring an initial first peak of the vertical electric field, (a) tower top unfiltered current, (b) tower top 650 KHz filtered current, (c) azimuthal magnetic field at $r = 20$ m, and (d) vertical electric field at $r = 22$ m (flash 572, stroke 5 of 8).

5.4.2.4 Abnormal leader – return stroke waveforms

About one quarter of measured vertical electric field waveforms (18 pulses out of 75) in the first data set feature an unusual waveform characterized by a positive leader field change followed by a bipolar return stroke field change with a zero crossing time at about $60 \mu\text{s}$. A representative data set is shown in Fig. 5.15. The reasons for this unexpected behavior at these close distances are presently unknown to the authors and calls for further research. In these cases, it was found that the early-time return stroke electric field change exhibits an oscillatory behavior which can be correlated to similar, but more pronounced oscillations discernible in the corresponding current waveform (as can be seen in the expanded views of current and electric field shown in Fig. 5.15e and Fig. 5.15f).

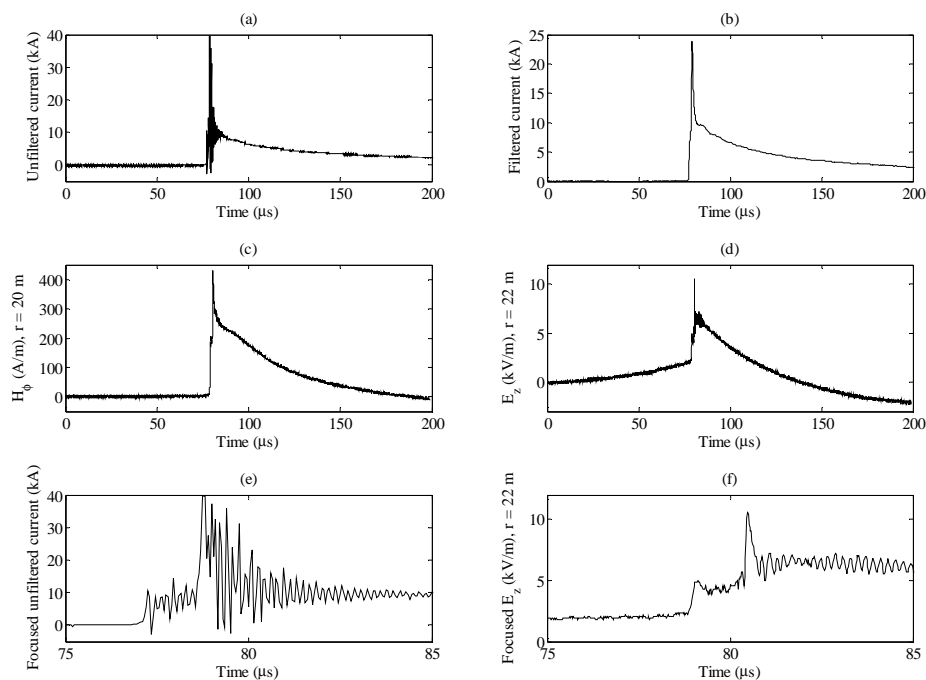


Fig. 5.15 Representative data of an abnormal leader-return stroke waveform recorded during first setup on 2007-11-12, (a) tower top unfiltered current, (b) tower top 650 KHz filtered current, (c) azimuthal magnetic field at $r = 20$ m, (d) vertical electric field at $r = 22$ m showing an increasing ramp for the vertical leader electric field. Expanded waveforms of the current and the electric field are shown in (e) and (f), respectively (flash 586, stroke 2 of 2).

5.4.3 Radial Electric Fields

It can be seen from Fig. 5.3 and Fig. 5.4 that the overall leader-return-stroke radial electric field waveforms are also characterized by asymmetrical V-shaped pulses. However, unlike the vertical fields, the bottom of the V is not associated with the transition from the leader to the return stroke. Rather, the horizontal field due to the return stroke is characterized by a short negative pulse of the order of 1 microsecond or so, starting with a fast negative excursion followed by a positive one. This can be clearly seen in Fig. 5.3e and Fig. 5.4e where we have presented expanded views of the radial electric field waveform.

Table 5.5 and Table 5.6 summarize the parameters associated with leader-return stroke radial electric field waveforms. The magnitudes of the radial electric field changes due to the leader ΔE_L and the width at half peak of the leader field pulse HW are defined and illustrated in Fig. 5.7b.

Table 5.5 Summary of the radial electric field

Date	Hour	Flash #	Stroke	ΔE_L (V/m)	HW (μ s)
2008-03-12	16:43:27	644 (22 m)	1	830	4
			2	390	13
2008-03-12	17:15:57	645 (22 m)	1*	573	6.5
			2*	337	6
			3*	157	15
			4*	332	3.5
			5*	1030	3
			6*	130	20
			7	570	7
			8	895	10
2008-07-20	15:07:17	682 (20 m)	1	85.0	10
			2	68	15
			3	35.7	23
2008-08-01	21:48:31	683 (20 m)	1	153	7
			2	401	15

* ICC pulse

Table 5.6 Minimum, mean, standard deviation, and maximum values of the radial electric field presented in Table 5.5

Number of events	ΔE_L (kV/m)				HW (μ s)			
	Min	Mean	St. Dev.	Max	Min	Mean	St. Dev.	Max
10 (22 m)	130	524.4	311.2	1030	3	8.8	5.6	20
5 (20 m)	35.7	401	147.5	401	7	14	6.1	23

The behaviour of the close electric field change due to the leader has been often analyzed assuming a uniformly charged leader (e.g., [137]). In this case, an analytical expression for the vertical electric field is available [141]. In the Appendix (Section 5.7), we derive an analytical expression for the radial electric field, assuming a uniform charge distribution along the leader with constant speed. The procedure for the vertical electric field was also drawn following the same approach as that used in [137]. The equations for the vertical and radial electric fields read (see Fig. 5.26 for the geometrical parameters)

$$E_z = \frac{\rho_L}{4\pi\epsilon_0} \left[-\frac{1}{\sqrt{r^2 + (H - z)^2}} + \frac{1}{\sqrt{r^2 + (H_B(t) - z)^2}} - \frac{(H - z)(H - H_B(t))}{[r^2 + (H - z)^2]^{\frac{3}{2}}} - \frac{1}{\sqrt{r^2 + (H + z)^2}} + \frac{1}{\sqrt{r^2 + (H_B(t) + z)^2}} - \frac{(H + z)(H - H_B(t))}{[r^2 + (H + z)^2]^{\frac{3}{2}}} \right] \tag{5.1}$$

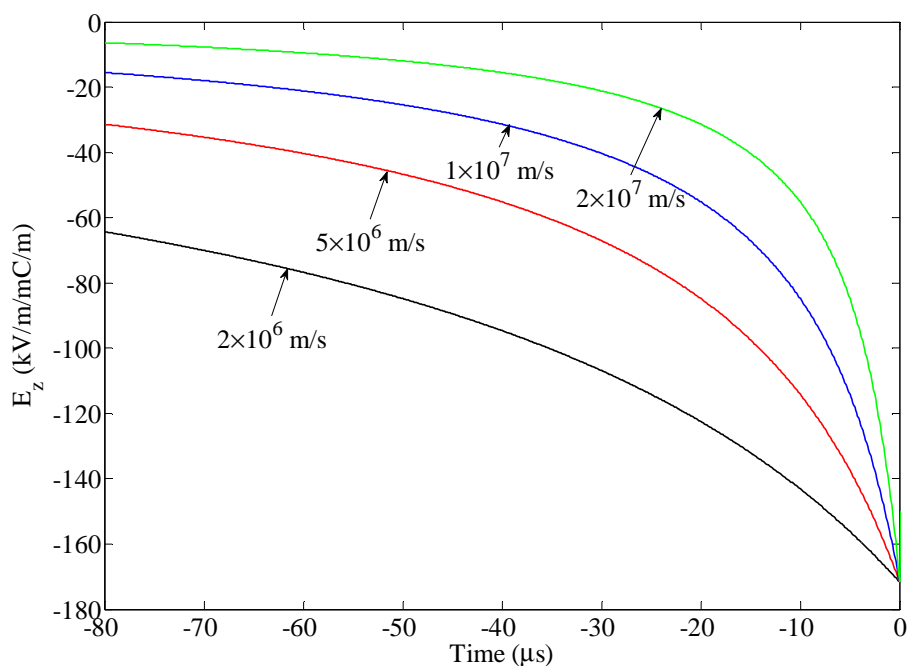
$$E_r = \frac{\rho_L r}{4\pi\epsilon_0} \left[\frac{H-z}{r^2\sqrt{r^2+(H-z)^2}} - \frac{H_B(t)-z}{r^2\sqrt{r^2+(H_B(t)-z)^2}} - \frac{H-H_B(t)}{\left[r^2+(H-z)^2\right]^{\frac{3}{2}}} \right. \\ \left. - \frac{H+z}{r^2\sqrt{r^2+(H+z)^2}} + \frac{H_B(t)+z}{r^2\sqrt{r^2+(H_B(t)+z)^2}} + \frac{H-H_B(t)}{\left[r^2+(H+z)^2\right]^{\frac{3}{2}}} \right] \quad (5.2)$$

in which $H_B(t) = \begin{cases} H - v_L t & \text{for } H > H_T \\ H_T & \text{for } H \leq H_T \end{cases}$, ρ_L is the leader channel linear charge density, v_L

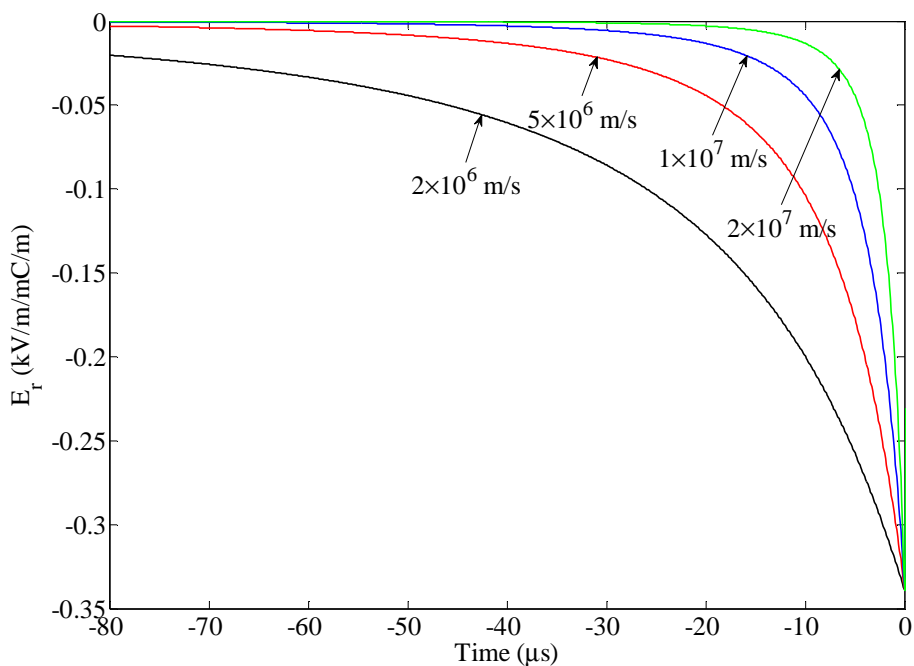
is the leader speed and H_T is the height of the tower.

Fig. 5.16 shows the vertical and radial leader electric field per unit charge density calculated at 20 m for a leader reaching the tower for four different values of the speed v_L : 2 m/ μ s, 5 m/ μ s, 10 m/ μ s, and 20 m/ μ s. These values are in the range of measured data [155]. The half widths of the calculated waveforms corresponding to the above speeds for vertical leader fields are 22.9 μ s, 14 μ s, 8.6 μ s, and 5 μ s, respectively, and for the radial leader fields they are 12.4 μ s, 5.5 μ s, 2.8 μ s, and 1.5 μ s, respectively.

The calculated half width values fall for the most part within the ranges observed in the experimental waveforms given in Table 5.3 and Table 5.5. It should be noted, however, that the calculated width of the V for the vertical field is about three times that of the horizontal field. This contrasts with the experimental data, for which this ratio is on average 1.34. This discrepancy could be attributed to several factors, namely the assumptions in the simplified model: uniform charge distribution and neglecting the presence of the tower and the contribution of charges induced on it.



(a)



(b)

Fig. 5.16 (a) Vertical, and (b) radial leader electric field changes at $r = 20 \text{ m}$ due a uniform charge distribution for different leader speeds.

Note that, on average, the vertical electric field is about 6 times as large as the horizontal electric field. As discussed in Section 5.3, the alignment of the measuring antenna is

extremely important because any tilt would cause a component of the vertical field to appear in the horizontal field signal. We added a tilt in simulations and observed its effect on the agreement between the simulated waveforms and their measured counterparts. We estimated thus the error in the alignment of the horizontal field sensor to be less than about 1 degree. This would result in a contamination of the horizontal field signal of less than 10%.

5.5 Test of Electromagnetic and Engineering Models for the Return Stroke

In this Section, we will use the obtained experimental data on vertical and horizontal electric fields radiated by lightning strikes to the Gaisberg tower to test models for the return stroke stage. We will consider two classes of models (e.g. [12]): (1) electromagnetic or Antenna-Theory (AT) models and (2) engineering models and more specifically the Modified Transmission Line model with exponential decay (MTLE) [37, 129]. The representation of the channel-base current and the modeling parameters will be described in the following subsections.

5.5.1 Channel-Base Current

For the comparison, we selected three sets of data associated with the third setup (see Fig. 5.1c), namely, the 2nd and 3rd strokes of the flash 682, and the 2nd stroke of the flash 683 (Table 5.5). It's worth noting that for the simulations a 750-kHz low pass filter has been applied to the measured current waveforms. The simulated waveforms of electrical fields due the currents filtered by this cut-off frequency showed a better agreement to those of measurement in particular in terms of rise-time. Fig. 5.17 shows the measured current waveforms corresponding to these return strokes.

For the case of the AT model (see Section 5.5.2), the filtered current waveforms are directly used as the exciting source at the top of the tower.

For the case of the engineering model (MTLE), for each event, the so-called 'undisturbed current' is represented using the sum of two Heidler's functions (Chapter 2, Section 2.2.1.4), the parameters of which being determined to reproduce in the best possible way the measured current waveform on the top of the tower:

$$i_0(h,t) = \begin{cases} \frac{I_{o1}}{\eta_1} \frac{(t/\tau_{11})^{N_1}}{1+(t/\tau_{11})^{N_1}} \exp(-t/\tau_{21}) + \frac{I_{o2}}{\eta_2} \frac{(t/\tau_{12})^{N_2}}{1+(t/\tau_{12})^{N_2}} \exp(-t/\tau_{22}) & t \geq 0 \\ 0 & t < 0 \end{cases} \quad (5.3)$$

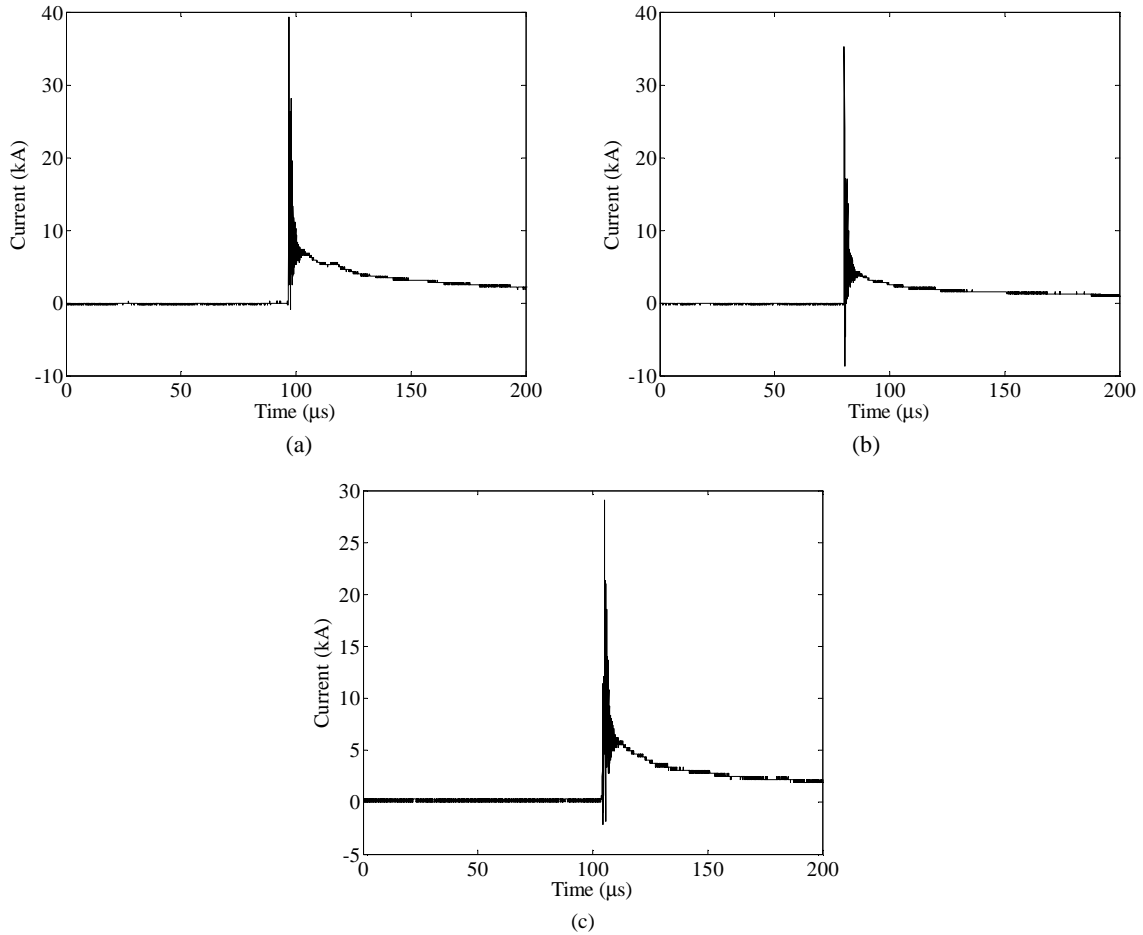


Fig. 5.17 Current records of (a) Flash 682, stroke 2/3, (b) Flash 682, stroke 3/3 (c) Flash 683, stroke 2/2

5.5.2 Antenna Theory Model (AT)

In the AT models, the elevated strike object is represented by conducting wires. The lightning return-stroke channel is modeled as a vertical wire antenna and the lightning return-stroke current is injected by a voltage source at the tip of the tower. The current distribution along the channel and along the tower is found by solving an electric field integral equation ([17]).

In this study, we used the Numerical Electromagnetics Code NEC-4 [58], a well-known and widely used computer code based on the Method of Moments for analyzing the electromagnetic response of antennas and scatterers. Compared to previous NEC versions,

such as NEC-2 used by Baba and Ishii [16], NEC-4 is numerically more efficient and can also model wires buried in the ground or penetrating from the air into the ground [57].

As illustrated in Fig. 5.18, the model for the strike object consists of a 60-m tall vertical wire connected to five inclined wires representing the tower legs. A radius of 0.05 m has been applied to all wires in the model.

In order to reproduce a return stroke speed along the lightning channel lower than the speed of light, distributed series inductances and resistances are included in the modeled channel [16]. The adopted values are those suggested by Baba and Ishii [16], namely $6 \mu\text{H/m}$ and $1 \Omega/\text{m}$, respectively. These values correspond to an equivalent return stroke speed of $120 \text{ m}/\mu\text{s}$. The wire structures representing the tower and the lightning channel were divided into 20-m length segments. The voltage source at the top of the strike object is determined by the desired current waveform on the top of the tower and by the input impedances of the lightning channel and the tower. The detailed procedure is explained in [17].

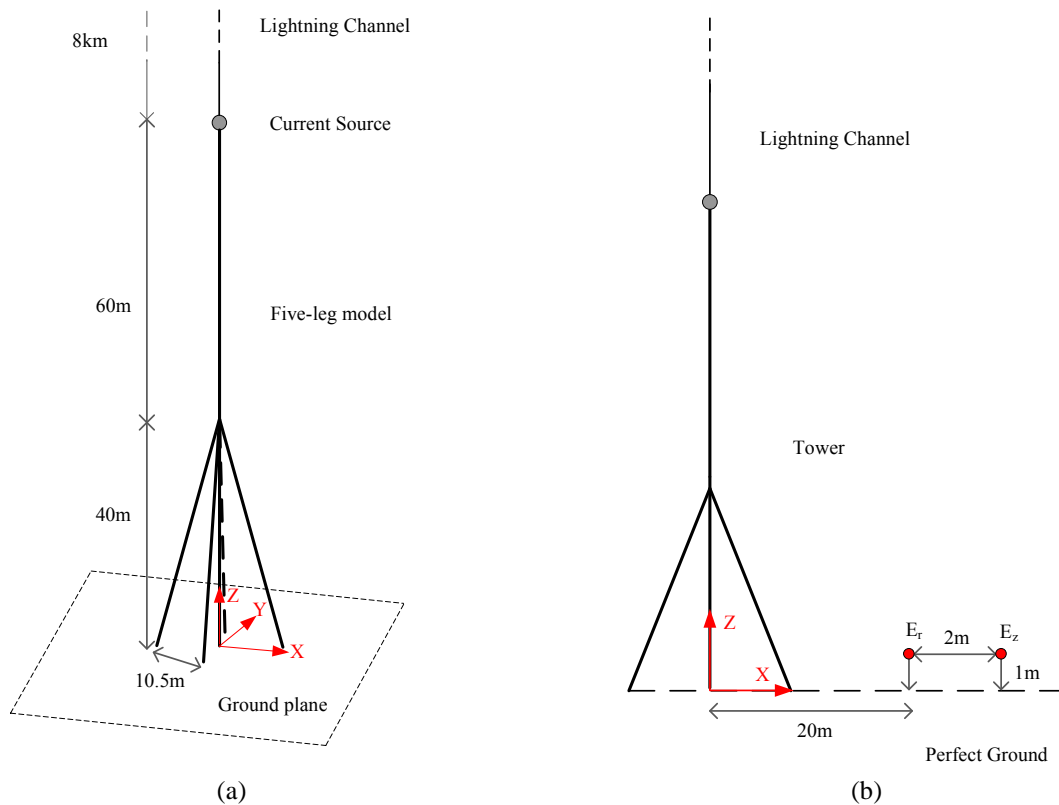


Fig. 5.18 (a) Proposed Five-Leg model for Gaisberg tower as used in NEC simulation, and (b) lateral view of the both tower and vertical and radial electric field sensors above a perfect conducting ground

5.5.3 Engineering Models

In Engineering Models, the presence of a struck object is included considering it as a uniform, lossless transmission line (see Chapter 2).

In this analysis, we adopted the MTLE model [37, 129] . A value of 2 km was assumed for the current decay constant λ [27], and the return stroke speed was assumed to be $v = 120$ m/ μ s.

The parameters of the Heidler’s functions (5.3) representing the current were determined using a trial-and-error approach to obtain the best match with the filtered recorded currents. The determined parameters for each event are presented in Table 5.7.

Table 5.7 Parameters for the undisturbed current, tower reflection coefficients, return-stroke speed, for the MTLE model

Flash	Stroke	v ($\times 10^8$ m/s)	ρ_g	ρ_t	I_{o1} (kA)	τ_{11} (μ s)	τ_{21} (μ s)	N_1	I_{o2} (kA)	τ_{12} (μ s)	τ_{22} (μ s)	N_2
682	2/3	1.2	0.9	-0.35	6.5	0.2	4.0	4	2.3	5.5	180	5
682	3/3	1.2	0.9	-0.35	3.7	0.18	3.8	3	0.9	5.7	40	5
683	2/2	1.2	0.9	-0.35	6.3	0.65	1.4	4	1.9	4.1	25	2

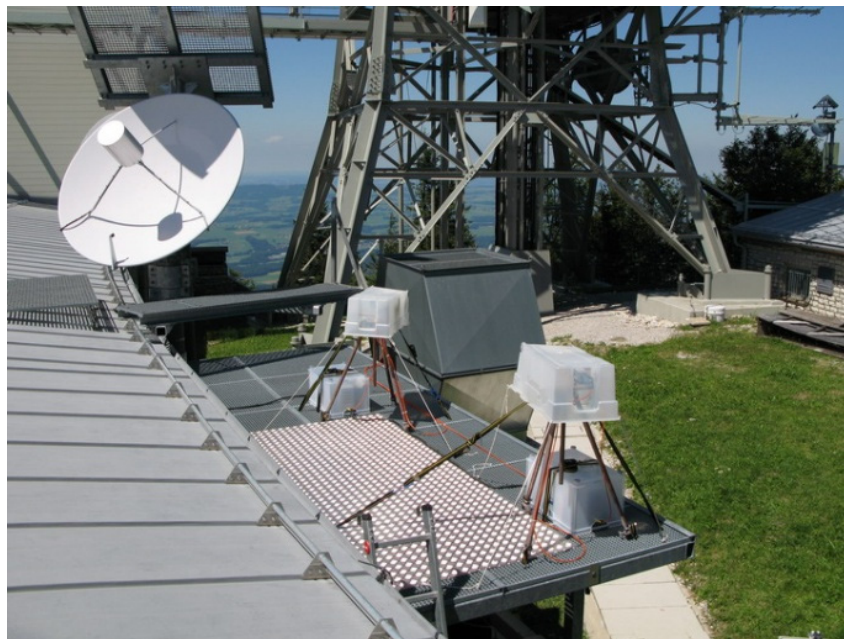


Fig. 5.19 Location of the two electric field sensors

5.5.4 Simulation Results and Comparison with Experimental Data

As shown earlier in Fig. 5.1, in the actual measurement setup the radial and vertical electric sensors were located 1 m above a metallic platform (see Fig. 5.19). A series of numerical

simulations were performed using NEC-4 in which the platform was modelled using wire-grid models. The obtained results revealed that ignoring the platform and considering the observation point at the same height (1 m) above a perfectly conducting ground would be a reasonable approximation. In NEC some wire-grid models could be proposed to take into account the presence of the metallic platform on the calculated electric fields.

This fact was also confirmed, as far as the vertical electric field is concerned, by the calibration campaign mentioned in Section 5.2.3 during which waveforms associated with distant lightning return strokes were measured using as reference a flat plate antenna located on the surface of the ground [147], and the enhancement effect of the metallic platform on the measured vertical electric fields was found to be negligible.

Fig. 5.20, Fig. 5.21 and Fig. 5.22 show the three data sets including

- the filtered current waveforms as well as the waveform obtained using the adopted representations using Heidler's functions,
- the radial electric fields recorded at $r = 20$ m, and
- the vertical electric fields recorded at $r = 22$ m.

Note that in these figures, we have only shown the electric field changes during the return stroke phase and deliberately ignored the field change during the preceding downward leader phase.

The measurements are then compared with the simulated results using the MTLE and electromagnetic (NEC-4) models (see Fig. 5.23, Fig. 5.24, and Fig. 5.25). It can be seen that both models predict electric field waveforms which are in reasonable agreement with measured waveforms. In general, the predicted fields by the electromagnetic model appear to be in better agreement with measured data, especially for the third event. The better performance of the electromagnetic model could be due to the fact that: (1) the measured current waveform is directly used as an input of the model, while an analytical representation is used for the MTLE model, and (2) the tower is represented in a more accurate way in the electromagnetic model.

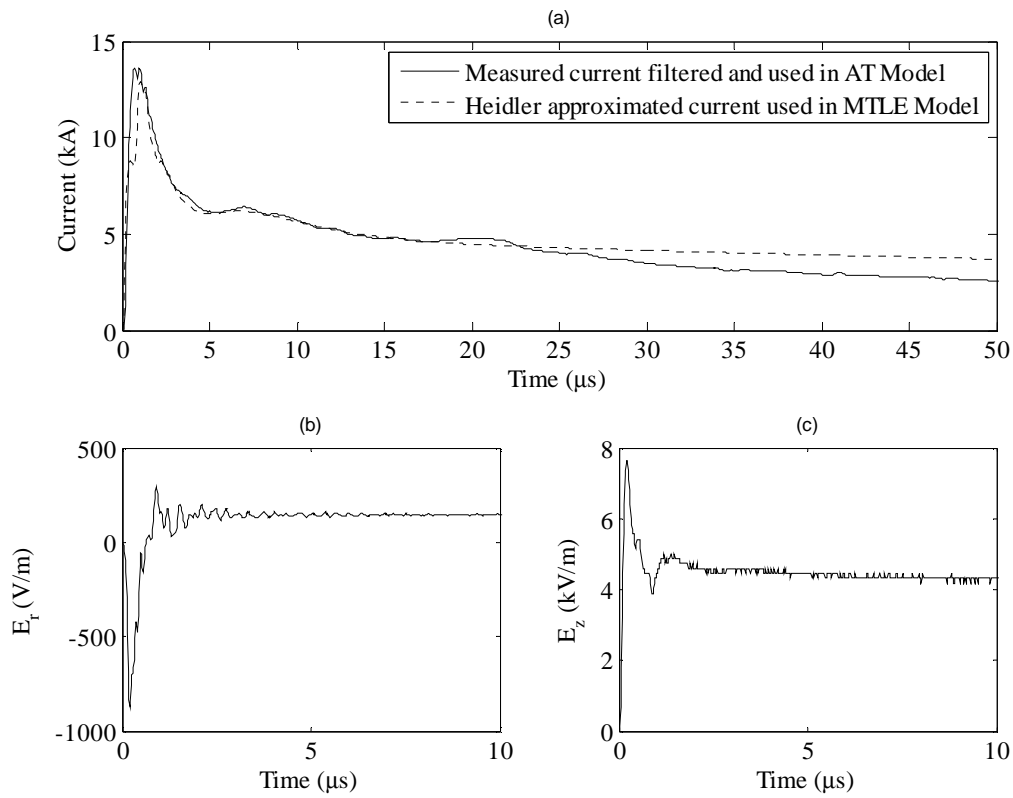


Fig. 5.20 Return stroke current, radial and vertical electric field due to the Flash 682, return stroke 2/3

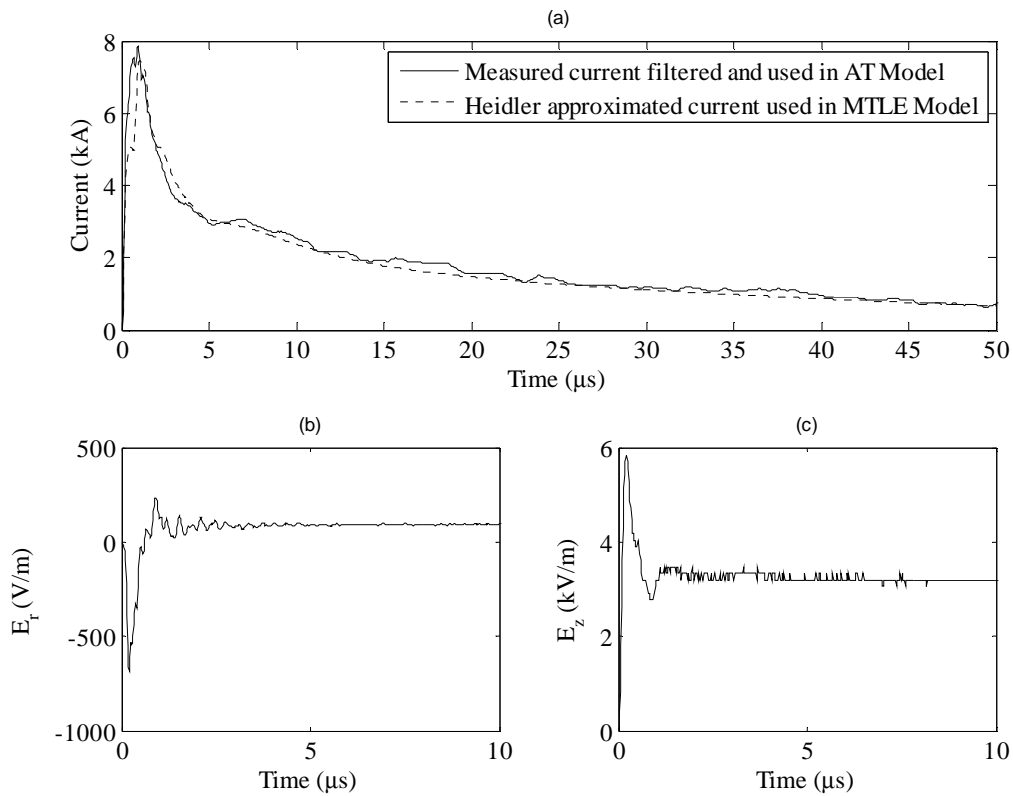


Fig. 5.21 Return stroke current, radial and vertical electric field due to the Flash 682, return stroke 3/3

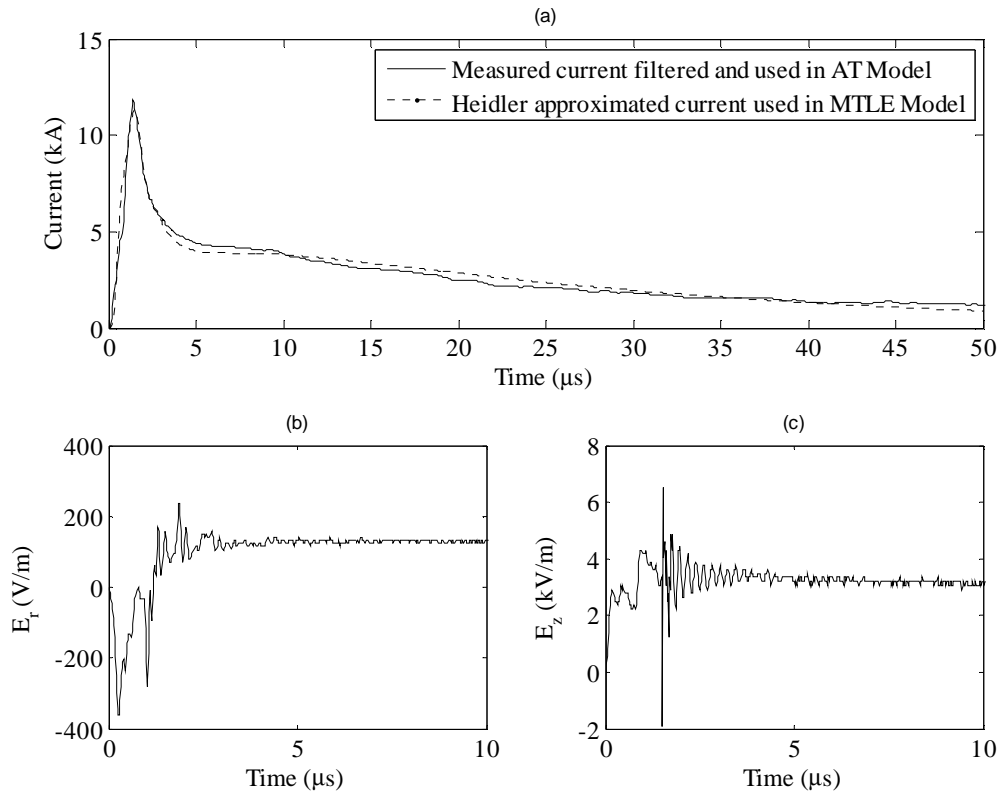


Fig. 5.22 Return stroke current, radial and vertical electric field due to the Flash 683, return stroke 2/2

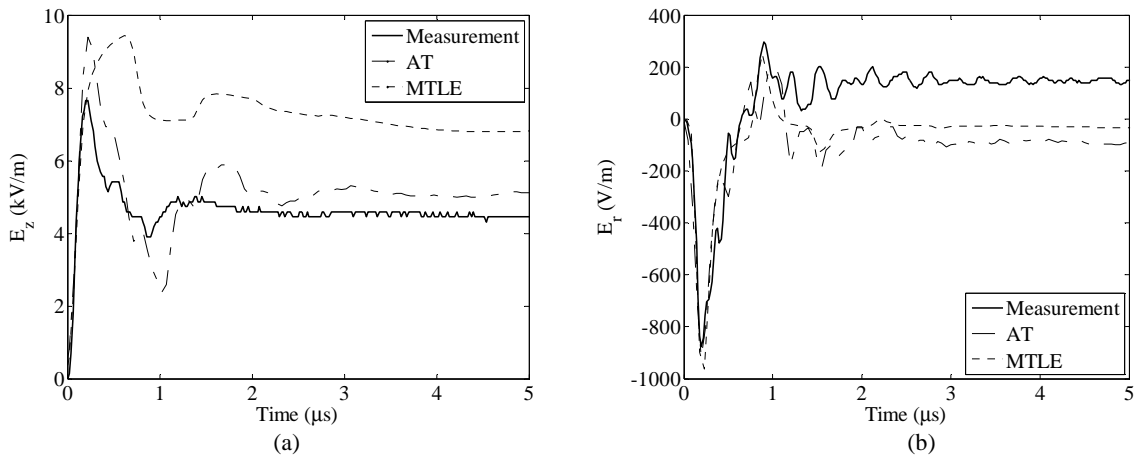


Fig. 5.23 (a) Vertical and (b) Radial electric field return stroke change due to the Flash 682, return stroke 2/3, measured, and simulated by AT and MTLE Engineering Models

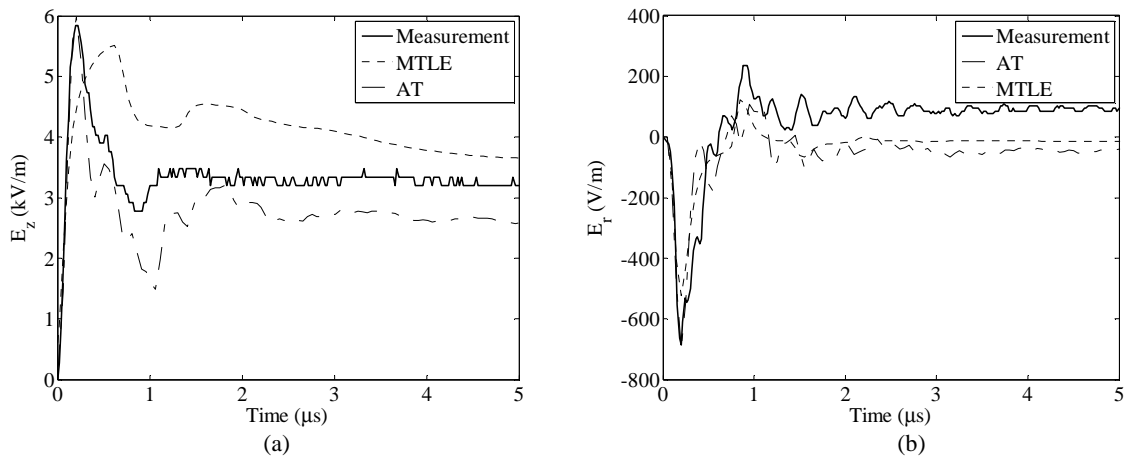


Fig. 5.24 (a) Vertical and (b) Radial electric field return stroke change due to the Flash 682, return stroke 3/3, measured, and simulated by AT and MTLE Engineering Models

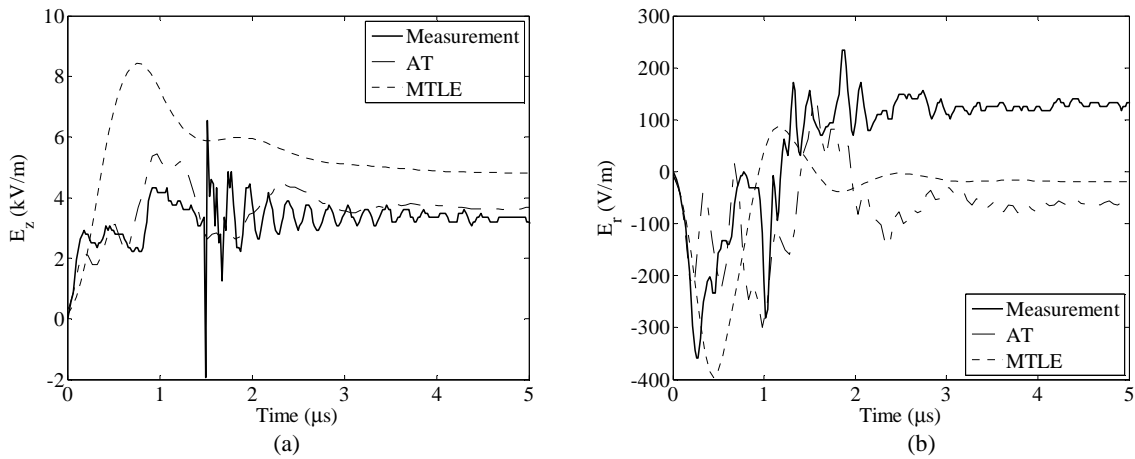


Fig. 5.25 (a) Vertical and (b) Radial electric field return stroke change due to the Flash 683, return stroke 2/2, measured, and simulated by AT and MTLE Engineering Models

5.6 Summary and Conclusions

Measurements of electric (vertical and radial) and azimuthal magnetic fields from leaders and return strokes associated with lightning strikes to the 100-m tall Gaisberg tower in Austria obtained in 2007 and 2008 were presented and discussed. The fields were measured at a distance of about 20 m from the tower. Simultaneously with the fields, return-stroke currents were also measured at the top of the tower. The data include simultaneous records of vertical and radial electric fields, which were obtained for the first time at such close distances.

The magnetic field waveforms are characterized by waveshapes similar to those of the incident current. However, the H-field peaks appear to be a factor of about 1.6 larger than the

values predicted by Ampere's law. This enhancement could be due to several possible causes, such as the proximity to the tower base and other close-by metallic structures.

The vertical and radial electric field waveforms appear as asymmetrical V-shaped pulses. For the vertical electric field, the initial, relatively slow, negative electric field change is due to the downward leader and the following fast positive field change is due to the upward return stroke phase of the lightning discharge. For the horizontal electric fields, however, the bottom of the V is not associated with the transition from the leader to the return stroke. The horizontal field change due to the return stroke is characterized by a short negative pulse of the order of 1 microsecond or so, starting with a fast negative excursion followed by a positive one.

We derived an analytical expression for the radial electric field, assuming a uniform charge distribution along the leader with constant speed. The calculated width of the V-shaped pulse of the vertical field is about three times that of the horizontal field, in contrast with the experimental data, for which this ratio is on average only 1.34.

The return-stroke vertical electric field changes appear to be significantly smaller than similar measurements obtained using triggered lightning. This finding confirms to some extent the shadowing effect of the tower which results in a significant decrease of the electric field at distances of about the height of the tower or less. The vertical and radial E-field changes due to the return stroke were also found to be larger on average than the leader electric field changes.

In a significant number of cases (33%), the vertical electric field waveform due to the return stroke is characterized by a first peak which exceeds the typical late-time flattening due to the electrostatic term. This is in contrast with similar measurements related to triggered lightning, in which such a first peak is absent. Around one quarter of the measured vertical electric field waveforms (18 pulses out of 75) feature an unusual waveform characterized by a positive leader field change followed by a bipolar return stroke field change with a zero crossing time of about 60 μs . The findings of this study call for further research to understand the reasons for the unexpected behavior of the electric field at these close distances.

Finally, the ability of two different models for the return stroke in reproducing measured vertical and horizontal electric fields was tested using the obtained measured data. The considered models were (1) the engineering MTLE model, and (2) the electromagnetic model implemented using NEC-4. It has been shown that both models predict electric field waveforms which are in reasonable agreement with measured waveforms. In general, the

predicted fields by the electromagnetic model appear to be in better agreement with measured data, because of the direct use of the measured current waveform as an input and the more accurate representation of the tower.

5.7 Appendix

The leader channel is assumed to propagate downward at a constant speed v_L from its initial height H along the z axis to the tower top level. The linear charge density along the leader ρ_L is assumed to be constant and time independent. The magnitude of the vertical [Rubinstein, et al., 1995] and radial components of the field change at a distance r from the strike point and a height z above ground due to an elemental section of the channel dz' at height z' can be written, including the effect of charge depletion in the cloud [150, 156], as the following (see Fig. 5.26)

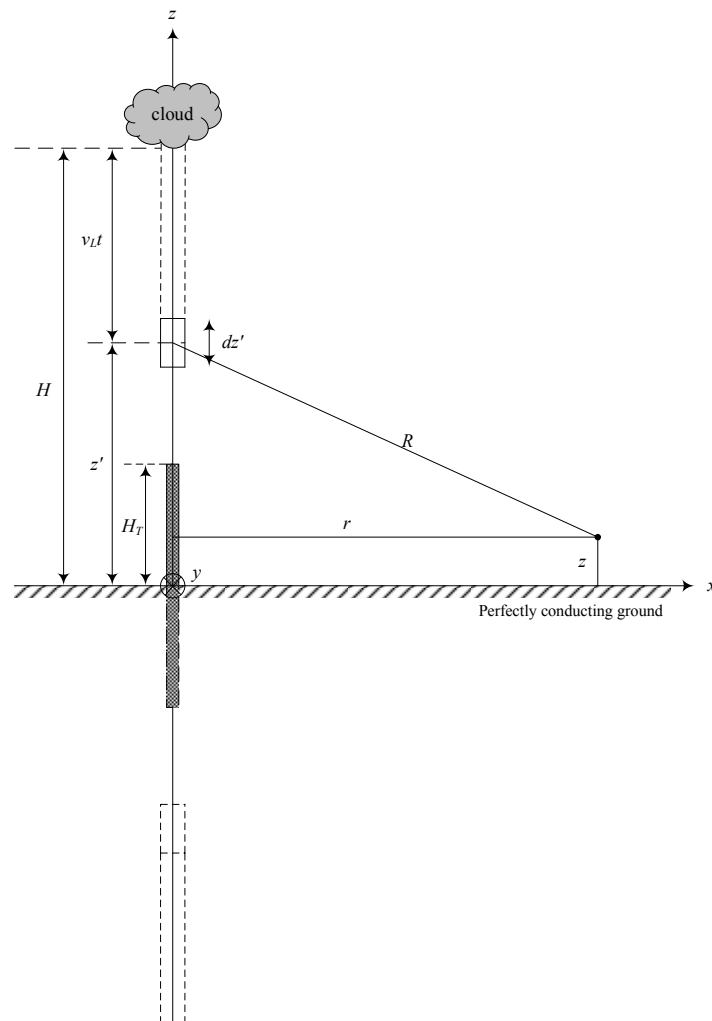


Fig. 5.26 Geometry for the calculation of electric field components of a vertical lightning channel in the presence of the tower above a perfectly conducting ground.

$$dE_z = \frac{\rho_L}{4\pi\epsilon_0} \left(\frac{z' - z}{\left[r^2 + (z' - z)^2 \right]^{\frac{3}{2}}} - \frac{H - z}{\left[r^2 + (H - z)^2 \right]^{\frac{3}{2}}} + \frac{z' + z}{\left[r^2 + (z' + z)^2 \right]^{\frac{3}{2}}} - \frac{H + z}{\left[r^2 + (H + z)^2 \right]^{\frac{3}{2}}} \right) dz' \quad (5.4)$$

$$dE_r = \frac{\rho_L}{4\pi\epsilon_0} \left(\frac{r}{\left[r^2 + (z' - z)^2 \right]^{\frac{3}{2}}} - \frac{r}{\left[r^2 + (H - z)^2 \right]^{\frac{3}{2}}} - \frac{r}{\left[r^2 + (z' + z)^2 \right]^{\frac{3}{2}}} + \frac{r}{\left[r^2 + (H + z)^2 \right]^{\frac{3}{2}}} \right) dz' \quad (5.5)$$

The overall field change at any time t is then obtained by integrating (5.3) and (5.4) from the height of the bottom of the leader at time t to the cloud charge center

$$E_z(t) = \int_{H-v_L t}^H dE_z dz' \quad (5.6)$$

$$E_r(t) = \int_{H-v_L t}^H dE_r dz' \quad (5.7)$$

Introducing (5.3) and (5.4) into (5.5) and (5.6) yields

$$E_z(t) = \frac{\rho_L}{4\pi\epsilon_0} \int_{H-vt}^H \left(\frac{z' - z}{\left[r^2 + (z' - z)^2 \right]^{\frac{3}{2}}} - \frac{H - z}{\left[r^2 + (H - z)^2 \right]^{\frac{3}{2}}} + \frac{z' + z}{\left[r^2 + (z' + z)^2 \right]^{\frac{3}{2}}} - \frac{H + z}{\left[r^2 + (H + z)^2 \right]^{\frac{3}{2}}} \right) dz' \quad (5.8)$$

$$E_r(t) = \frac{\rho_L}{4\pi\epsilon_0} \int_{H-vt}^H \left(\frac{r}{\left[r^2 + (z' - z)^2 \right]^{\frac{3}{2}}} - \frac{r}{\left[r^2 + (H - z)^2 \right]^{\frac{3}{2}}} - \frac{r}{\left[r^2 + (z' + z)^2 \right]^{\frac{3}{2}}} + \frac{r}{\left[r^2 + (H + z)^2 \right]^{\frac{3}{2}}} \right) dz' \quad (5.9)$$

After applying integration, we obtain the expressions for the vertical and radial components of the electric field due to the leader, which are given in equations (5.1) and (5.2).

Chapter 6

Effect of Nearby Buildings on Electromagnetic Fields from Lightning

6.1 Introduction

Sensors used for the measurement of lightning electric and magnetic fields are often placed close to or on top of buildings or other structures [34, 136, 146, 157-159]. Metallic beams and other conducting parts in those structures may cause enhancement or attenuation effects on the measured fields. Rubinstein et al. [157] used simultaneous measurements of lightning electric fields at the top of a building and at ground level to estimate an enhancement factor for the electric field of about 1.5 for their 17-floor building. Bonyadi-Ram et al. [146] presented a theoretical analysis in which the building on which the electric field was evaluated was represented by a metallic wire-grid model. Their results imply that the enhancement factor for the electric field is about 2.3 for a 10-m high building and increases with the height of the structure. Bermudez et al. [34] and Pavanello et al. [136] compared electromagnetic fields associated with lightning strikes to the Toronto CN Tower measured on the roofs of buildings at different distances from the tower with theoretical estimations. Their results suggest that both the electric and the magnetic fields may have been enhanced by the presence of the buildings, although the degree of enhancement was actually more significant for the electric field than for the magnetic field. Baba and Rakov [159] applied the finite-difference time-domain (FDTD) method to evaluate the effect of a building on the vertical component of electric field radiated by nearby lightning. Their computation results show that

the magnitude of the E-field on the roof of a 20-m building is about 1.5 times greater than that at the same horizontal distance on the ground surface in the absence of the building.

In this chapter, we present an experimental analysis for the evaluation of the distortion introduced by a building on the electric and magnetic fields from lightning [123-124, 160]. A numerical analysis using the Numerical Electromagnetics Code NEC-4 [58] is also presented to support the experimental data.

6.2 Considered configurations and simulation parameters

Experimental waveforms from distant natural lightning were recorded during the summers 2006 and 2007. Electric and magnetic field waveforms were measured simultaneously at two different locations, on the roof of a building (the Power Systems Laboratory of the Swiss Federal Institute of Technology, Lausanne, Switzerland) and on the ground. The building is located on the Campus of the Swiss Federal Institute of Technology in Lausanne, on the north of Lake Geneva.

The field derivatives were recorded using flat plate antennas (for the vertical E-field) and two magnetic loops (for the two magnetic field components H_x and H_y) [161]. The sensors outputs were connected via 20-m long 50Ω double-shielded cables (RG214U type) to a digitizer.

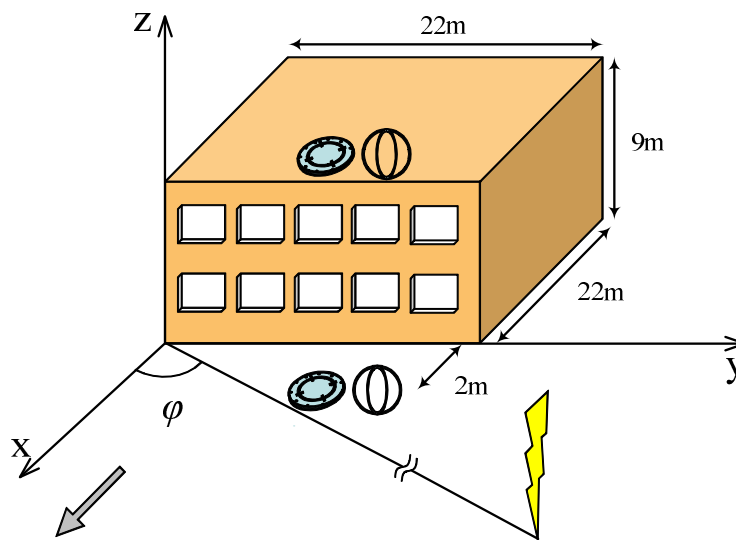


Fig. 6.1 Experimental Setup 1

The angle of incidence of the lightning electromagnetic field was determined using the magnetic direction finding technique [1] from the two components H_x and H_y of the magnetic

field measured on the roof of the building. Here we implicitly made the assumption that the magnetic field components on the roof were not affected by the presence of the building, or that both components of the H-field were affected equally.

Three different setups were considered and are described hereafter.

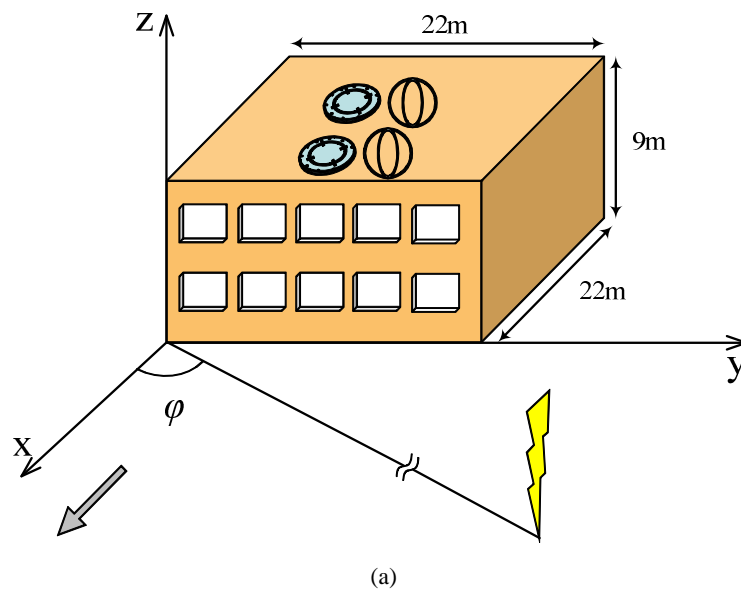


Fig. 6.2 Experimental setup 2 (a) and location of the sensors on the rooftop (b).

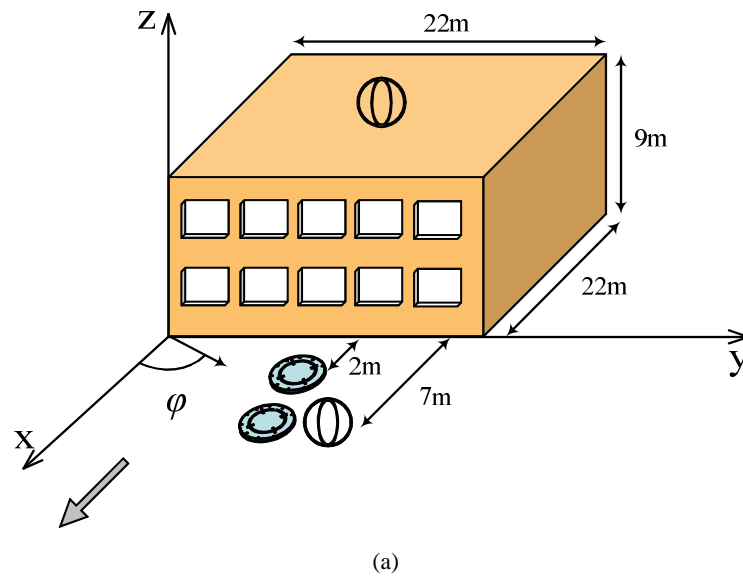


Fig. 6.3 Experimental setup 3 (a) and location of the sensors on the ground (viewed from the rooftop) (b).

Setup 1. illustrates the placement of the antennas for the first setup. The coordinate system used throughout this chapter is also shown in the same figure. The sensors on the roof are located approximately 1-m away from the southern edge and equidistant from the corners, while those on the ground are located about two meters away from the building façade and half way along it [123].

Setup 2. Fig. 6.2 shows the location of the antennas for the second setup. Sets of electric and magnetic field sensors are located on the roof of the building, one in the center and the other near the southern edge (1 m away from the edge and half way along it).

Setup 3. The arrangement of the antennas used for the third setup is shown in Fig. 6.3 Both sets of electric field sensors are located on the ground at 2 and 7 m from the southern edge, as shown in the figure. The magnetic field is measured on the roof center and at 7 m from the southern edge.

6.3 Experimental results

6.3.1 Setup One

We analyzed 4 flashes occurred on July 5th, 2006. These flashes were identified as negative cloud-to-ground strikes by their field signatures.

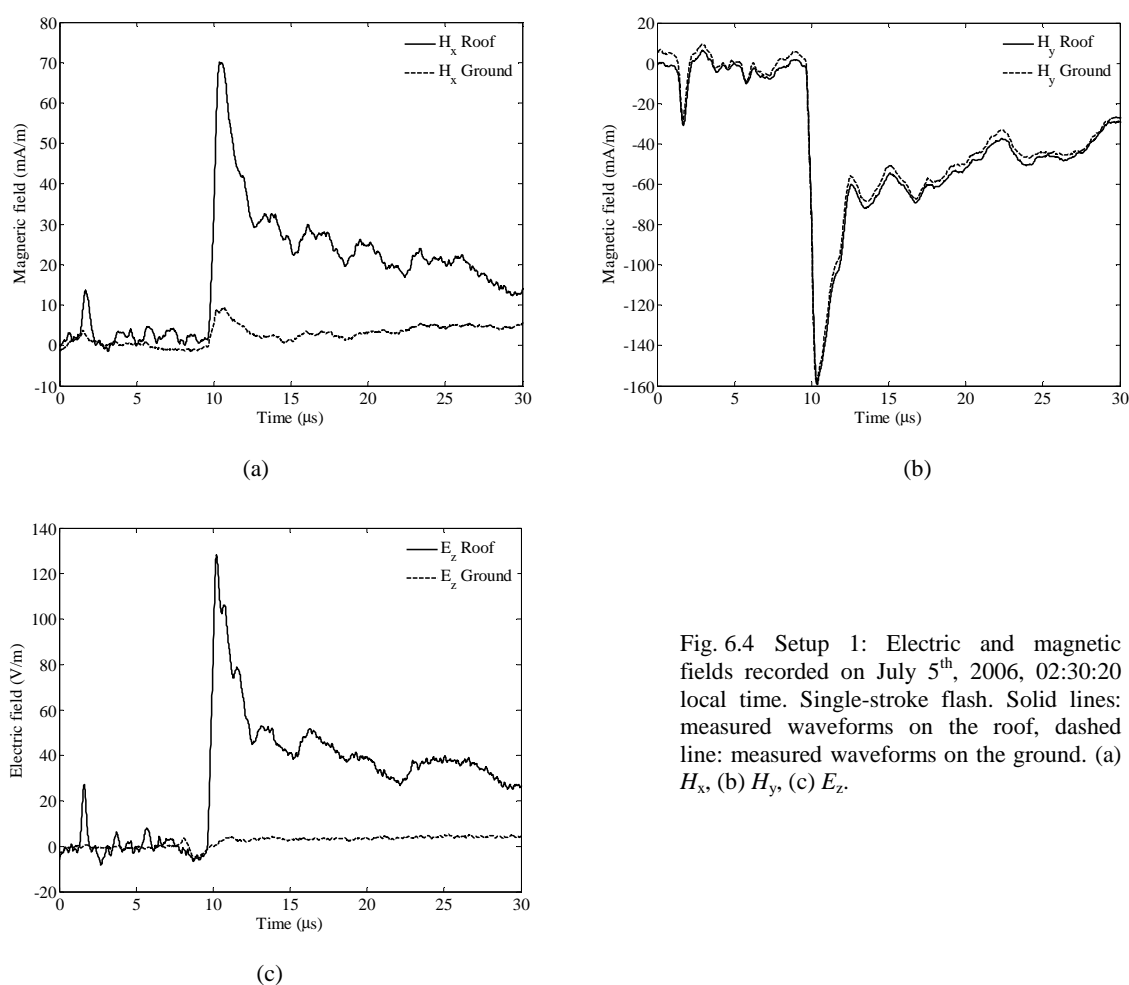


Fig. 6.4 Setup 1: Electric and magnetic fields recorded on July 5th, 2006, 02:30:20 local time. Single-stroke flash. Solid lines: measured waveforms on the roof, dashed line: measured waveforms on the ground. (a) H_x , (b) H_y , (c) E_z .

Fig. 6.4 presents one typical set of measurements consisting of simultaneous records of vertical electric fields and horizontal magnetic fields (H_x and H_y) on the roof of the building and on the ground, corresponding to a single-stroke flash occurred at 02:30:20 local time, July 5th 2006. Stepped leader pulses are clearly visible in the waveforms before the onset of the return stroke pulse. Table 6.1 summarizes some salient parameters (angle of incidence, field peaks) for 13 strokes out of the four flashes recorded on July 5th, 2006. Table 6.2 presents the ratios of electromagnetic field peaks on the roof to those measured on the ground, as well as the values for the wave impedances.

Table 6.1 Setup 1: Parameters of the events recorded on July 5th, 2006

Flash	Incidence Angle (degrees)	Event Number	Inter-Event Interval (ms)	E_{Ground} (V/m)	E_{Roof} (V/m)	$H_{\text{X}}^{\text{Ground}}$ (mA/m)	$H_{\text{X}}^{\text{Roof}}$ (mA/m)	$H_{\text{Y}}^{\text{Roof}}$ (mA/m)	$H_{\text{Y}}^{\text{Ground}}$ (mA/m)
2006-07-05, 02:28:00	63	1/5		5.8	183.5	42.5	247.8	-128.8	-136.2
		2/5	45.6	4.3	52.7	11.6	70.1	-35.5	-32.7
		3/5	67.9	5.9	90.2	17.6	122.3	-60.9	-62.9
		5/5	117.9	2.0	54.6	14.7	71.3	-35.2	-32.7
2006-07-05, 02:30:20	23	1/1		3.7	128.1	9.22	70.1	-159.4	-158.1
2006-07-05, 02:32:27	60	1/5		6.5	125.2	30.5	180	-66.6	-70.8
		2/5	66.0	5.4	101.4	22.1	148.9	-55.8	-58.7
		3/5	41.3	4.8	70.8	17.8	98.4	-36.5	-37.3
		4/5	50.2	5.1	67.8	19.5	100.1	-36	-45.6
		5/5	52.7	2.4	35.3	5.42	51.4	-19.2	-19.8
2006-07-05, 03:07:47	107	5/8	35.1	22.4	179.2	44.2	263	85.8	86.2
		7/8	525.8	10.9	108.1	33.3	163.4	49.3	54.2

Table 6.2 Setup 1: Ratios of electric and magnetic field peaks and wave impedances

Flash	Incidence Angle (degrees)	Event Number	$\frac{E_{\text{Roof}}}{E_{\text{Ground}}}$	$\frac{H_{\text{X}}^{\text{Roof}}}{H_{\text{X}}^{\text{Ground}}}$	$\frac{H_{\text{Y}}^{\text{Roof}}}{H_{\text{Y}}^{\text{Ground}}}$	$\frac{E_{\text{Ground}}}{H_{\text{Ground}}} (\Omega)$	$\frac{E_{\text{Roof}}}{H_{\text{Roof}}} (\Omega)$	$\frac{E_{\text{Ground}}}{H_{\text{Roof}}} (\Omega)$
2006-07-05, 02:28:00	63	1/5	31.7	5.8	0.9	40.5	657.1	20.7
		2/5	12.3	6.0	1.1	123.9	670.7	54.7
		3/5	15.2	7.0	1.0	90.8	660.2	43.4
		5/5	26.9	4.9	1.1	56.6	686.7	25.5
2006-07-05, 02:30:20	23	1/1	34.7	7.6	1.0	23.3	735.6	21.2
2006-07-05, 02:32:27	60	1/5	19.1	5.9	0.9	84.8	652.3	34.1
		2/5	18.7	6.7	0.9	86.6	637.7	34.1
		3/5	14.9	5.5	1.0	114.9	675	45.2
		4/5	13.3	5.1	0.8	103.2	638	48.1
		5/5	15.0	9.5	1.0	114.5	643.2	42.8
2006-07-05, 03:07:47	107	5/8	8.0	6.0	1.0	231.4	647.8	81
		7/8	9.9	4.9	0.9	170.9	633.0	63.7

It can be seen from Table 6.1 and Table 6.2 that the electric field peak on the roof is one order of magnitude greater than that measured on the ground. On the other hand, the magnetic field component H_y is nearly identical on the ground and on the roof. However, the H_x component on the ground has a peak value 5 to 10 times lower than that of the same component measured on the roof.

As discussed in [123], the obtained results suggest an enhancement of the vertical electric field measured on the roof of the building, in line with the conclusions of [34, 136, 146, 157-159]. The enhancement referred to in the mentioned studies is defined as the ratio of the fields on top of a building to the corresponding fields in the absence of the building. Since we measured our electric field two meters from the building, the fact that the ratio of the E-field peak on the roof to the E-field peak on the ground is about 10-30 suggests an attenuation of the E-field measured on the ground [123].

The fact that the magnetic field component at ground level perpendicular to the building façade, H_x , is considerably lower than the same component on the roof is thought to be essentially due to currents induced on the metallic structure of this façade [123]. These currents flow predominantly in the yz plane and they generate therefore a magnetic field in the x direction.

As can be seen in the 4th column of Table 6.2, a great disparity can be observed for the ratio of the electric field on the roof and that on the ground. For example, the first flash presents ratios of 31.7, 12.3, 15.2 and 26.9. Since all the measured fields for those strokes come from the same direction and propagated along the same path, they are expected to be submitted to the same attenuation and distortion effects. The fact that the ratio varies to such significant extent can be essentially due to two reasons: (1) the differences in the rise-times of the fields and possible frequency dependence of the building effect, and (2) the fact that the E-field waveforms on the ground were characterized by very low magnitudes (see Fig. 6.4c) and hence might have been affected by noise.

In order to estimate the amount of enhancement/attenuation of the electromagnetic field components, the following approach based on the wave impedance is proposed. Since all the events recorded in this study correspond to distant lightning strikes (some tens of kilometers), the field is essentially radiation and the electric field peak to magnetic field peak ratio should be equal to the free space wave impedance, 377Ω . We also assume that the magnetic field components measured on the roof are not affected by the presence of the building. This assumption, which will be tested in Section 4, is supported by the fact that the two horizontal

field components measured on the roof of the building are not expected to be significantly affected by the currents induced on the roof, which flow predominantly in the same horizontal plane. The last two columns in Table 6.2 present the ratio of the electric field peaks on the roof and on the ground to the magnetic field peaks on the roof. It can be seen that the ratio of the field peaks on the roof ranges from 630 to 735 Ω , with a mean value of 640.4 Ω and a standard deviation of 10.46 Ω . These values indicate that the enhancement of the electric field on the roof is about 1.7 to 1.9. The ratio of the E-field peak on the ground to the E-field peak on the roof (last column of Table 6.2) ranges from 20 Ω to 80 Ω . Comparing these values to the free-space wave impedance suggests that the reduction of the electric field at ground ranges from 5 to 20.

6.3.2 Setup Two

We analyzed 10 flashes occurred on June 20th and 21st, 2007. All these flashes were identified as negative cloud-to-ground strikes by their field signatures. Fig. 6.5 presents one typical set of measurements consisting of simultaneous records of electric and magnetic fields recorded on July 20th 2007. Table 6.3 summarizes parameters for 12 strokes out of the recorded 10 flashes. It can be seen that the vertical electric field at the edge of the rooftop is only slightly enhanced compared to the same component measured on the roof center (average: 5.67%). No significant difference was found between the y-component of the magnetic field at the two locations. However, the magnetic field x-component on the edge was significantly larger than that of the center (average 29.75%).

Table 6.4 presents the ratios of electromagnetic field peaks on the roof to those measured on the ground, as well as the values for the wave impedances. Assuming again that the magnetic field components measured on the roof center are not affected by the presence of the building, the enhancement of the electric field can be evaluated by examining the last two columns in Table 6.4 which present the ratio of the electric field peaks on the roof center and on the roof edge to the magnetic field peaks on the roof center. It can be seen that the ratio of the field peaks on the roof ranges from 590 to 807 Ω , with a mean value of 686.64 Ω and a standard deviation of 77.67 Ω . These values indicate that the enhancement of the electric field on the roof is about 1.5 to 2.

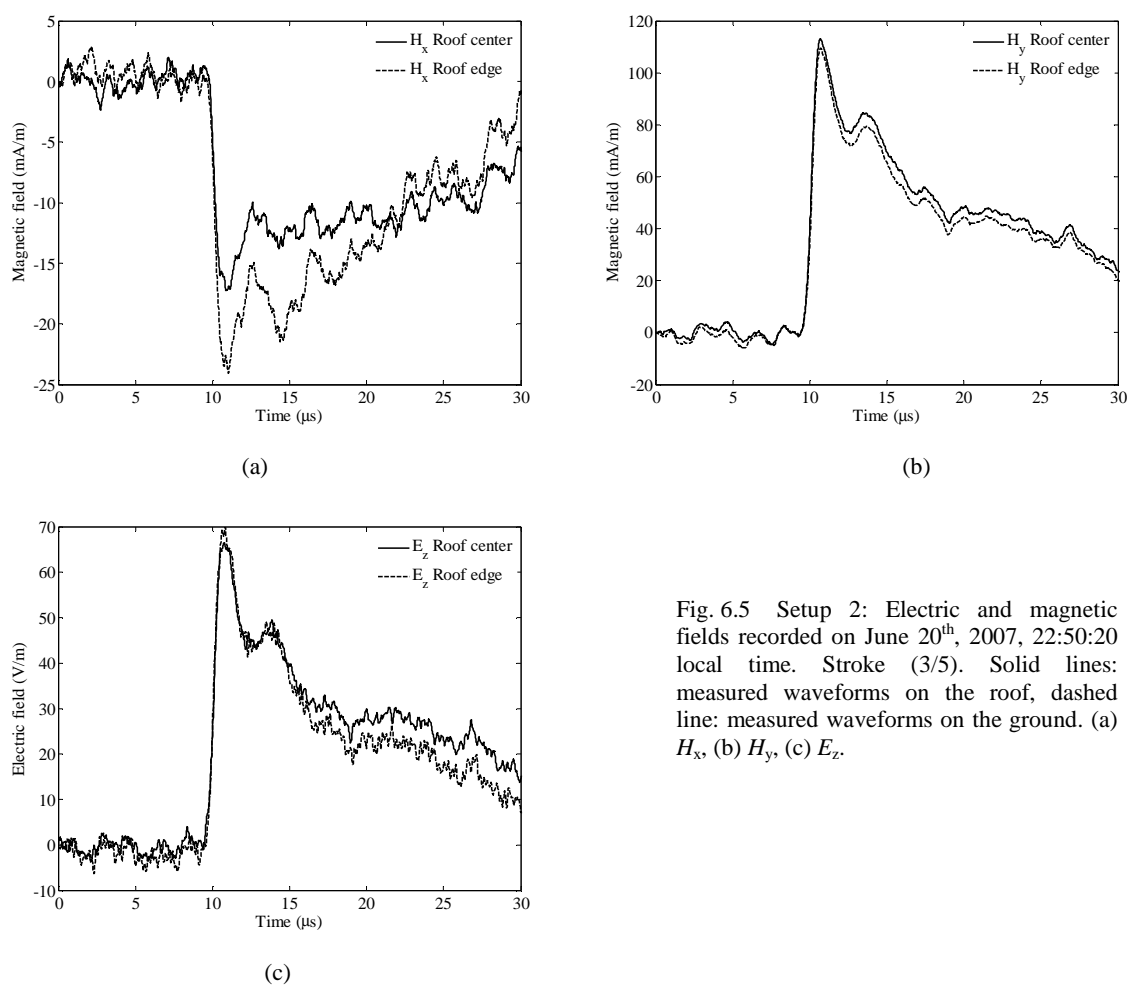


Fig. 6.5 Setup 2: Electric and magnetic fields recorded on June 20th, 2007, 22:50:20 local time. Stroke (3/5). Solid lines: measured waveforms on the roof, dashed line: measured waveforms on the ground. (a) H_x , (b) H_y , (c) E_z .

Table 6.3 Setup 2: Parameters of the events recorded on June 20th and 21st, 2007

Flash	Incidence Angle (degrees)	Event Number	Inter-Event Interval (ms)	E_{Centre} (V/m)	E_{Edge} (V/m)	H_X^{Centre} (mA/m)	H_Y^{Centre} (mA/m)	H_X^{Edge} (mA/m)	H_Y^{Edge} (mA/m)
2007-06-20, 22:50:20	-171	2/5	172	73.46	69.7	-16.5	116.8	-25.1	111.8
		3/5	134	66.56	70	-17.3	113.1	-24.1	109.5
		5/5	0.2	78.38	83	-19.9	132.2	-29.9	125.9
2007-06-20, 23:42:48	161	1/2		53.69	57.1	30	84.9	36.3	82.3
2007-06-20, 23:43:03	-50	1/1		28.97	28.89	-31.8	-27.1	-38.8	-29.2
2007-06-20, 23:48:40	-48	1/1		27.63	29.4	-29.3	-26	-37.7	-28.5
2007-06-20, 23:49:57	-60	1/3		93.25	99.5	-121.6	-69.8	-150.2	-76
2007-06-20, 23:50:23	-59	1/1		52.94	60.21	-63.9	-38.5	-76.9	-45
2007-06-20, 23:52:33	-51	3/3	103.9	40.51	44.69	-46.5	-37.9	-56.8	-42.7
2007-06-20, 23:59:42	-48	3/4	56.78	37.18	37.08	-39.9	-35.4	-50	-37.5
2007-06-21, 00:03:03	-48	1/1		38.45	43.5	-40.3	-36.9	-47.8	-42.4
2007-06-21, 01:10:49	-170	1/1		53.8	58.14	-16.8	97.6	-22.5	93.6

Table 6.4 Setup 2: Ratios of electric and magnetic field peaks and wave impedances

Flash	Incidence Angle (degrees)	Event Number	$\frac{E_{\text{Edge}}}{E_{\text{Centre}}}$	$\frac{H_x^{\text{Edge}}}{H_x^{\text{Centre}}}$	$\frac{H_y^{\text{Edge}}}{H_y^{\text{Centre}}}$	$\frac{E^{\text{Centre}}}{H^{\text{Centre}}} (\Omega)$	$\frac{E_{\text{Edge}}}{H^{\text{Centre}}} (\Omega)$
2007-06-20, 22:50:20	-171	2/5	0.95	1.52	0.96	622.7	590.9
		3/5	1.05	1.39	0.97	581.7	611.8
		5/5	1.06	1.5	0.95	586.3	620.8
2007-06-20, 23:42:48	161	1/2	1.06	1.21	0.97	596.3	634.1
2007-06-20, 23:43:03	-50	1/1	0.99	1.22	1.08	693.4	691.5
2007-06-20, 23:48:40	-48	1/1	1.06	1.29	1.1	705.3	750.5
2007-06-20, 23:49:57	-60	1/3	1.07	1.24	1.09	665.1	709.6
2007-06-20, 23:50:23	-59	1/1	1.14	1.2	1.17	709.6	807.1
2007-06-20, 23:52:33	-51	3/3	1.1	1.22	1.13	675.3	745
2007-06-20, 23:59:42	-48	3/4	0.99	1.25	1.06	697	695.2
2007-06-21, 00:03:03	-48	1/1	1.13	1.19	1.15	703.7	796.1
2007-06-21, 01:10:49	-170	1/1	1.08	1.34	0.96	543.2	587.1

6.3.3 Setup Three

We measured one flash occurred on July 1st, 2007 for this configuration and which was identified as a negative cloud-to-ground strike by its field signatures. Fig. 6.6 presents one typical set of measurements consisting of simultaneous records of electric and magnetic fields recorded on July 20th 2007. Table 6.5 summarizes parameters for the 2 strokes out of the recorded flash. It can be seen that the vertical electric field at 2 m from the building is significantly smaller in magnitude than that measured at 7 m from the building, presumably less affected by the building shadowing effect. In agreement with the results obtained for the setup 1, the magnetic field x-component at ground level perpendicular to the building façade, H_x , is considerably lower than the same component on the roof. However, it is found for this configuration that the H_y component at ground level is also lower (to a lesser degree) compared to the same component measured on the roof.

Table 6.6 presents the ratios of electromagnetic field peaks, as well as the values for the wave impedances. It can be seen that the wave impedance for the field measured at 7 m from the building façade is nearly equal to the free space wave impedance. This could be considered as an indication that at this location, electric and magnetic field components are very little affected by the building. On the other hand, the ratios of the electric field at 7 m from the building to the magnetic field on the roof center are 261.9 and 269.7 Ω for first and second stroke respectively. Assuming that the magnetic field on the roof center is unaffected by the building, this would indicate that both the electric and magnetic fields at 7 m from the building façade are still affected by the shadowing effect, despite the fact that their ratio is close to the free space wave impedance.

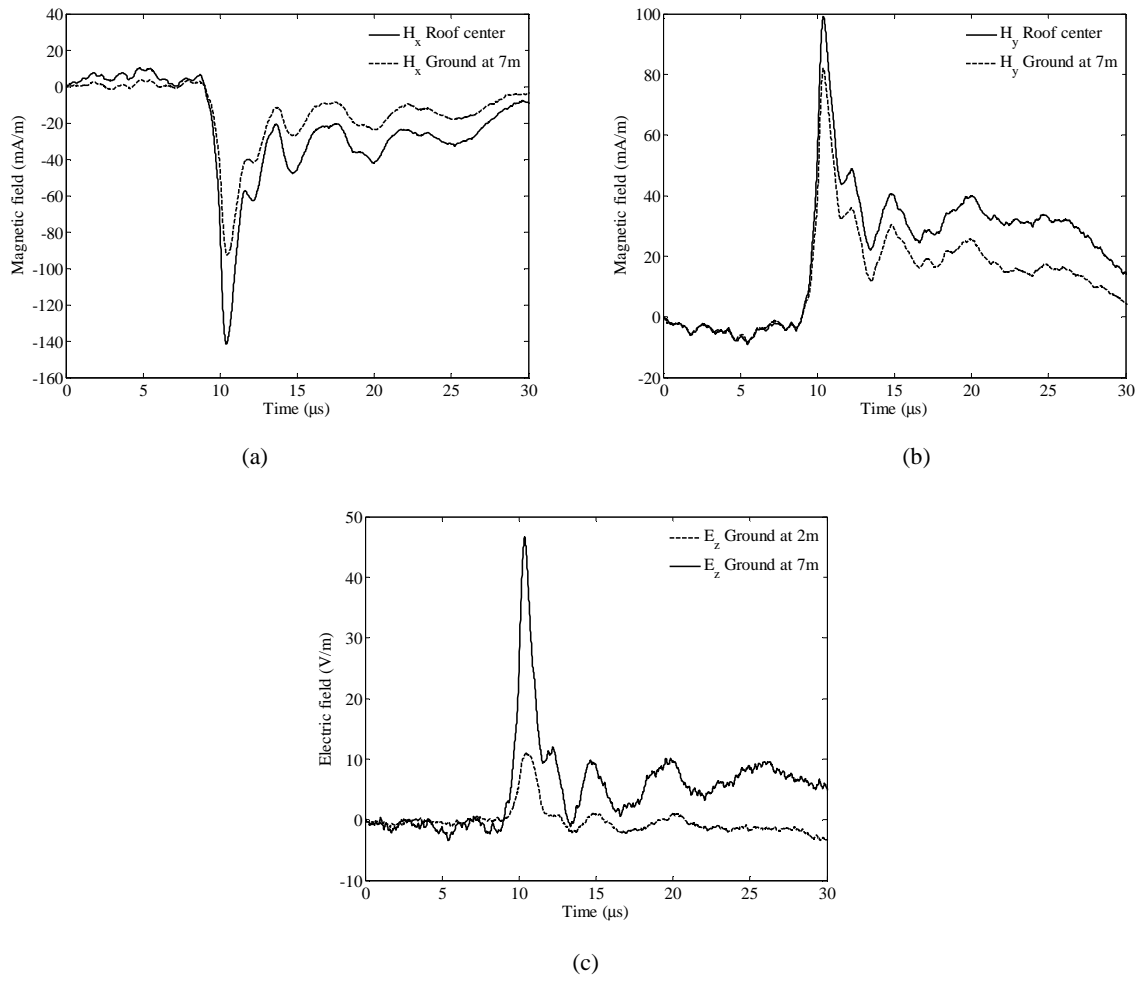


Fig. 6.6 Setup 3: Electric and magnetic fields recorded on July 1st, 2007, 17:15:06 local time. Stroke (3/3). Solid lines: measured waveforms on the roof, dashed line: measured waveforms on the ground. (a) H_x , (b) H_y , (c) E_z .

Table 6.5 Setup3: Parameters of the events recorded on July 1st, 2007

Flash	Incidence Angle (degrees)	Event Number	Inter-Event Interval (ms)	E_{Ground}^{2m} (V/m)	E_{Ground}^{7m} (V/m)	H_X^{Roof} (mA/m)	H_Y^{Roof} (mA/m)	H_X^{Ground} (mA/m)	H_Y^{Ground} (mA/m)
2007-07-01, 17:15:06	-125	1/3		10.6	44.7	-139	99	-93	84.2
		3/3	66.8	11.04	46.62	-141.6	99.2	-92.7	81.9

Table 6.6 Setup3: Ratios of electric and magnetic field peaks and wave impedances

Flash	Incidence Angle (degrees)	Event Number	$\frac{E_{Ground}^{7m}}{E_{Ground}^{2m}}$	$\frac{H_X^{Roof}}{H_X^{Ground}}$	$\frac{H_Y^{Roof}}{H_Y^{Ground}}$	$\frac{E_{Ground}^{2m}}{H_{Ground}^{7m}}$ (Ω)	$\frac{E_{Ground}^{2m}}{H_{Roof}^{Roof}}$ (Ω)	$\frac{E_{Ground}^{7m}}{H_{Ground}^{7m}}$ (Ω)	$\frac{E_{Ground}^{7m}}{H_{Roof}^{Roof}}$ (Ω)
2007-07-01, 17:15:06	-125	1/3	4.22	1.49	1.17	78.0	62.1	356.3	261.9
		3/3	4.22	1.53	1.21	81.3	63.9	376.9	269.7

6.4 Simulations

In the analysis presented in this section, we made use of the Numerical Electromagnetics Code NEC-4 [9], a well-known and widely used computer code based on the Method of Moments for analyzing the electromagnetic response of antennas and scatterers. The building was represented using a very simplified wiregrid parallelepiped structure consisting of 12 wires (see Fig. 6.7). Each wire was subdivided into 10 segments and the radius of all wires was 5 cm. The incident field used was a plane wave with a waveshape typical of a lightning return-stroke far field and with an angle of incidence corresponding to the event presented in Fig. 6.4 (July 5th 2006, 02:30:20), which corresponds to the setup 1.

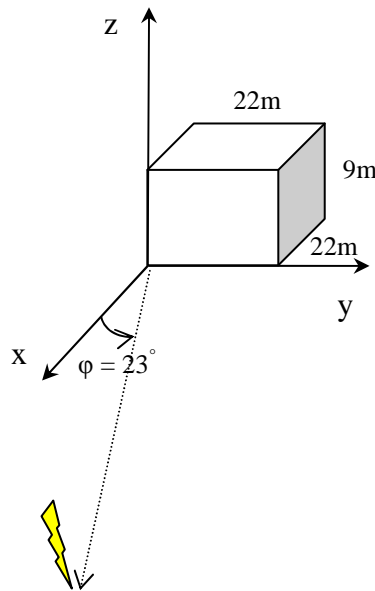


Fig. 6.7 Wiregrid model for the building and the configuration for the NEC-4 computation corresponding to the event recorded on July 5th, 2006, 02:30:20 local time.

The resulting computed electric and magnetic fields are shown in Fig. 6.8. Table 6.7 presents, for comparison, the ratios of the electric and magnetic field peaks and the wave impedances determined from the measured waveforms and from the simulations. Despite noticeable differences between simulations and measurements, which are believed to be essentially due to the oversimplified model for the building, it can be seen that the computed results are qualitatively in agreement with the observed data and show the same trends.

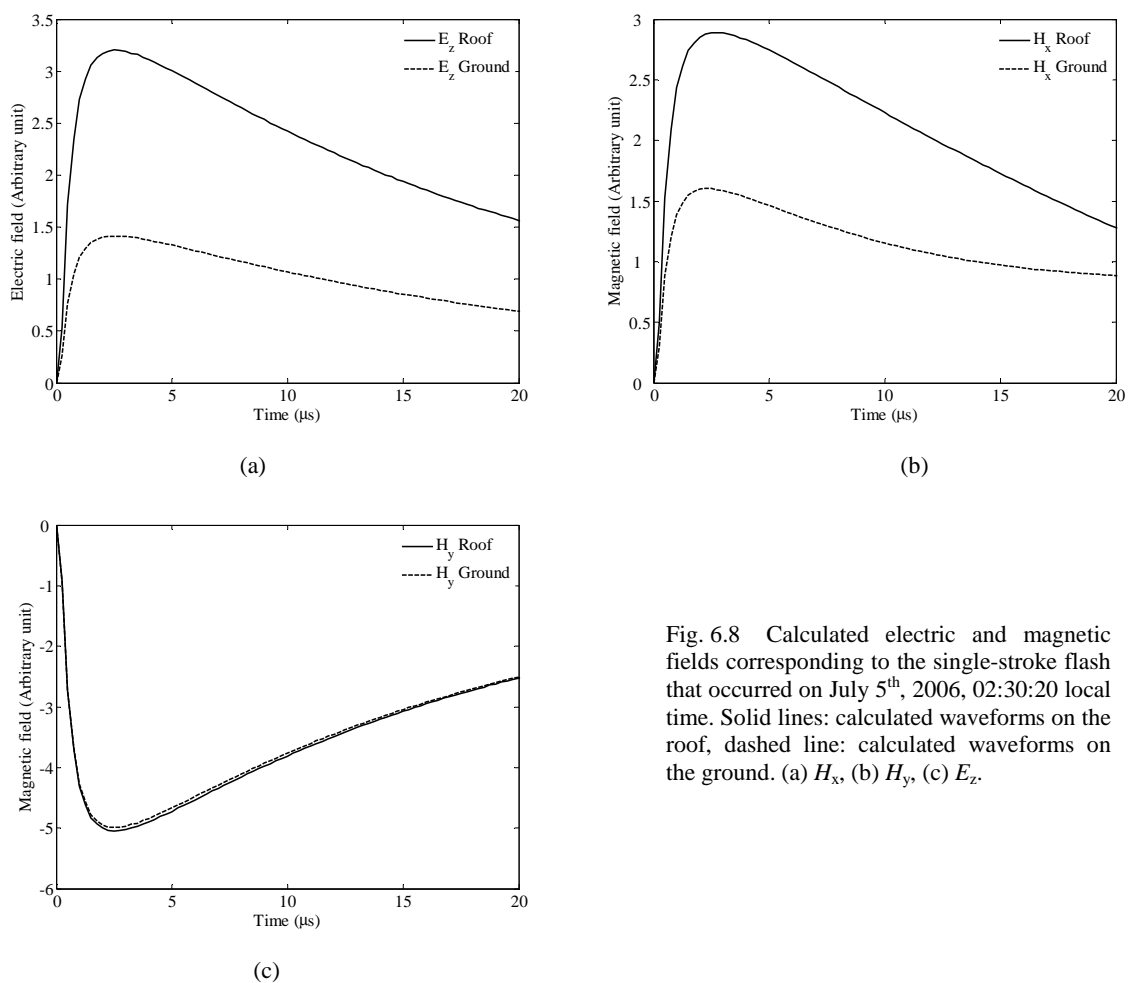


Fig. 6.8 Calculated electric and magnetic fields corresponding to the single-stroke flash that occurred on July 5th, 2006, 02:30:20 local time. Solid lines: calculated waveforms on the roof, dashed line: calculated waveforms on the ground. (a) H_x , (b) H_y , (c) E_z .

Table 6.7 Ratios of electric and magnetic field peaks and wave impedances. Comparison between measurements and simulations. Event July 5th, 2006 -02:30:20

2006-02-05, 02:30:20	$\frac{E_{Roof}}{E_{Ground}}$	$\frac{H_X^{Roof}}{H_X^{Ground}}$	$\frac{H_Y^{Roof}}{H_Y^{Ground}}$	$\frac{E_{Ground} (\Omega)}{H_{Ground}}$	$\frac{E_{Roof}}{H_{Roof} (\Omega)}$	$\frac{E_{Ground} (\Omega)}{H_{Roof}}$
Simulation	2.3	1.8	1.0	269.5	550.7	243.3
Measurement	34.7	7.6	1.0	23.3	735.6	21.2

Table 6.8 Percentage of difference between computed electric and magnetic field components in the presence of the building and with the building removed, leaving only the ground plane

Percentage	E_{Roof}	E_{Ground}	H_X^{Roof}	H_Y^{Roof}	H_X^{Ground}	H_Y^{Ground}
Simulation	47 %	-35 %	27 %	-5 %	-29 %	-6 %

Table 6.8 presents the difference, expressed as a percentage, between the calculated fields in the presence of the building and those obtained without the building. The results confirm (i) the enhancement of the electric field on the roof and (ii) the attenuation of the electric field on the ground. The results also confirm that the H_y component is very little affected by the building whereas the H_x component on the ground is attenuated. The results also indicate an enhancement of the H_x component on the roof, which is in agreement with the experimental results obtained for the setup 2.

6.5 Conclusions

We presented experimental waveforms radiated from distant natural lightning recorded during the summers of 2006 and 2007. Electric and magnetic field waveforms were measured simultaneously on the roof of a building (the Power Systems Laboratory of the Swiss Federal Institute of Technology, Lausanne, Switzerland) and on the ground at different distances away from it. The fields were recorded using flat plate antennas (for the E-field) and magnetic loops (for the H-field). The results suggest that the measured electric field on the roof of the building could be enhanced by a factor of 1.7 to 1.9, whereas the electric fields on the ground experience a significant reduction by a factor ranging from 5 to 20. Also, it is shown that for a sensor located on the ground close to a building, the magnetic field component perpendicular to the building can experience significant attenuation, presumably due to the effect of the induced currents in the building. The magnetic field on the roof of the building seems not to be significantly affected by the building.

Simulations using the Numerical Electromagnetic Code (NEC-4) were also carried out in which the building was represented using a simple wiregrid model. The simulation results support in essence the findings of the experimental analysis, despite quantitative differences which are ascribed, at least in part, to the oversimplified model of the building.

Chapter 7

Summary, Conclusions and Perspectives

7.1 Summary and conclusions

The focus of this thesis was the analysis and modeling of lightning strikes to tall structures in view of the characterization of generated electromagnetic fields. The work comprised both theoretical investigations and experimental measurements with the aim of improving our current understanding of lightning to tall structures and associated electromagnetic fields.

Chapter 2 reviewed recent progress in the modeling of lightning strikes to tall towers and associated experimental data obtained during the last decade or so. Two types of return stroke models namely the Engineering Models, and the Electromagnetic or Antenna-Theory (AT) models, extended to take into account the presence of a tall strike object were discussed. It was emphasized that the engineering models are characterized by a discontinuity at the return stroke wavefront which requires special care when calculating the electromagnetic fields. In addition, this discontinuity cannot be considered as physically plausible.

It was also shown that none of the two classes of models were able to reproduce the far field zero crossing of the electromagnetic fields, nor the narrow undershoot observed in the waveforms of the electromagnetic fields associated with lightning strikes to the Toronto CN Tower.

The chapter highlighted some important questions raised by different research groups in the past few years which call for further investigations. These questions were as follows:

(1) No systematic theoretical analysis nor experimental data are available for electromagnetic fields in the immediate vicinity of a tall structure struck by lightning. The characterization of nearby electromagnetic fields is particularly important in the analysis of the interaction to nearby electrical and electronics systems.

(2) Why do lightning return stroke models not reproduce the far-field zero crossing associated with lightning to tall structures? How should these models be revised to be able to reproduce such an effect?

(3) How should the engineering models be revised in order to remove the associated current discontinuity at the return stroke wavefront?

(4) It is well-known that the measurements of electromagnetic fields from lightning are affected by the presence of nearby buildings and metallic structures. However, no systematic and quantitative analysis of such an effect is presently available in the literature.

The work presented in this thesis addresses all the above questions.

In Chapter 3, a detailed theoretical analysis of electromagnetic field characteristics in the immediate vicinity of a tower struck by lightning was presented. It was shown that the electric field generated by a lightning return stroke to a tall structure can change polarity at very close distance range, typically at distances of about one tenth the height of the struck object or so. This change in the polarity appearing as a negative excursion preceded by a short (some tens of nanoseconds) initial positive excursion, seems to be a specific signature of very close vertical electric fields. Two different theoretical explanations of such an inversion of polarity were given, the first based on general field equations for a perfectly-conducting ground, and the second based on the equation derived by Baba and Rakov for the case when the return stroke wave front speed is assumed to be equal to the speed of light and the reflection coefficient at the top of the tall structure is zero. A simple equation was derived which provides an estimate of the critical distance below which such an inversion of polarity might occur. It was also shown that the inversion of polarity depends on the value for the reflection coefficient at the base of the tower and might disappear for reflection coefficients close to 1. On the other hand, other parameters such as the return stroke speed, the reflection coefficient at the top of the tower, and the adopted return stroke model seemed not to have an impact on the inversion of polarity. Simulation results also showed that the electric field peak at distances beyond the height of the tower or so exhibits the typical $1/r$ dependence. At closer distances, however, the E-field peak features a saturation, due to the so-called tower

shadowing effect. This shadowing effect results in a substantial decrease of nearby electric field. On the other hand, the magnetic field peak varies inversely proportional to the horizontal distance and does not depend significantly on the presence of an elevated strike object.

In Chapter 4, an improved version of the engineering models for return-strokes to tall structures was proposed which accounts for (1) the presence of possible reflections at the return stroke wavefront, and, (2) a return stroke initiation above the structure due to an upward connecting leader. We also proposed an elegant iterative solution that can be easily implemented into computer simulation programs to take into account in a straightforward way multiple reflections occurring at the discontinuities at the tower ends and at the return stroke wavefront.

Simulation results for the magnetic fields were compared with experimental waveforms associated with lightning strikes to the CN Tower (553 m). It was shown that taking into account the reflections at the return-stroke wavefront results in better reproducing the fine structure of the magnetic field waveforms, including the double-peak, the early narrow undershoot and the far-field zero crossing. The results also suggested that the typical double-peak response of the radiated fields from tall structures might be due to the combined effect of upward-connecting leader and reflections at the return stroke wavefront.

Chapter 5 presented and discussed obtained measurements of electric (vertical and radial) and magnetic fields from leaders and return strokes associated with lightning strikes to the Gaisberg tower in Austria obtained in 2007 and 2008. The Gaisberg tower is a 100-m tall radio tower located 1287 m above sea level on the top of a mountain 5 km east of the city of Salzburg, Austria. The fields were measured at a distance of about 20 m from the tower. Simultaneously with the fields, return-stroke currents were also measured at the top of the tower. The data include simultaneous records of vertical and radial electric fields, which were obtained for the first time at such close distances. The whole measurement campaign includes three different measurement setups. Each setup includes records of lightning current waveforms measured on the top of the tower. In the first setup (from May 1st, 2007 to September 10th, 2007), we measured the vertical electric field and the azimuthal magnetic field, respectively at 22 m and 20 m from the center of the tower. In the second setup (from September 11th, 2007 to June 31st, 2008), we obtained records of the radial electric field and

azimuthal magnetic field, respectively at 22 m and 20 m from the center of the tower. Finally, for the third setup (from July 1st, 2008 to August 1st, 2008), we measured the vertical and radial components of the electric field at 22 m and 20 m from the tower, respectively.

A total of 13 upward initiated flashes containing 40 ICC pulses (pulses superimposed on the ICC, the initial continuing current typical for upward initiated flashes) and 44 return-strokes were recorded during the whole measuring campaign, although the sample size was different depending on the studied quantities and examined features for each data set.

It was found that the magnetic field waveforms are characterized by waveshapes similar to those of the incident current. However, the H-field peaks appear to be a factor of about 1.6 larger than the values predicted by Ampere's law. This enhancement could be due to several possible causes, such as the proximity to the tower base and other close-by metallic structures.

It was also observed that the vertical and radial electric field waveforms appear as asymmetrical V-shaped pulses. For the vertical electric field, the initial, relatively slow, negative electric field change is due to the downward leader and the following fast positive field change is due to the upward return stroke phase of the lightning discharge. For the horizontal electric fields, however, the bottom of the V is not associated with the transition from the leader to the return stroke. The horizontal field change due to the return stroke is characterized by a short negative pulse of the order of 1 microsecond or so, starting with a fast negative excursion followed by a positive one.

In addition, an analytical expression for the radial electric field, assuming a uniform charge distribution along the leader with constant speed was derived. The calculated width of the V-shaped pulse of the vertical field is about three times that of the horizontal field, in contrast with the experimental data, for which this ratio is on average only 1.34.

It was also shown that the return-stroke vertical electric field changes appear to be significantly smaller than similar measurements obtained using triggered lightning. This finding confirms to some extent the shadowing effect of the tower, predicted by the theoretical analysis of Chapter 3, which results in a significant decrease of the electric field at distances of about the height of the tower or less. The vertical and radial E-field changes due to the return stroke were also found to be larger on average than the leader electric field changes.

In a significant number of cases (33%), the vertical electric field waveform due to the return stroke was characterized by a first peak which exceeded the typical late-time flattening due to the electrostatic term. This is in contrast with similar measurements related to triggered

lightning, in which such a first peak is absent. About one quarter of the measured vertical electric field waveforms (18 pulses out of 75) feature an unusual waveform characterized by a positive leader field change followed by a bipolar return stroke field change with a zero crossing time of about 60 μs .

Finally, the ability of two different models for the return stroke in reproducing measured vertical and horizontal electric fields was tested using the obtained measured data. The considered models were (1) the engineering MTLE model, and (2) the electromagnetic model implemented using NEC-4. It was shown that both models predict electric field waveforms which are in reasonable agreement with measured waveforms. In general, the predicted fields by the electromagnetic model appear to be in better agreement with measured data, because of the direct use of the measured current waveform as an input and the more accurate representation of the tower.

Chapter 6 was devoted to effect of nearby buildings on electromagnetic fields from lightning. Indeed, sensors used for the measurement of lightning electric and magnetic fields are often placed close to or on top of buildings or other structures. Metallic beams and other conducting parts in those structures may cause enhancement or attenuation effects on the measured fields. Experimental waveforms radiated from distant natural lightning recorded during the summers of 2006 and 2007 were presented. Electric and magnetic field waveforms were measured simultaneously on the roof of a building (the Power Systems Laboratory of the Swiss Federal Institute of Technology, Lausanne, Switzerland) and on the ground at different distances away from it. The fields were recorded using flat plate antennas (for the E-field) and magnetic loops (for the H-field). The results suggested that the measured electric field on the roof of the building could be enhanced by a factor of 1.7 to 1.9, whereas the electric fields on the ground experienced a significant reduction by a factor ranging from 5 to 20. Also, it was shown that for a sensor located on the ground close to a building, the magnetic field component perpendicular to the building can experience significant attenuation, presumably due to the effect of the induced currents in the building. The magnetic field on the roof of the building seems not to be significantly affected by the building.

Simulations using the Numerical Electromagnetic Code (NEC-4) were also carried out in which the building was represented using a simple wire-grid model. The simulation results supported in essence the findings of the experimental analysis, despite quantitative differences which are ascribed, at least in part, to the oversimplified model of the building.

7.2 Perspectives

A number of ideas appeared during the course of this study and as a result of the findings of the theoretical investigations and experimental campaigns which definitely deserve further research. The main ideas are discussed hereafter.

The improved version presented in Chapter 4 in which possible reflections at the return stroke wavefront and the presence of an upward connecting leader are considered represent certainly a significant improvement in the modeling of return strokes to tall structures. The improved model was found indeed successful to reproduce the early undershoot, the far field zero crossing and the double peak structure of the field, features that original models were not able to reproduce. The new model also allows, to the extent that the upper reflection coefficient for the current is set to -1, to naturally remove the physically unreasonable discontinuity on the return stroke wavefront. Even though a current reflection coefficient set to -1 corresponds to an open-circuit condition, the situation of a return-stroke is quite different from a traditional transmission line in the sense that the channel is not static and extends in length as a function of time. As mentioned in Chapter 4, Heidler and Hopf [130-131] coped with this problem by defining a reflection coefficient which is given by $\rho_c = (v - c) / (v + c)$, v and c being respectively the return stroke speed and the speed of light. However, the above equation is based on simplified assumptions and a more detailed analysis is required to describe boundary conditions at the end of an extending transmission line.

The experimental campaign carried out in Austria revealed a number of interesting questions which call for further investigations. It was found that in a significant number of cases, the vertical electric field waveform due to the return stroke is characterized by a first peak which exceeds the typical late-time flattening due to the electrostatic term, in contrast with similar measurements related to triggered lightning, in which such a first peak is absent. As of today, the reason for this effect is not quite well understood. Also, some of the measured vertical electric field featured an abnormal waveform characterized by a positive leader field change followed by a bipolar return stroke field change, never observed in available measurements obtained using triggered lightning. Possible reasons for this could include the contribution of the charges induced on the tower to the very close electric field, nonuniform charge distribution along the channel, inclination of the channel.

Work is already in progress to address the raised issues.

References

- [1] V. A. Rakov and M. A. Uman, *Lightning: physics and effects*: Cambridge University Press, 2003.
- [2] Dugan, R, *et al.*, *Electrical Power Systems Quality*: Mc Graw-Hill, 1996.
- [3] S. Guerrieri, *et al.*, "On the influence of elevated strike objects on directly measured and indirectly estimated lightning currents," *IEEE Transactions on Power Delivery*, vol. 13, pp. 1543-55, 1998.
- [4] V. A. Rakov, "Transient response of a tall object to lightning," *IEEE Transactions on Electromagnetic Compatibility*, vol. 43, pp. 654-61, 2001.
- [5] F. Rachidi, "Modeling Lightning Return Strokes to Tall Structures: A Review," *Journal of Lightning Research*, vol. 1, pp. 16-31, January 2007.
- [6] R. J. Fisher, *et al.*, "Parameters of triggered-lightning flashes in Florida and Alabama," *Journal of Geophysical Research*, vol. 98, pp. 22887-902, 1993.
- [7] V. A. Rakov, "Lightning Discharges Triggered Using Rocket-and-Wire Techniques," in *Recent Research Development on Geophysics*. vol. 2, R. Signpost, Ed., ed India, 1999, pp. 141-171.
- [8] F. Heidler, *et al.*, "Lightning Currents Measured at a Telecommunication Tower from 1992 to 1998," in *14th International Zurich Symposium on Electromagnetic Compatibility*, Zurich, Switzerland, 2001, p. 6.
- [9] M. A. O. Schroeder, *et al.*, "Lightning current statistical analysis: Measurements of Morro do Cachimbo Station - Brazil," in *26th ICLP (International Conference on Lightning Protection)*, Cracow, Poland, 2002.
- [10] T. Narita, *et al.*, "Observation of current waveshapes of lightning strokes on transmission towers," *IEEE Transactions on Power Delivery*, vol. 15, pp. 429-35, 2000.
- [11] H. Pichler, *et al.*, "Statistics of lightning current parameters measured at the Gaisberg Tower," in *18th International Lightning Detection Conference (ILDC)*, Helsinki, Finland, 2004, p. 6.
- [12] V. A. Rakov and M. A. Uman, "Review and evaluation of lightning return stroke models including some aspects of their application," *IEEE Transactions on Electromagnetic Compatibility*, vol. 40, pp. 403-26, 1998.
- [13] F. Rachidi, *et al.*, "The Effect of Vertically-Extended Strike Object on the Distribution of Current Along the Lightning Channel," *Journal of Geophysical Research*, vol. 107, p. 4699, 2002.
- [14] A. S. Podgorski and J. A. Landt, "Numerical analysis of the lightning-CN tower interaction," in *6th Symposium and Technical Exhibition on Electromagnetic Compatibility*, Zurich, Switzerland, 1985.
- [15] F. Heidler and T. Zundl, "Influence of tall towers on the return stroke current," in *Aerospace and Ground Conference on Lightning and Static Electricity*, Williamsburg, USA, 1995.
- [16] Y. Baba and M. Ishii, "Numerical electromagnetic field analysis of lightning current in tall structures," *IEEE Transactions on Power Delivery*, vol. 16, pp. 324-8, 2001.
- [17] B. Kordi, *et al.*, "Application of the antenna theory model to a tall tower struck by lightning," *Journal of Geophysical Research*, vol. 108, 2003.
- [18] R. F. Harrington, *Field computation by Moment Methods*. New York: IEEE & Wiley, 1993.

- [19] S. Visacro and F. H. Silveira, "Evaluation of lightning current distribution along the lightning discharge channel by a hybrid electromagnetic model," *Journal of Electrostatics*, vol. 60, pp. 111-120, 2004.
- [20] F. H. Silveira, *et al.*, "Lightning effects on the vicinity of elevated structures," in *International Conference on Lightning Protection ICLP*, Avignon, France, 2004, pp. 291-296.
- [21] V. A. Rakov and F. Rachidi, "Overview of Recent Progress in Lightning Research and Lightning Protection," *IEEE Transactions on Electromagnetic Compatibility*, vol. 51, pp. 428-442, 2009.
- [22] T. Zundl, "Lightning current and LEMP calculations compared to measurements gained at the Peissenberg tower," in *22nd ICLP (International Conference on Lightning Protection)*, Budapest, Hungary, 1994, pp. 1-6.
- [23] S. Guerrieri, *et al.*, "Extension of two return stroke models to consider the influence of elevated strike objects on the lightning return stroke current and the radiated electromagnetic field: comparison with experimental results," *EMC '96 ROMA. International Symposium on Electromagnetic Compatibility. Univ. Rome 'La Sapienza', Rome, Italy*, vol. 2, 1996.
- [24] S. Guerrieri, *et al.*, "Effects of Traveling-Waves of Current on the Initial Response of a Tall Franklin Rod," in *ICLP2000*, Rhode, Greece, 2000, pp. 94-99.
- [25] I. Rusan, *et al.*, "Comparison of measured and computed electromagnetic fields radiated from lightning strikes to the Toronto CN tower," in *23rd International Conference on Lightning Protection (ICLP)*, Florence, 1996, pp. 297-303.
- [26] H. Motoyama, *et al.*, "Electromagnetic field radiation model for lightning strokes to tall structures," *IEEE Transactions on Power Delivery*, vol. 11, pp. 1624-32, 1996.
- [27] F. Rachidi, *et al.*, "Current and electromagnetic field associated with lightning return strokes to tall towers," *IEEE Transactions on Electromagnetic Compatibility*, vol. 43, pp. 356-367, August 2001 2001.
- [28] W. Janischewskyj, *et al.*, "Comparison of lightning electromagnetic field characteristics of first and subsequent return strokes to a tall tower 1. Magnetic field," in *24th ICLP (international conference on lightning Protection)*, Birmingham, U.K., 1998, pp. 245-251.
- [29] W. Janischewskyj, *et al.*, "Lightning electric field characteristics of first and subsequent return strokes to a tall tower," *Eleventh International Symposium on High Voltage Engineering*, vol. 467, 1999.
- [30] V. Shostak, *et al.*, "Electromagnetic fields of lightning strikes to a tall tower: a model that accounts for upward-connecting discharges," in *25th ICLP (International Conference on Lightning Protection)*, Rhodes, Greece, 2000, pp. 60 - 65.
- [31] V. Shostak, *et al.*, "Return-stroke current modeling of lightning striking a tall tower accounting for reflections within the growing channel and for upward-connecting discharges," in *11th International Conference on Atmospheric Electricity*, Guntersville, U.S.A., 1999, pp. 123-6.
- [32] H. Goshima, *et al.*, "Characteristics of electromagnetic fields due to winter lightning stroke current to a high stack," *Transactions of the Institute of Electrical Engineers of Japan, Part B*, vol. 120, pp. 44-9, 2000.
- [33] J. L. Bermudez, *et al.*, "Determination of Reflection Coefficients at the Top and Bottom of Elevated Strike Objects Struck by Lightning," *Journal of Geophysical Research*, vol. 108, pp. 4413, doi: 10.1029/2002JD002973, 2003.
- [34] J. L. Bermudez, *et al.*, "Far-field - current relationship based on the TL model for lightning return strokes to elevated strike objects," *IEEE Transactions on Electromagnetic Compatibility*, vol. 47, pp. 146-159, February 2005 2005.

- [35] Y. Baba and V. A. Rakov, "Lightning electromagnetic environment in the presence of a tall grounded strike object," *Journal of Geophysical Research*, vol. 110, 2005.
- [36] R. Rusan, *et al.*, "Comparison of measured and computed electromagnetic fields radiated from lightning strikes to the Toronto CN tower," in *23rd ICLP (International Conference on Lightning Protection)*, Florence, Italy, 1996, pp. 297-303.
- [37] F. Rachidi and C. A. Nucci, "On the Master, Uman, Lin, Standler and the Modified Transmission Line lightning return stroke current models," *Journal of Geophysical Research*, vol. 95, pp. 20389-94, 1990.
- [38] G. V. Cooray, "On the concepts used in return stroke models applied in engineering practice," *IEEE Trans. on Electromagnetic Compatibility*, vol. 45, pp. 101-108, February 2003 2002.
- [39] Y. Baba and V. A. Rakov, "On the use of lumped sources in lightning return stroke models," *Journal of Geophysical Research*, vol. 110, 2005.
- [40] M. Shigihara and A. Piantini, "Estimation of lightning currents from measurements performed on elevated objects," in *28th International Conference on Lightning Protection (ICLP)*, Kanazawa, Japan, 2006, pp. 213-218.
- [41] V. Shostak, *et al.*, "Modeling of the electromagnetic field associated with lightning return strokes to a complex tall tower," in *26th ICLP (International Conference on Lightning Protection)*, Cracow, Poland, 2002, pp. 167-172.
- [42] V. Shostak, *et al.*, "Expanding the modified transmission line model to account for reflections within the continuously growing lightning return stroke channel," in *IEEE Power Engineering Society Summer Meeting*, Piscataway, USA, 2000.
- [43] J. L. Bermudez, *et al.*, "On the use of transmission line theory to represent a nonuniform vertically-extended object struck by lightning," in *2003 IEEE Symposium on Electromagnetic Compatibility (EMC)*, Boston, USA, 2003.
- [44] Y. Baba and V. A. Rakov, "On the interpretation of ground reflections observed in small-scale experiments simulating lightning strikes to towers," *IEEE Transactions on Electromagnetic Compatibility*, vol. 47, 2005.
- [45] A. Shoory, *et al.*, "On the Propagation of Current Pulses along Tall Structures Struck by Lightning," in *2010 Asia-Pacific Symposium on Electromagnetic Compatibility*, Beijing, China, 2010.
- [46] D. Pavanello, *et al.*, "Return Stroke Current Profiles and Electromagnetic Fields Associated with Lightning Strikes to Tall Towers: Comparison of Engineering Models," in *International Conference on Lightning Protection, ICLP 2004*, Avignon, France, 2004.
- [47] C. A. Nucci, *et al.*, "Lightning return stroke current models with specified channel-base current: a review and comparison," *Journal of Geophysical Research*, vol. 95, pp. 20395-408, 1990.
- [48] D. Pavanello, *et al.*, "Electromagnetic Field Radiated by Lightning to Tall Towers: Treatment of the Discontinuity at the Return Stroke Wavefront," *Journal of Geophysical Research*, vol. 109, 2004.
- [49] O. Beierl, "Front Shape Parameters of Negative Subsequent Strokes Measured at the Peissenberg Tower," in *21st ICLP (International Conference on Lightning Protection)*, Berlin, Germany, 1992, pp. 19-24.
- [50] E. Montandon and B. Beyeler, "The Lightning Measuring Equipment on the Swiss PTT Telecommunications Tower at St. Chrischona, Switzerland," in *22nd ICLP (International Conference on Lightning Protection)*, Budapest, Hungary, 1994, p. 6.

- [51] J. C. Willett, *et al.*, "An experimental test of the 'transmission-line model' of electromagnetic radiation from triggered lightning return strokes," *Journal of Geophysical Research*, vol. 93, pp. 3867-78, 1988.
- [52] M. R. Gavric, "Iterative method for waveshape restoration of directly measured lightning flash currents," *IEE Proceedings Generation, Transmission and Distribution*, vol. 149, pp. 66-70, 2002.
- [53] W. Janischewskyj, *et al.*, "Collection and use of lightning return stroke parameters taking into account characteristics of the struck object," in *23rd ICLP (International Conference on Lightning Protection)*, Florence, Italy, 1996, pp. 16-23.
- [54] A. S. Podgorski and J. A. Landt, "Three dimensional time domain modelling of lightning," *IEEE Transactions on Power Delivery*, vol. PWRD-2, pp. 931-938, 1987.
- [55] R. Moini, *et al.*, "An antenna theory model for the lightning return stroke," in *12th International Zurich Symposium on Electromagnetic Compatibility*, Zurich, Switzerland, 1997, pp. 149-152.
- [56] E. Petrache, *et al.*, "Lightning Strikes to Elevated Structures: Influence of Grounding Conditions on Currents and Electromagnetic Fields," in *IEEE International Symposium on Electromagnetic Compatibility*, Chicago, 2005.
- [57] E. Petrache, *et al.*, "Influence of the finite ground conductivity on the transient response to lightning of a tower and its grounding," in *28th General Assembly of International Union of Radio Science (URSI)*, New Delhi, India., 2005.
- [58] G. J. Burke, "Numerical Electromagnetics Code NEC-4 Method of Moments," Lawrence Livermore National Laboratory UCRL-MA-109338, 1992.
- [59] R. Moini, *et al.*, "A new lightning return stroke model based on antenna theory," *Journal of Geophysical Research*, vol. 105, pp. 29693-702, 2000.
- [60] M. Rubinstein, "An approximate formula for the calculation of the horizontal electric field from lightning at close, intermediate, and long range," *IEEE Transactions on Electromagnetic Compatibility*, vol. 38, pp. 531-5, 1996.
- [61] F. Rachidi, *et al.*, "Influence of a lossy ground on lightning-induced voltages on overhead lines," *IEEE Transactions on Electromagnetic Compatibility*, vol. 38, pp. 250-263, 1996.
- [62] A. K. Agrawal, *et al.*, "Transient response of multiconductor transmission lines excited by a nonuniform electromagnetic field," *IEEE Transactions on Electromagnetic Compatibility*, vol. 22, pp. 119-29, May 1980.
- [63] D. Pavanello, *et al.*, "On the calculation of Electromagnetic Fields Radiated by Lightning to Tall Structures," in *International Conference on Lightning Protection, ICLP 2004*, Avignon, France, 2004.
- [64] M. Rubinstein and M. A. Uman, "Transient electric and magnetic fields associated with establishing a finite electrostatic dipole, revisited," *IEEE Transactions on Electromagnetic Compatibility*, vol. 33, pp. 312-20, 1991.
- [65] M. Rubinstein and M. A. Uman, "On the radiation field turn-on term associated with traveling current discontinuities in lightning," *Journal of Geophysical Research*, vol. 95, pp. 3711-13, 1990.
- [66] D. M. Le Vine and J. C. Willett, "Comment on the transmission line model for computing radiation from lightning," *Journal of Geophysical Research*, vol. 97, pp. 2601-2610, 1992.
- [67] R. Thottappillil and V. A. Rakov, "On different approaches to calculating lightning electric fields," *Journal of Geophysical Research*, vol. 106, pp. 14191-14205, 2001.

- [68] R. Thottappillil, *et al.*, "Distribution of charge along the lightning channel: relation to remote electric and magnetic fields and to return-stroke models," *Journal of Geophysical Research*, vol. 102, pp. 6987-7006, 1997.
- [69] R. Thottappillil, *et al.*, "Treatment of retardation effects in calculating the radiated electromagnetic fields from the lightning discharge," *Journal of Geophysical Research*, vol. 103, pp. 9003-13, 1998.
- [70] V. Cooray, *et al.*, "On the constraints imposed by the close electric field signature on the equivalent corona current in lightning return stroke models," in *International Conference on Lightning Protection (ICLP 2004)*, Avignon, France, 2004, pp. 116-121.
- [71] D. Pavanello, *et al.*, "Propagation effects on the electromagnetic field radiated by lightning to tall towers," in *VIII International Symposium on Lightning Protection, SIPDA*, Sao Paulo, Brazil, 2005.
- [72] V. Cooray, "Effects of propagation on the return stroke radiation fields," *Radio Science*, vol. 22, pp. 757-68, 1987.
- [73] D. Pavanello, *et al.*, "Electromagnetic environment in the immediate vicinity of a tower struck by lightning," in *EUROEM'2004*, Magdeburg, Germany, 2004.
- [74] S. Miyazaki and M. Ishii, "Influence of elevated stricken object on lightning return-stroke current and associated fields," in *International Conference on Lightning Protection ICLP*, Avignon, France, 2004, pp. 122-127.
- [75] A. Baños, *Dipole Radiation in the Presence of a Conducting Half-Space*. Oxford, 1966.
- [76] A. Sommerfeld, "The propagation of electromagnetic waves in wireless telegraphy," *Annual Physics*, vol. 81, pp. 1135-1153, 1926.
- [77] F. Delfino, *et al.*, "An Algorithm for the Exact Evaluation of the Underground Lightning Electromagnetic Fields," *IEEE Transactions on Electromagnetic Compatibility*, vol. 49, pp. 401-411, 2007.
- [78] F. Delfino, *et al.*, "Lightning return stroke current radiation in presence of a conducting ground: 1. Theory and numerical evaluation of the electromagnetic fields," *Journal of Geophysical Research*, vol. 113, 2008.
- [79] F. Delfino, *et al.*, "Lightning return stroke current radiation in presence of a conducting ground: 2. Validity assessment of simplified approaches," *Journal of Geophysical Research*, vol. 113, 2008.
- [80] F. Delfino, *et al.*, "Evaluation of underground lightning electromagnetic fields," in *International Symposium on Electromagnetic Compatibility EMC Europe 2006*, Barcelona, Spain, 2006.
- [81] M. Rubinstein, "An approximate formula for the calculation of the horizontal electric field from lightning at close, intermediate, and long range," *IEEE Trans. on Electromagnetic Compatibility*, vol. 38, pp. 531-535, 1996.
- [82] V. Cooray, "Horizontal fields generated by return strokes," *Radio Science*, vol. 27, pp. 529-37, 1992.
- [83] J. R. Wait, "Concerning the horizontal electric field of lightning," *IEEE Transactions on Electromagnetic Compatibility*, vol. 39, p. 186, 1997.
- [84] A. Shoory, *et al.*, "Analysis of lightning-radiated electromagnetic fields in the vicinity of lossy ground," *IEEE Transactions on Electromagnetic Compatibility*, vol. 47, pp. 131- 145, 2005.
- [85] V. Cooray, "Some considerations on the "Cooray-Rubinstein" formulation used in deriving the horizontal electric field of lightning return strokes over finitely conducting ground," *IEEE Transactions on Electromagnetic Compatibility*, vol. 44, pp. 560-566, 2002.

- [86] C. F. Barbosa and J. O. S. Paulino, "An Approximate Time-Domain Formula for the Calculation of the Horizontal Electric Field from Lightning," *IEEE Transactions on Electromagnetic Compatibility*, vol. 49, pp. 593-601, 2007.
- [87] C. Caligaris, *et al.*, "Cooray-Rubinstein Formula for the Evaluation of Lightning Radial Electric Fields: Derivation and Implementation in the Time Domain," *IEEE Transactions on Electromagnetic Compatibility*, vol. 50, pp. 194-197, 2008.
- [88] V. Cooray, "Underground electromagnetic fields generated by the return strokes of lightning flashes," *IEEE Transactions on Electromagnetic Compatibility*, vol. 43, pp. 75-84, February 2001 2001.
- [89] E. Petrache, *et al.*, "Lightning-Induced Voltages on Buried Cables", Part I: Theory," *IEEE Transactions on Electromagnetic Compatibility*, vol. 47,, p. August 2005, 2005.
- [90] P. Degauque and A. Zeddani, "Remarks on the transmission-line approach to determining the current induced on above-ground cables," *IEEE Transactions on Electromagnetic Compatibility*, vol. 30, pp. 77-80, 1988.
- [91] P. A. Tirkas, *et al.*, "Finite-Difference Time-Domain Method for Electromagnetic Radiation, Interference, and Interaction with Complex Structures," *IEEE Transactions on electromagnetic Compatibility*, vol. 35, pp. 192-203, 1993.
- [92] M. Paolone, *et al.*, "A New Finite Difference Time Domain Scheme for the Evaluation of Lightning Induced Overvoltages on Multiconductor Overhead Lines," in *5th Int. Conf. on Power System Transients*, Rio de Janeiro, 2001.
- [93] C. A. F. Sartori and J. R. Cardoso, "An analytical-FDTD method for near LEMP calculation," *IEEE Transactions on Magnetics*, vol. 36, pp. 1631-1634, 2000.
- [94] C. Yang and B. Zhou, "Calculation methods of electromagnetic fields very close to lightning," *IEEE Transactions on Electromagnetic Compatibility*, vol. 46, pp. 133-141, 2004.
- [95] A. Mimouni, *et al.*, "Electromagnetic environment in the immediate vicinity of a lightning return stroke," *Journal of Lightning Research*, vol. 2, pp. 64-75, 2007.
- [96] A. Mimouni, *et al.*, "A finite-difference time-domain approach for the evaluation of electromagnetic fields radiated by lightning to tall structures," *Journal of Electrostatics*, vol. 866, pp. 504-513, 2008.
- [97] Y. Baba and V. A. Rakov, "On the mechanism of attenuation of current waves propagating along a vertical perfectly conducting wire above ground: application to lightning," *IEEE Transactions on Electromagnetic Compatibility*, vol. 47, pp. 521-532, 2005.
- [98] Y. Baba and V. A. Rakov, "Electromagnetic fields at the top of a tall building associated with nearby lightning return strokes," *IEEE Transactions on Electromagnetic Compatibility*, vol. 49, pp. 632-643, 2007.
- [99] K. Berger, *et al.*, "Parameters of lightning flashes," *Electra. no.*, vol. 41, pp. 23-37, 1975.
- [100] S. Visacro, *et al.*, "Statistical analysis of lightning current parameters: Measurements at Morro do Cachimbo Station," *Journal of Geophysical Research*, vol. 109, D01105, doi:10.1029/2003JD003662, 2004.
- [101] V. A. Rakov, "A Review of the Interaction of Lightning with Tall Objects," *Recent Res. Devel. Geophysics, Research Signpost, India*, vol. 5, pp. 57-71, 2003.
- [102] Y. Baba and V. A. Rakov, " Influences of the Presence of a Tall Grounded Strike Object and an Upward Connecting Leader on Lightning Currents and Electromagnetic Fields," *IEEE Transactions on Electromagnetic Compatibility*, pp. 886-892, 2007.

- [103] S. Visacro and F. H. Silveira, "Lightning current waves measured at short instrumented towers: The influence of sensor position," *Geophysical Research Letters*, vol. 32, L18804, doi:10.1029/2005GL023255, 2005.
- [104] J. Takami and S. Okabe, "Observational Results of Lightning Current on Transmission Towers," *IEEE Transactions on Power Delivery*, vol. 22, pp. 547-556, 2007.
- [105] G. Diendorfer, *et al.*, "Some Parameters of Negative Upward Initiated Lightning to the Gaisberg Tower (2000 - 2007)," *IEEE Transactions on Electromagnetic Compatibility*, 2009.
- [106] T. R. McComb, *et al.*, "Preliminary measurements of lightning flashes to the C.N. Tower in Toronto," *Canadian Electrical Engineering Journal*, vol. 5, pp. 3-9, 1980.
- [107] W. Janischewskyj, *et al.*, "Statistics of lightning strikes to the Toronto Canadian National Tower (1978-1995)," *IEEE Transactions on Power Delivery*, vol. 12, pp. 1210-1221, 1997.
- [108] A. Hussein, *et al.*, "Current waveform parameters of CN Tower," *Journal of Electrostatics*, vol. 60, pp. 149-162, 2004.
- [109] M. Miki, *et al.*, "Initial stage in lightning initiated from tall objects and in rocket-triggered lightning," *Journal of Geophysical Research*, vol. 110, D02109, doi:10.1029/2003JD004474, 2005.
- [110] D. Flache, *et al.*, "Initial-stage pulses in upward lightning: Leader/return stroke versus M-component mode of charge transfer to ground," *Geophys. Res. Lett.*, vol. 35, L13812, doi:10.1029/2008GL034148, 2008.
- [111] D. Pavanello, *et al.*, "On Return-Stroke Currents and Remote Electromagnetic Fields Associated with Lightning Strikes to Tall Structures. Part II: Experiment and Model Validation," *Journal of Geophysical Research*, vol. 112, 2007.
- [112] Y. T. Lin, *et al.*, "Characterization of lightning return stroke electric and magnetic fields from simultaneous two-station measurements," *Journal of Geophysical Research*, vol. 84, pp. 6307-14, 1979.
- [113] W. Janischewskyj, *et al.*, "Propagation of lightning current within the CN Tower," in *CIGRE Study Committee 33 Colloquium*, Toronto, Canada, 1997.
- [114] G. Diendorfer, *et al.*, "Evaluation of lightning location data employing measurements of direct strikes to a radio tower," Session 2002 CIGRE, Paris, France 2002.
- [115] A. Mosaddeghi, *et al.*, "On the Inversion of Polarity of the Electric Field at Very Close Range from a Tower Struck by Lightning," *Journal of Geophysical Research*, vol. 112, 2007.
- [116] D. Wang, *et al.*, "Luminous propagation of lightning attachment to CN tower," *Journal of Geophysical Research*, vol. 100, pp. 11661-7, 1995.
- [117] M. A. Uman, *et al.*, "The electromagnetic radiation from a finite antenna," *American Journal of Physics*, vol. 43, pp. 33-8, 1975.
- [118] A. Zeddani and P. Degauque, "Current and Voltage Induced on Telecommunications Cable by a lightning return stroke," in *Lightning Electromagnetics*, R. L. Gardner, Ed., ed New York: Hemisphere, 1990, pp. 377-40.
- [119] R. Thottappillil, *et al.*, "Return stroke transmission line model for stroke speed near and equal that of light," *Geophysical Research Letters*, vol. 28, pp. 3593-6, 2001.
- [120] A. Mosaddeghi, *et al.*, "Electric and Magnetic Fields at Very Close Range from a Lightning Strike to a Tall Object," in *19th International Zurich Symposium on Electromagnetic Compatibility*, Singapore, 2008.

- [121] A. Mosaddeghi, *et al.*, "On the bipolar waveform of electric field at very close range from a tower struck by lightning," in *29th International Conference on Lightning Protection ICLP*, Uppsala, Sweden, 2008.
- [122] D. Pavanello, *et al.*, "Ability of engineering models to reproduce electromagnetic fields from lightning return strokes to tall towers," in *29th International Conference on Lightning Protection (ICLP)*, Uppsala, Sweden, 2008.
- [123] A. Mosaddeghi, *et al.*, "Distortion of electric and magnetic fields from lightning due to close-by metallic structures," in *7th International Symposium and Exhibition on Electromagnetic Compatibility and Electromagnetic Ecology*, St. Petersburg, Russia, 2007.
- [124] A. Mosaddeghi, *et al.*, "Effect of Nearby Buildings on Electromagnetic Fields from Lightning," *Journal of Lightning Research*, vol. 1, pp. 52-60, 2009.
- [125] A. Mosaddeghi, *et al.*, "On the effect of possible reflections at the return stroke wavefront on radiated fields from lightning strikes to tall structures," in *X International Symposium on Lightning Protection (SIPDA)*, Curitiba, Brazil, 2009.
- [126] A. Mosaddeghi, *et al.*, "Radiated Fields from Lightning Strikes to Tall Structures: Effect of Upward Connecting Leader and Reflections at the Return Stroke Wavefront " *IEEE Transactions on Electromagnetic Compatibility*, in press, 2010.
- [127] T. Takashima and R. Ishibashi, "Electric fields in dielectric multilayers calculated by digital computer," *IEEE Tras. Electr. Insul.*, vol. EI-13, pp. 37-44, 1978.
- [128] Y. Baba and V. A. Rakov, "Influence of strike object grounding on close lightning electric fields," *Journal of Geophysical Research*, vol. 113, D12109, doi:10.1029/2008JD009811, 2008.
- [129] C. A. Nucci, *et al.*, "On lightning return stroke models for LEMP calculations," in *19th International Conference on Lightning Protection (ICLP)*, Graz, Austria, 1988.
- [130] F. Heidler and C. Hopf, "Influence of the lightning channel termination on the lightning current and lightning electromagnetic impulse," in *international aerospace and ground conference on lightning and static electricity*, Mannheim, 1994, pp. 65-74.
- [131] W. Schulz and G. Diendorfer, "Properties of an extended Diendorfer Uman return stroke model [lightning]," *Ninth International Symposium on High Voltage Engineering. Inst. High Voltage Eng, Graz, Austria*, vol. 9, 1995.
- [132] I. K. Boev, "Radiated Electric and Magnetic Fields Caused by Lightning Return Strokes to the Toronto CN Tower," Doctor of Philosophy, Graduate Department of Electrical and Computer Engineering University of Toronto, Toronto, 2010.
- [133] A. Lafković, *et al.*, "Evaluation of the Performance Characteristics of the North American Lightning Detection Network Based on Tall-Structure Lightning," *IEEE Transactions on Electromagnetic Compatibility*, vol. 50, pp. 630-641, 2008.
- [134] V. Shostak, *et al.*, "Electromagnetic Field associated with Lightning Return Strokes to a Tall Structure: Influence of Channel Geometry," in *2003 IEEE Bologna PowerTech Conference*, Bologna, Italy, 2003, pp. 524-527.
- [135] V. Shostak, *et al.*, "Modeling of lightning return strokes at a complex tall structure," in *XIIIth International Symposium on High Voltage Engineering (ISH)*, Delft, Netherlands, 2003, p. 6.
- [136] D. Pavanello, *et al.*, "On return stroke currents and remote electromagnetic fields associated with lightning strikes to tall structures: Part I: Computational Models," *Journal of Geophysical Research*, vol. 112, 2007 2007.

- [137] M. Rubinstein, *et al.*, "Characterization of vertical electric fields 500 m and 30 m from triggered lightning," *Journal of Geophysical Research*, vol. 100, pp. 8863-72, 1995.
- [138] D. E. Crawford, *et al.*, "The close lightning electromagnetic environment: dart-leader electric field change versus distance," *Journal of Geophysical Research*, vol. 106, pp. 14,909-14,917, July 27, 2001.
- [139] J. Schoene, *et al.*, "Statistical Characteristics of the Electric and Magnetic Fields and Their Time Derivatives 15 m and 30 m from Triggered Lightning," *Journal of Geophysical Research*, vol. 108, No. D6, 4192, doi:10.1029/2002JD002698, 2003.
- [140] V. A. Rakov, *et al.*, "Close electric field signatures of dart leader/return stroke sequences in rocket-triggered lightning showing residual fields, J. Geophys. Res., 110.," *Journal of Geophysical Research*, vol. 110, 2005.
- [141] M. A. Uman, *The lightning discharge* vol. 39. Florida, USA: Academic Press, Inc., 1987.
- [142] M. A. Uman, *et al.*, "Electric fields close to triggered lightning," *EMC '94 Roma. International Symposium on Electromagnetic Compatibility. Univ. Rome, Rome, Italy*, vol. 2, 1994.
- [143] R. J. Fisher and G. H. Schnetzer, "1993 triggered lightning test program: Environments within 20 meters of the lightning channel and small area temporary protection concepts," Sandia Matl. Lab, Albuquerque, N.M. SAND94-0311, 1994.
- [144] V. A. Rakov, *et al.*, "New insights into lightning processes gained from triggered-lightning experiments in Florida and Alabama," *Journal of Geophysical Research*, vol. 103, pp. 14117-30, 1998.
- [145] M. Rubinstein, "On the estimation of stroke detection efficiency by comparison of adjacent lightning location systems," in *22nd International Conference on Lightning Protection (ICLP)*, Budapest, Hungary, 1994.
- [146] S. Bonyadi Ram, *et al.*, "The effects of tall buildings on the measurement of electromagnetic fields due to lightning return strokes," in *2001 IEEE EMC International Symposium*, Montreal, Canada, 2001, pp. 1001-1004.
- [147] A. Mosaddeghi and H. Pichler, "Analysis of measurements of currents and associated electromagnetic fields at Gaisberg tower," EPFL-ALDIS, Lausanne-Vienna2009.
- [148] G. Diendorfer, "Gaisberg tower measurements, edited," 2009.
- [149] F. Rachidi, *et al.*, "On the measurement and calculation methods of lightning horizontal electric fields," in *MOCA-09*, Montreal, Canada, 2009.
- [150] E. M. Thomson, *et al.*, "Horizontal electric fields from lightning return strokes," *Journal of Geophysical Research*, vol. 93, pp. 2429-41, 1988.
- [151] K. Michishita, *et al.*, "Measurement of horizontal electric fields associated with distant cloud-to-ground strokes," *Journal of Geophysical Research*, vol. 101, pp. 3861-3867, 1996.
- [152] M. Miki, *et al.*, "Electric Fields Near Triggered Lightning Channels Measured with Pockels Sensors," *Journal of Geophysical Research*, vol. 107(D16), 10.1029/2001JD001087, 2002.
- [153] C. F. Barbosa, *et al.*, "Measured and modeled horizontal electric field from rocket-triggered lightning," *IEEE Transactions on Electromagnetic Compatibility*, vol. 50, pp. 913-920, 2008.
- [154] V. A. Rakov, "Lightning discharges triggered using rocket-and-wire techniques," *recent res. Devel. Geophysics*, vol. 2, pp. 141-171, 1999.

- [155] D. M. Jordan, *et al.*, "Observed dart leader speed in natural and triggered lightning," *Journal of Geophysical Research*, vol. 97, pp. 9951-7, 1992.
- [156] M. A. Uman, "Lightning discharge," *Academic Press, London, UK*, 1987.
- [157] M. Rubinstein, *et al.*, "Analysis of Multi-Station Cloud Lightning Electric Field Pulses Recorded with the Swiss LPATS Network," in *22nd ICLP (International Conference on Lightning Protection)*, Budapest, Hungary, 1994, p. 6.
- [158] J. L. Bermudez, *et al.*, "On the enhancement of electric and magnetic fields from lightning due to close-by metallic structures," in *European Electromagnetics EUROEM'2004*, Magdeburg, Germany, 2004.
- [159] Y. Baba and V. A. Rakov, "Electric fields at the top of tall building associated with nearby lightning return strokes," in *18th Zurich International Symposium on Electromagnetic Compatibility*, Munich, 2007, pp. 179-182.
- [160] A. Mosaddeghi, *et al.*, "An experimental analysis of the effect of nearby buildings on electromagnetic fields from lightning " in *29th International Conference on Lightning Protection ICLP*, Uppsala, Sweden, 2008.
- [161] D. Pavanello, "Electromagnetic Radiation from Lightning Return Strokes to Tall Structures," Ph.D. Ph.D., Swiss Federal Institute of Technology (EPFL), Lausanne, 2007.

Curriculum Vitae

Name: Seyed Abbas MOSADDEGHI

Born on June 10, 1980, Iranian

Email: abbas.mosaddeghi@gmail.com

Education

- 2006-2010 Ph.D. in Electrical Engineering, **Ecole Polytechnique Fédérale de Lausanne (EPFL)**, SWITZERLAND
- 2002- 2005 M.Sc. in Electrical Engineering, Communications and Electromagnetics, **Amirkabir University of Technology**, Tehran, IRAN
- 1998-2002 B.Sc. in Electrical Engineering, Telecommunications, **Sharif University of Technology**, Tehran, IRAN

Professional experience

Research and teaching assistant in the field of electromagnetic compatibility and lightning at the EMC Laboratory of EPFL.

Journal Papers

- A. Mosaddeghi, F. Rachidi, M. Rubinstein, F. Napolitano, D. Pavanello, V. Shostak, W. Janischewskyj and M. Nyffeler, "Radiated Fields from Lightning Strikes to Tall Structures: Effect of Upward Connecting Leader and Reflections at the Return Stroke Wavefront", in press, *IEEE Trans. on Electromagnetic Compatibility*, 2011
- A. Mosaddeghi, A. Shoory, F. Rachidi, G. Diendorfer, H. Pichler, D. Pavanello, M. Rubinstein, P. Zwiack, and M. Nyffeler, "Lightning Electromagnetic Fields at Very Close Distances Associated with Lightning Strikes to the Gaisberg Tower", *Journal of Geophysical Research*, 115, D17101, doi:10.1029/2009JD013754, 2010
- A. Mosaddeghi, A. Shoory, F. Rachidi, M. Rubinstein, G. Diendorfer, H. Pichler, D. Pavanello, and M. Nyffeler, "Close-Range Electric Fields Associated with Lightning Strikes to the Austrian Gaisberg Tower", *International Journal of Plasma Environmental Science & Technology*, Vol.4, No.1, 2010
- V. Shostak, W. Janischewskyj, F. Rachidi, A. Mosaddeghi, M. Rubinstein, and G. Kovenya, "Some Aspects on Lightning Protection of Wind Turbines", *International Journal of Plasma Environmental Science & Technology*, Vol.4, No.1, 2010
- A. Mosaddeghi, D. Pavanello, F. Rachidi, M. Rubinstein, and P. Zwiack, "Effect of Nearby Buildings on Electromagnetic Fields from Lightning", *Journal of Lightning Research*, 1:52-60, 2009
- A. Mosaddeghi, D. Pavanello, F. Rachidi, M. Rubinstein, "On the Inversion of Polarity of the Electric Field at Very Close Range from a Tower Struck by Lightning", *Journal of Geophysical Research*, 112, D19113, doi:10.1029/2006JD008350, 2007

Conference Papers

- A. Mosaddeghi, A. Shoory, F. Rachidi, G. Diendorfer, H. Pichler, D. Pavanello, M. Rubinstein, P. Zwiack, and M. Nyffeler, "Vertical and Radial Electric Fields from Leaders and Return Strokes Associated with Lightning Strikes to the Gaisberg Tower", *30th International Conference on Lightning Protection (ICLP)*, Cagliari, Italy, September 2010
- A. Mosaddeghi, F. Rachidi, M. Rubinstein, D. Pavanello, V. Shostak, W. Janischewskyj, and E. Petrache, "On the Effect of Possible Reflections at the Return Stroke Wavefront on Radiated Fields From Lightning Strikes to Tall Structures", *X International Symposium on Lightning Protection (X SIPDA)*, Curitiba, Brazil, November 2009
- A. Mosaddeghi, F. Rachidi, M. Rubinstein, G. Diendorfer and H. Pichler et al. "Close-Range Electromagnetic Fields Associated with Lightning Strikes to the Austrian Gaisberg Tower", *4th International Workshop on Electromagnetic Radiation from Lightning to Tall Structures*, Montreal, Canada, July 2009.
- A. Mosaddeghi, A. Mimouni, F. Rachidi, M. Rubinstein and W. G. Diendorfer et al., "Vertical and Horizontal Components of the Electric Field Associated with Lightning Strikes to the Gaisberg Tower", *4th International COST Symposium on Lightning Physics and Effects*, Vienna, Austria, May 2009

Curriculum Vitae

G. Diendorfer, A. Mosaddeghi, D. Pavanello, H. Pichler, F. Rachidi, M. Rubinstein, "Electric and Magnetic Field Measurements at Very Close Range Associated with Lightning Strikes to the Austrian Gaisberg Tower", *2008 URSI General Assembly, Chicago, USA*, August 2008

A. Mosaddeghi, D. Pavanello, F. Rachidi, M. Rubinstein, "Electric and Magnetic Fields at Very Close Range from a Lightning Strike to a Tall Object", *19th International Zurich Symposium On Electromagnetic Compatibility, Singapore*, May 2008

A. Mimouni, A. Mosaddeghi, F. Rachidi, M. Rubinstein, "Electromagnetic Fields Very Near to a Tall Tower Struck by Lightning: Influence of the Ground Conductivity", *European Electromagnetics International Symposium EUROEM 2008, Lausanne, Switzerland*, July 2008

A. Mosaddeghi, D. Pavanello, F. Rachidi, M. Rubinstein, P. Zweiacker, "An experimental Analysis of the Effect of Nearby Buildings on Electromagnetic Fields from Lightning", *29th International Conference on Lightning Protection (ICLP), Uppsala, Sweden*, June 2008

A. Mosaddeghi, D. Pavanello, F. Rachidi, M. Rubinstein, "On the Bipolar Waveform of Electric Field at Very Close Range from a Tower Struck by Lightning", *29th International Conference on Lightning Protection (ICLP), Uppsala, Sweden*, June 2008

D. Pavanello, A. Mosaddeghi, F. Rachidi, M. Rubinstein, W. Janischewskyi, V. Shostak, A.M. Hussein, C.A. Nucci, J.S. Chang, "Ability of engineering models to reproduce electromagnetic fields from lightning return strokes to tall towers", *29th International Conference on Lightning Protection (ICLP), Uppsala, Sweden*, June 2008

G. Diendorfer, A. Mosaddeghi, D. Pavanello, H. Pichler, F. Rachidi, M. Rubinstein, "Electromagnetic Fields from Lightning Strikes to the Gaisberg Tower", *3rd International COST Symposium on Lightning Physics and Effects, Vienna, Austria*, April 2008.

A. Mosaddeghi, D. Pavanello, F. Rachidi, M. Rubinstein, P. Zweiacker, "Distortion of electric and magnetic fields from lightning due to close-by metallic structures", *7th International Symposium and Exhibition on Electromagnetic Compatibility and Electromagnetic Ecology, St. Petersburg, Russia*, June 26-29, 2007

A. Mosaddeghi, D. Pavanello, F. Rachidi, M. Rubinstein, P. Zweiacker, "Effect of Nearby Buildings on Electric and Magnetic Fields from Lightning", *2nd International COST Symposium on Lightning Physics and Effects, Vienna, Austria*, April 2007

A. Mosaddeghi, D. Pavanello, F. Rachidi, M. Rubinstein, "Electromagnetic Environment at Very Close Range from a Tower Struck by Lightning", *2nd International COST Symposium on Lightning Physics and Effects, Vienna, Austria*, April 2007

Honors

Best paper awarded for the paper entitled "On the Bipolar Waveform of Electric Field at Very Close Range from a Tower Struck by Lightning" at the *29th International Conference on Lightning Protection (ICLP), Uppsala, Sweden*, June 2008

Invited presentation on "Electromagnetic disturbances generated by lightning discharge" at the *ITU-T SG5 (Environment and Climate Change) Meeting, Geneva, Switzerland*, 24 November 2010

Qualified and financially supported by European Cooperation in Science and Technology (COST) Action P18 (The Physics of Lightning Flash and Its Effects) for two Short Term Scientific Missions (STSM):

- COST-STSM-P18-04458, Vienna, Austria, 02-06 March 2009, "Lightning Measurement Analysis of Gaisberg Tower in Salzburg, Austria.". The STSM has been selected for oral presentation at *COST P18 Final MC and Evaluation Conference, Stockholm, Sweden, 23-24 November 2009*.
- COST-STSM-P18-02726, Uppsala, Sweden, 20-26 May 2007, "Design and fabrication of a current sensor for measuring the tower currents during lightning strike."

Languages

Persian (native), English (fluent), French (fluent), German (basic knowledge)